Title
The structure and function of colicin Ia

Author
Ghosh, Partho

Publication Date
1992

Peer reviewed|Thesis/dissertation

The Structure and Function of colicin Ia

by

Partho Ghosh

DISSERTATION

Submitted in partial satisfaction of the requirements for the degree of

DOCTOR OF PHILOSOPHY

in

Biochemistry

in the

GRADUATE DIVISION

of the

UNIVERSITY OF CALIFORNIA

San Francisco

For my family:
my late Father,
my Mother,
Dhrubo,
and
Stephanie

Acknowledgements

Something very good but very difficult to describe happens during the course of graduate school. In part it is due to the task undertaken: to solve problems whose answers, if they exist at all, have yet to be found. Doing this successfully requires quite a bit of luck but also the insight and clarity of vision about how to go about solving the problem. Developing these may be what graduate school is all about and also what is most difficult about graduate school. It is a harrowing challenge when rather than finding the answer from one's teacher, one must become one's own teacher. Teaching oneself all alone is extremely difficult and worse yet dull, so I was very lucky to have a group of professors and peers who made the process lively, exciting, and worthwhile.

I was also lucky to be able to have the time to work on a challenging problem. At times extremely frustrating, in the end it allowed me to learn x-ray crystallography, a subject I have thoroughly enjoyed for its elegance and symmetry, and to work on an intriguing scientific problem. The structure of colicin Ia during many late nights at the synchrotron transfigured into Polyphemus, tearing limb from limb, but during the mental restitution of day became Circe, singing siren songs of more experiments and more data.

My first experience in crystallography came with Bill Montfort who taught me about precession camera, the Ewald sphere, and TS crystals in my rotation in this lab. I even had a chance to collect data

in San Diego with Bill, Bob Stroud, and Janet Finer-Moore. My next instruction in crystallography was with Seunghyon Choe, when we were scanning films in West Lafayette, Indiana (Purdue). Seunghyon had collected the first diffraction beyond 6 Å for colicin Ia at SSRL, which had just opened. The crystals had been grown by Nancy Helmers after some initial work by Susan Hershenson. From speaking with Jordan Konisky, I understand that the first crystals were grown in 1979 when he was on sabbatical in Herb Boyer's lab. In any case, Seunghyon and I spent two weeks in Michael Rossman's lab scanning and processing all of his films. During the next couple of months, Seunghyon was a very good and capable teacher regarding the scaling of data, the MIR method, and difference Pattersons. I was lucky to be able to ask him numerous questions and learn from him even as he was racing to finish his own Ph. D. thesis.

During the first year in Bob's lab, I decided to try some functional experiments with colicin Ia. Stephanie Mel and I found a cell pellet of colicinogenic cells, struck some of this out on LB plates, and we were off producing and purifying our own colicin Ia.

Jim Hudspeth was very kind to provide space and equipment in his lab to try out colicin Ia channel recording experiments. Stephanie and I tried for months to get current recordings from colicin Ia, and through an insight of Stephanie's that we should wait longer for hexane to evaporate from the lipid monolayer, we were able to get membranes successfully and to finally record colicin Ia channels. This led to the experiments described in the first two chapters. Rob Moore was involved in getting the MA-β peptide

synthesized and in the initial channel recordings. For analysis of these channels, Bill Roberts and his programs were of immeasurable importance and later Fernan Jaramillo was very generous with his time and programs as well. Joe Howard and Aniruddha Das were sources of advice in the Hudspeth lab, and Richard Jacobs provided much appreciated technical assistance. Juan Korenbrot also provided greatly appreciated lab space for analysis of these channels and critical discussion. For experiments with the channel-forming fragment of colicin Ia described in Chapter 2, Larry Miercke was of unlimited expertise regarding column chromotography. It never ceased to amaze me how devoted he is to that science. For all the channel experiments, I was very fortunate to have the advice and critical comments of Michael Shuster.

When I moved back from the functional aspects of channels to the structural, I was lucky to have a rich environment. I am indebted to many people for helping me to collect data at synchrotrons. Early on, Michael Shuster and Thomas Earnest were particularly good comrades during late nights at SSRL. I thank Thomas for his efforts at freezing colicin Ia. Eric Fauman, Earl Ruttenber, Ramu, Doug Freymann, Paul Foster, Bob Rose, Kathy Perry, and lately Anton Krukowski have also lent a much appreciated hand at SSRL and Brookhaven. Stephanie was the only person I could convince to accompany to the cold climes of CHESS (until Michael Wiener arrived) for three separate visits. I am indebted for this and am currently paying off this debt. I am lucky to have had Michael Wiener come into the project for setting up the flash freezing

technique with Doug Freymann and making it work. I am also greatly indebted to Sasha Kamb for an enormous amount of help in setting up the mutagenesis of colicin Ia.

I am also grateful for the conversations and ideas that have a natural way of occurring over the years. I appreciated having Mike McCarthy, Julie Earnest, Michael Shuster, and later Sasha Kamb and Michael Wiener with whom to discuss membrane proteins. I am very glad to have been able to discuss structure with Ramu, Eric Fauman, Chris Bystroff, and lately David Baker. Eric and Ramu have also been great sources of programs.

I also thank all my squash friends. They have always honed my competitive edge but more importantly have provided a needed diversion.

I owe an immense amount to my best friend throughout these years, Stephanie Mel. As she realizes, I write this with only a severely restricted amount of time before our plane to Thailand leaves, so I cannot do our friendship justice on these pages. I will have to express it elsewhere.

Lastly, I thank Bob Stroud for being a friend and a great teacher of crystallography. I have most appreciated his openness.

The structure and function of colicin Ia

by

Partho Ghosh

Abstract

The x-ray crystal structure of the channel-forming bacteriocin colicin Ia has been solved to low resolution using five derivatives, four of wild-type colicin Ia and of a serine to substitution mutant. The structure shows that this 70 kD molecule is "Y"-shaped, containing three very α-helical domains. One of the arms of the "Y", termed Arm 2, probably corresponds to an 18 kD channel-forming fragment of colicin Ia, which was found to form channels that differ substantially from those formed by intact colicin Ia. The 18 kD channels have shorter open times, larger conductances than the intact molecule ion channels. Additionally, while colicin Ia conducts current only at negative voltages, the 18 kD fragment continues to conduct current but at a lower flux than at negative voltages. The presence of an additional sub-domain in Arm 2 besides the helices that corresponds to the 18 kD fragment helices supports the interpretation that portions upstream of the 18 kD fragment may be involved in forming the intact molecule ion channel. The other arm of the "Y", termed Arm 1, probably contains residue 171, as determined from a difference Fourier of a mercurial derivative of mutant S171C. The 18 kD channel-forming fragment contains sequences that are capable of forming amphipathic

α -helices. The channel-forming activity of such amphipathic α -helical sequences have been investigated by channel-recordings from a 27-amino acid sequence derived from the nicotinic acetylcholine receptor (nAChR), MA-β. This peptide was found to form very stable ion channels, supporting the notion that amphipathic α-helical sequences are capable of forming ion channels, but found not to mimic the properties of the nAChR. The structure of colicin Ia represents the first step in understanding the mechanism of membrane insertion and ion channel-formation and -function of this molecule.

Table of Contents

List of Tables

exclusive of Chapter One

List of Figures

exclusive of Chapter One

INTRODUCTION

A fundamental property of cells is the isolation of an interior milieu from an exterior environment by means of a lipid bilayer membrane. Were it not for the fact that cells incorporate proteins into their membranes, this enclosure would preclude cells from communicating with their environment. Instead, cells possess various transmembrane receptors and ion channels to relay signals from the exterior to the cell's interior. In understanding the structural basis for transmembrane signaling, ion channels pose perhaps the most challenging problem: unlike most other transmembrane proteins, an ion channel's site of action is within the hydrophobic core of the membrane, through which it creates an aqueous path (Hille, 1984). In addition, ion channels are highly significant signal transducers, as evidenced by their prevalence within the nervous system. The focus of this thesis is the structural basis of ion channel formation and function.

In particular, the functional and structural properties of the bacterial, ion channel-forming protein colicin Ia have been investigated through single channel recording and x-ray diffraction techniques. Colicin Ia is a member of the ion channel-forming family of colicins which includes colicins A, B, E1, Ib, K, and N as well (for review see Cramer, et al., 1990; Pattus, et al., 1990). The colicins are soluble, bactericidal proteins that function by forming lethal, transmembrane ion channels. The lethal action of these proteins were noted early in the study of bacterial genetics and physiology (Jacob, et al., 1952; Fredericq, 1958; Nomura, 1963; Luria, 1964).

These proteins are induced by the SOS response (Morlon, et al., 1983; Waleh & Johnson, 1985; Mankovich, et al., 1986; Salles, et al., 1987) and are synthesized as soluble, cytoplasmic proteins. They are then released into the extracellular medium through a mechanism that does not involve the normal bacterial secretion pathway (Zhang, et al., 1985; Baty, et al., 1987; Cavard, et al., 1987). They bind to a specific, outer membrane receptor of another bacterium and translocate across the periplasmic space to the inner membrane, where they form the transmembrane ion channel. Colicinogenic strains are immune to the killing effect of their particular colicin because they constitutively produce an immunity protein, which is located in the inner membrane and blocks the action of the colicin (Weaver, et al., 1981b; Geli, et al., 1986).

The colicins require low pH (< 4) and negatively charged lipids for attachment and insertion into membranes (Pattus, et al., 1983; Davidson, et al., 1984b; Davidson, et al., 1985; Shiver, et al., 1987; Jakes, et al., 1990; Mel, 1992). In forming the ion channel, the colicins follow single-hit kinetics and stoichiometric studies seem to indicate that only one molecule is necessary to form a channel (Bruggemann & Kayalar, 1986; Peterson & Cramer, 1987; Slatin, 1988; Levinthal, et al., 1991). However, the association state of the channel is still not completely resolved. These channels are voltage-dependent, opening only at negative cellular potentials, and are relatively non-selective (Schein, et al., 1978; Weaver, et al., 1981a; Seta, et al., 1983; Raymond, et al., 1986; Nogueira & Varanda, 1988).

Yet, the colicins do discriminate between cations and anions in a manner dependent on pH. For example, at pH 6.0 in negatively charged membranes, colicin E1 is cation selective, but at pH 4.5 it becomes anion selective (Cleveland, et al., 1983). The diameter of the colicin channel as determined from colicin E1 is 8 Å at the narrowest point, but the average diameter is probably 12-16 Å (Raymond, et al., 1985).

In terms of primary structure, the ion channel-forming activities of colicins A and E1 have been isolated to the carboxy-terminal third of each intact molecule (Ohno-Iwashita & Imahori, 1982; Carmen Martinez, et al., 1983; Baty, et al., 1988; Baty, et al., 1990). The carboxy-terminal domains of the ion channel-forming colicins share little primary sequence identity, but do share sequences capable of forming amphipathic α-helices. It seems a likely possibility that these amphipathic α-helices form the lining of the ion channel. In this model, the amphipathic α-helices would have their hydrophilic surfaces facing outward into solution in the soluble state of the protein, but facing inward and thereby forming the channel lining in the transmembrane state (Davidson, et al., 1984a; Pattus, et al., 1985; Shiver, et al., 1989). In fact, the structure of the soluble form of the channel-forming fragment of colicin A reveals that it does possess amphipathic α-helices which have their hydrophilic surfaces facing outward (Parker, et al., 1989; Parker, et al., 1990; Parker, et al., 1992).

The amphipathic α-helix model was the impetus for testing

whether a peptide capable of forming an amphipathic α-helix would form ion channels. It was noted that the nicotinic acetylcholine receptor (nAChR), a ligand-gated ion channel found at the vertebrate neuromuscular junction, possesses four hydrophobic, putative transmembrane α-helical segments (M1-M4) and one amphipathic, putative transmembrane α-helical segment (MA) (Finer-Moore & Stroud, 1984). These putative segments are ~27 amino acids long and therefore the correct length to span the bilayer. Since transmembrane segments are much easier to identify by primary sequence analysis for nAChR than for colicin Ia, a sequence from nAChR rather than colicin Ia was used to test the model. A peptide having the sequence of the MA segment from the β subunit of nAChR was synthesized by solid-phase chemistry and found to form stable, long-lived ion channels in planar lipid bilayers. However, the ion channel properties of the peptide were very different from those of nAChR. For structural studies, crystals were grown from this peptide using acetonitrile, but these proved to be highly disordered as determined by x-ray diffraction. The properties of MA-β and the utility of using peptides as mimics of electrophysiological ion channels are discussed in Chapter 1.

To determine whether those sequences in colicin Ia capable of forming amphipathic α-helices were responsible for forming the ion channel, the molecule was proteolyzed. The carboxy-terminal quarter, which possesses these amphipathic sequences, was isolated through tryptic cleavage and purified. Rigorous tryptic cleavage of

the molecule reveals that this carboxy-terminal fragment is likely a structural domain of the protein. By incorporation into artificial phospholipid bilayers, this fragment was found to form ion channels, but the properties of these channels are very different from those of the intact colicin Ia channel. The relationship of this fragment to intact colicin Ia as well as to fragments of other colicins is discussed in Chapter 2.

As a means to understanding the mechanism of insertion of colicin Ia into membranes and subsequent ion channel formation, the soluble form of the molecule was crystallized. Multiple isomorphous (MIR) methods and site-directed mutagenesis were used to solve the x-ray diffraction structure. The result is a model of colicin Ia composed of 28 α-helical fragments without sequence as yet having been fit. However, the model suggests a relationship of functional and structural domains, and this along with the methods and results of structure determination are presented in Chapter 3.

References

Baty, D., Frenette, M., Lloubes, R., Geli, V., Howard, S. P., Pattus, F. & Lazdunski, C. (1988) *Mol. Microbiol. 2,* 807-811.

Baty, D., Lakey, J., Pattus, F. & Lazdunski, C. (1990) *Eur. J. Biochem. 189,* 409-413.

Baty, D., Lloubès, R., Geli, V., Lazdunski, C. & Howard, S. P. (1987) *EMBO J. 6,* 2463-2468.

Bruggemann, E. P. & Kayalar, C. (1986) *Proc. Nat. Acad. Sci. USA 83,* 4273-4276.

Carmen Martinez, M., Lazdunski, C. & Pattus, F. (1983) *EMBO J. 2,* 1501-1507.

Cavard, D., Baty, D., Howard, S. P., Verheij, H. M. & Lazdunski, C. (1987) *J. Bacteriol. 169,* 2187-2194.

Cleveland, M. v., Slatin, S., Finkelstein, A. & Levinthal, C. (1983) *Proc. Nat. Acad. Sci U.S.A. 80,* 3706-3710.

Cramer, W. A., Cohen, F. S., Merrill, A. R. & Song, H. Y. (1990) *Mol.*

Microbiol. 4, 519-526.

Davidson, V. L., Brunden, K. R. & Cramer, W. A. (1985) *Proc. Nat. Acad. Sci U.S.A. 82,* 1386-1390.

Davidson, V. L., Brunden, K. R., Cramer, W. A. & Cohen, F. S. (1984a) *J. Membr. Biol. 79,* 105-118.

Davidson, V. L., Cramer, W. A., Bishop, L. J. & Brunden, K. R. (1984b) *J. Biol. Chem. 259,* 594-600.

Finer-Moore, J. & Stroud, R. M. (1984) *Proc. Nat. Acad. Sci. U.S.A. 81,* 155-159.

Fredericq, P. (1958) *Symp. Soc. Exptl. Biol. 12,* 104-122.

Geli, V., Baty, D., Crozel, V., Morlon, J., Lloubès, R., Pattus, F. & Lazdunski, C. (1986) *Mol. Gen. Genet. 202,* 455-460.

Hille, B. (1984) *Ionic Channels of Excitable Membranes,* Sinauer Associates, Inc., Sunderland, Mass.

Jacob, F., Siminovitch, L. & Wollman, E. L. (1952) *Ann. Inst. Pasteur 83,* 295-315.

Jakes, K. S., Abrams, C. K., Finkelstein, A. & Slatin, S. L. (1990) *J. Biol. Chem. 265,* 6984-6991.

Levinthal, F., Todd, A. P., Hubbell, W. L. & Levinthal, C. (1991) *Proteins: Struct. Func. Genet. 11,* 254-262.

Luria, S. E. (1964) *Ann. Inst. Pasteur 107,* 67-73.

Mankovich, J. A., Hsu, C. & Konisky, J. (1986) *J. Bacteriol. 168,* 228-236.

Mel, S. F. (1992) Ph. D., University of California, San Francisco.

Morlon, J., Lloubes, R., Varenne, S., Chartier, M. & Lazdunski, C. (1983) *J. Mol. Biol. 170,* 271-285.

Nogueira, R. A. & Varanda, W. A. (1988) *J. Membr. Biol. 105,* 143-153.

Nomura, M. (1963) *Cold Spring Harbor Symposia on Quantitative Biology 28,* 315-324.

Ohno-Iwashita, Y. & Imahori, K. (1982) *J. Biol. Chem. 257,* 6446-6451.

Parker, M. W., Pattus, F., Tucker, A. D. & Tsernoglou, D. (1989) *Nature*

337, 93-96.

Parker, M. W., Postma, J. P. M., Pattus, F., Tucker, A. D. & Tsernoglou, D. (1992) *J. Mol. Biol. 224,* 639-657.

Parker, M. W., Tucker, A. D., Tsernoglou, D. & Pattus, F. (1990) *Trends Biochem. Sci. 15,* 126-129.

Pattus, F., Heitz, F., Martinez, C., Provencher, S. W. & Lazdunski, C. (1985) *Eur. J. Biochem. 152,* 681-689.

Pattus, F., Martinez, M. C., Dargent, B., Cavard, D., Verger, R. & Lazdunski, C. (1983) *Biochemistry 22,* 5698-5703.

Pattus, F., Massotte, D., Wilmsen, H. U., Lakey, J., Tsernoglou, D., Tucker, A. & Parker, M. W. (1990) *Experientia 46,* 180-192.

Peterson, A. A. & Cramer, W. (1987) *J. Membr. Biol. 99,* 197-204.

Raymond, L., Slatin, S. L. & Finkelstein, A. (1985) *J. Membr.Biol. 84,* 173-181.

Raymond, L., Slatin, S. L., Finkelstein, A., Liu, Q. & Levinthal, C. (1986) *J. Membr. Biol. 92,* 255-268.

Salles, B., Weisemann, J. M. & Weinstock, G. M. (1987) *J. Bacteriol. 169,* 5028-5034.

Schein, S. J., Kagan, B. L. & Finkelstein, A. (1978) *Nature 276,* 159-163.

Seta, P., d'Epenoux, B., Sandeaux, R., Pattus, F., Lazdunski, C. & Gavach, C. (1983) *Biochem. Biophys. Res. Commun. 113,* 765-771.

Shiver, J. W., Cramer, W. A., Cohen, F. A., Bishop, L. J. & de Jong, P. J. (1987) *J. Biol. Chem. 262,* 14273-14281.

Shiver, J. W., Peterson, A. A., Widger, W. R., Furbacher, P. N. & Cramer, W. A. (1989) *Methods Enzymol. 172,* 439-461.

Slatin, S. L. (1988) *Int. J. Biochem. 20,* 737-744.

Waleh, N. S. & Johnson, P. H. (1985) *Proc. Nat. Acad. Sci. U.S.A. 82,* 8389-8393.

Weaver, C. A., Kagan, B. L., Finkelstein, A. & Konisky, J. (1981a) *Biochim. Biophys. Acta 645,* 137-142.

Weaver, C. A., Redborg, H. & Konisky, J. (1981b) *J. Bacteriol. 148,* 817-828.

Zhang, S., Faro, A. & Zubay, G. (1985) *J. Bacteriol. 163,* 174-179.

CHAPTER 1
Ion Channels Formed by a Highly Charged Peptide

Reprinted with permission from Ghosh, P. & Stroud, R. M. (1991) Ion Channels Formed by a Highly Charged Peptide. *Biochemistry 30,* 3551-3557. 1991 American Chemical Society.

Reprinted from Biochemistry, 1991, 30.

Ion Channels Formed by a Highly Charged Peptide†

Partho Ghosh and Robert M. Stroud*
Department of Biochemistry and Biophysics, University of California, San Francisco, California 94143
Received March 29, 1990; Revised Manuscript Received January 10, 1991

ABSTRACT: A peptide (MA-β) corresponding to a segment of the nicotinic acetylcholine receptor (AChR) that has amphipathic α-helical periodicity forms ion channels in artificial phospholipid bilayers. The MA-β ion channels are very stable, comprise two discrete conductance states, and undergo rapid, flickering-type closings. The discrete-conductance ion channels formed by MA-β contrast with the continuous-conductance ion channels formed by a peptide (M2-δ) identical in sequence with M2 [Oiki, S., Danho, W., Madison, V., & Montal, M. (1988) *Proc. Natl. Acad. Sci. U.S.A. 85*, 8703–8707], a putative transmembrane segment of the AChR. Neither MA-β nor M2-δ sufficiently mimics the electrophysiological properties of the native AChR. We suggest that peptide ion channels can be classified into at least three general groups: discrete-conductance channels, such as MA-β; continuous-conductance channels, such as M2-δ; and membrane disruptors, such as those formed by short, amphipathic α-helical peptides.

Ion channel proteins mediate the transmembrane transduction of electrical and chemical signals between cells and between cellular compartments (Hille, 1984). A problem in understanding the mechanism of action of these proteins is in identifying the residues that constitute the ion-conducting channel. This problem is addressed for the nicotinic acetylcholine receptor (AChR), a well-studied ion channel which is found at the vertebrate neuromuscular junction. The AChR, a ligand-gated and cation-selective channel, is a heteropentamer of four homologous subunits ($\alpha\beta\alpha\gamma\delta$), which are arranged quasi-symmetrically around the ion channel. This 298-kDa protein complex possesses a 2.5-nm-wide, extracellular infundibulum, which presumably contains the entrance to the ion channel (Ross et al., 1977). The ion channel narrows from this large entrance to an apparent diameter of ~0.7 nm within the membrane (Mitra et al., 1989; Kistler et al., 1982).

The lining of the transmembrane portion of the ion channel is most likely formed by five quasi-equivalent segments, one from each subunit of the AChR, in pentameric arrangement. Each subunit of the AChR contains four primarily hydrophobic, putative α-helical transmembrane segments, M1 through M4, as well as a sequence having amphipathic α-helical periodicity, MA. Primary sequence analysis focused attention on MA as a possible ion channel forming segment because of its amphipathic α-helical periodicity (Finer-Moore & Stroud, 1984) (Figure 1a). However, recent experimental evidence indicates that the M2 region (Figure 1b) is a more likely candidate for the ion channel lining segment (Noda et al., 1983). Although generally hydrophobic, the M2 segment has three to five serines or threonines, depending on the subunit, which could contribute to the hydrophilic center of the ion channel. Mutagenesis of the M2 region (Imoto et al., 1988; Leonard et al., 1988) and photolabeling studies using channel blockers (Giraudat et al., 1987; Oberthür et al., 1986) have indicated a key role for this segment in ion channel function. The $GABA_A$ and glycine receptors, which are ligand-gated, anion-selective ion channels and are similar in sequence to the AChR, possess a segment resembling M2 but lack an MA-like segment (Grenningloh et al., 1987; Schofield et al., 1987).

A peptide (M2-δ) corresponding to the M2 region of the δ-subunit has been found to form ion channels in artificial phospholipid bilayers (Oiki et al., 1988a). To determine whether the MA region also possesses ion channel forming capability, a peptide (MA-β) corresponding to MA from the β-subunit of *Torpedo californica* AChR was synthesized, and its ion channel activity was assayed in artificial phospholipid bilayers. We present the electrophysiological properties of MA-β and discuss the relative properties of MA-β, M2-δ, and native AChR channels.

Experimental Procedures

Synthesis and Purification of Peptides. The 27 amino acid MA-β peptide (Figure 1a) and a 19-amino acid peptide (AL), which is unrelated to the AChR in sequence (Figure 1c), were synthesized by using solid-phase, stepwise *tert*-butoxycarbonyl (*t*-Boc)[1] chemistry and PAM resins on an Applied Biosystems 430A automated peptide synthesizer. They were purified by reverse-phase HPLC on a C_{18} column, using a 0–70% AcN gradient containing 0.1% TFA (Figure 2a). The purity and homogeneity of the peptides were verified by direct amino acid analysis. The identity and purity of the MA-β peptide were further determined by mass spectrometry (Figure 2b), which showed that no other peptide species besides MA-β was present. The MA-β and AL peptides are water-soluble to concentrations of at least 10 g/L.

Formation of Artificial Phospholipid Bilayers. Artificial phospholipid bilayers were formed on the tip of tight-seal pipets (Coronado & Latorre, 1983; Suarez-Isla et al., 1983). A Corning lead glass 1080 pipet, which had been pulled so that its tip resistance was 1–20 MΩ, was filled with a buffered salt solution and placed into a 2-mL bath containing the same salt solution. Five to ten microliters of a 1 g/L solution of soybean asolectin (Associated Concentrates), which had been purified (Kagawa & Racker, 1971) and solubilized in hexane, was spread on the approximately 100 mm^2 surface of the bath solution. Membrane-sealed tips were formed by allowing the hexane to evaporate for 10 min and then by removing and

† This work was supported by NIH Grant GM24485 and NSF Grant DMB8615712 (to R.M.S.) and partially by NIH Grants NS20429 and NS22389 (to A. J. Hudspeth). P.G. is a recipient of an NSF Predoctoral Fellowship and was partially supported by a grant from the Lucille P. Markey Charitable Trust.
* Author to whom correspondence should be addressed.

[1] Abbreviations: *t*-Boc, *tert*-butoxycarbonyl; PAM, phenylacetamidomethyl; AcN, acetonitrile; TFA, trifluoroacetic acid; Tris, tris(hydroxymethyl)aminomethane; EDTA, ethylenediaminetetraacetic acid; EGTA, [ethylenebis(oxyethylenenitrilo)]tetraacetic acid; HEPES, *N*-(2-hydroxyethyl)piperazine-*N*′-2-ethanesulfonic acid.

0006-2960/91/0430-3551$02.50/0

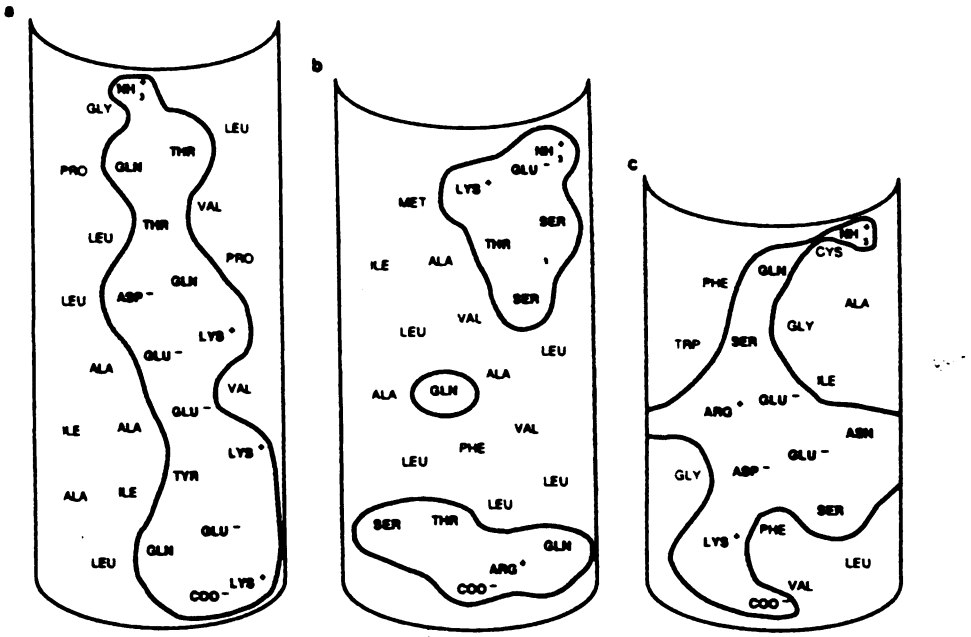

FIGURE 1: Sequences of the MA-β peptide (a), M2-δ (b), and AL peptide (c) are depicted on a helical net representation. The outlined areas correspond to polar amino acids, and the amino and carboxy terminii groups of each peptide. (a) The MA-β peptide sequence corresponds to residues 424–450 of the β-subunit of the *Torpedo californica* AChR, except at the ultimate carboxy-terminal residue, where a glutamate is replaced by a lysine. (b) The M2-δ sequence corresponds to residues 259–281 of the δ-subunit of the *Torpedo californica* AChR. (c) The AL peptide's sequence is not related to the AChR's.

reinserting the pipet in the salt solution. With a success rate of 80–90%, this procedure yielded electrically stable membrane-sealed tips with a resistance of 5–100 GΩ. The MA-β peptide was added to the unstirred bath solution to a final concentration ranging from 0.5 to 50 mg/L; the AL peptide was added to a final concentration ranging from 0.1 to 100 mg/L. Ion channels typically appeared 10–20 min after the introduction of the MA-β peptide into the bath solution. While lower concentrations of MA-β failed to yield ion channels within the 5–6 h duration of the experiment, higher concentrations tended to lyse the membrane seal.

Channel Recordings. A voltage-clamp amplifier (EPC-5, List Electronic) was used to set the transmembrane potential and to measure ionic currents. Ground potential was defined as that of the bath, so the reported potentials represent those of the trans compartment; the cis compartment is defined as the compartment to which peptide was added. The sign convention is that for recording from cell-attached or outside-out membrane patches: current into the pipet is defined as positive and shown as an upward deflection. Current and voltage records were filtered at 1.0 kHz with an 8-pole Butterworth filter and stored on FM recording tape. The tapes were digitized at 100 μs per point for analysis. Because of the time resolution of filtering, only events of duration 1 ms or greater were examined.

Results

MA-β Peptide Forms Very Stable Ion Channels. The 27 amino acid MA-β peptide has the potential to form an amphipathic α-helix, having 4 negatively and 3 positively charged residues on one side of the α-helix (Figure 1a; Table I). The peptide is identical with the MA segment of the β-subunit of *Torpedo californica* AChR (Stroud & Finer-Moore, 1985) except at position 27, where a lysine is substituted for a glutamate. The glutamate at position 27 is not conserved in other AChR subunits and in β-subunits from other species, and is generally replaced by a positively charged amino acid. This residue was altered to compensate for the extra negative charge present on the carboxy terminus of the peptide, and to promote α-helix formation by placing a positive charge at the negative end of the helix dipole.

The MA-β peptide forms very stable ion channels in artificial phospholipid bilayers (Figure 3a). The majority of recordings resulted in multiple, open ion channels (Figure 3c), each of which appeared sequentially. On the basis of three separate recordings showing the presence of a single channel, the open time of the MA-β peptide channel was estimated to be on the order of many seconds to minutes. These three recordings also showed that an opening is eventually followed by closure to a quiescent, fully closed state whose lifetime is many seconds to minutes. This closure is differentiable from flickering-type closings, which occur throughout an opening and result in partial or full closure of the channel for several milliseconds (Figure 3b). The channel remains in these brief, partially or fully closed states 4% of the total open time and in the fully open state 96% of the total open time, indicating that the flickering-type closings are a minor fraction of the peptide channel's activity. Neither the latency of appearance nor the open lifetimes of MA-β ion channels appeared to be dependent on the transmembrane potential.

To determine whether these ion channels resulted uniquely from MA-β peptide's action, channel recordings were carried out for a second peptide, AL, which was synthesized and purified in a manner parallel to that of MA-β. AL peptide's sequence, which is unrelated to the AChR's and eight amino acids shorter than MA-β's, contains five charged residues and possesses amphipathic α-helical periodicity, although less pronounced than MA-β's (Figure 1c, Table I). The AL

Table I Some Ion Channel Forming Peptides

peptide	no of amino acids	α-helical amphipathicity[a]	max power[b]	frequency of max power[c]	conductance class
MA-β	27	7.66	9.40	1/3.4	discrete
$(LSSLLSL)_3$[d]	21	6.43	6.43	1/3.5	discrete
alamethicin[e]	20	3.11	4.39	1/2.8	discrete
M2-β[f]	23	2.21	7.65	1/10.0	continuous
sodium channel peptide[g]	22	2.17	7.68	1/2.8	continuous
AL	19	4.01	6.55	1/3.8	disruptor
$(LSSLLSL)_2$[d]	14	6.43	6.43	1/3.5	disruptor

[a] The Fourier transform with respect to the hydrophobicities of the amino acids in the peptide (Finer-Moore & Stroud, 1984) were calculated according to $I(\nu) = 100[(1/n)\sum_{j=1}^{n} H_j \exp(2\pi ij\nu)]^2$, where $I(\nu)$ is the power spectrum of hydrophobicities, n is the number of amino acids in the peptide, H_j is the hydrophobicity of residue j in kilocalories per mole (Eisenberg et al., 1982), and ν is the frequency. The value reported is the power at a frequency of 1/3.5 residues^{-1}, corresponding to the periodicity of an α-helix. The larger the value, the more marked is the amphipathic α-helical periodicity. [b] The maximum value in the Fourier transform of hydrophobicities, which was calculated for frequencies between 0.0 and 0.5. [c] The frequency at which the maximum value in the Fourier transform occurs, reported in units of residues^{-1}. [d] Lear et al. (1988). [e] The sequence is Ac-XPXAXAQXVXGLXPVXXEQY (Cascio & Wallace, 1988), in which Ac represents an acetyl group, X represents α-aminoisobutyric acid, and Y represents phenylalaninol. For the Fourier-transform analysis, the hydrophobicity of the α-aminoisobutyric acid residues was approximated by the hydrophobicity of glutamic acid, and the hydrophobicity of phenylalaninol was approximated by the hydrophobicity of phenylalanine. [f] Oiki et al. (1988a). [g] The sequence of this peptide is DPWNWLDFTVITFAYVTEFVDL (Oiki et al., 1988b).

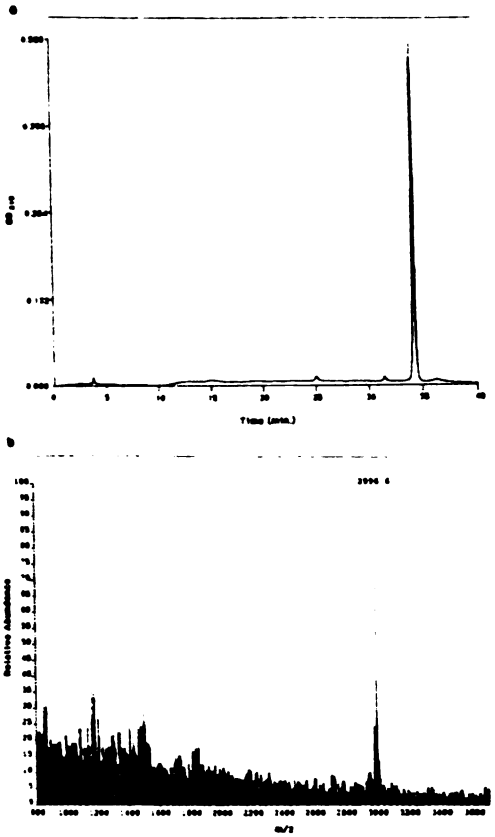

FIGURE 2: (a) Reverse-phase HPLC of purified MA-β. The peptide was applied to a C_{18} column and was eluted with a 0–70% AcN linear gradient containing 0.1% TFA. The gradient reached 70% AcN in 35 min, and the flow rate was 1 mL/min. (b) Liquid secondary ion mass spectrum (LSIMS) of purified MA-β. The single peak present corresponds to MA-β, whose calculated m/z is 2996.7 (for the MH^+ species). The experimentally measured mass is noted above the peak.

peptide did not produce square-waveform transitions in ionic current; instead, it infrequently gave rise to irregular increases in membrane conductance (Figure 3d). The difference between the action of the two peptides suggests that discrete-conductance ion channels, such as those resulting from MA-β, can be distinguished from membrane-disrupting events, such as those caused by AL.

MA Peptide Has Primarily Two Open-Channel Conductance Levels. The MA peptide primarily forms channels of two types, a high-conductance channel of 12.5 pS (±0.2) and a low-conductance channel of 8.6 pS (±0.2) in 500 mM NaCl (Figure 4). For both conductance-type channels, the ionic current is directly proportional to the applied transmembrane voltage and is equal in magnitude at positive and negative transmembrane voltages. The high-conductance type channel is observed more frequently, constituting 69% of all openings, while the low-conductance type constitutes 30% of all openings. Channels of even lower conductance, 4–6 pS in 500 mM NaCl, were observed infrequently, representing 1% of all openings. Both high- and low-conductance channels display similar long-lived openings and flickering-type closings.

To determine whether the high- and low-conductance channels constitute independent states, the magnitude of transitions between conductance levels was analyzed (Figure 5). Both 8.5- and 12.5-pS transitions, corresponding to steps between fully closed and fully open states for the low- and high-conductance channels, respectively, are found. However, the 4.0-pS step which would account for a transition between the low-conductance state and the high-conductance state is absent, indicating that the low- and high-conductance channels are independent and do not interconvert.

Between 140 and 1000 mM NaCl, the conductance of the two channel types increases linearly as a function of salt concentration and does not saturate. In this range, the rate of increase in the conductance of the high-conductance channel is 5.9 pS/M NaCl and of the low-conductance channel 4.9 pS/M. Although the linear relationship accounts for the behavior of the two channel types at concentrations of NaCl greater than 140 mM, it is not valid at lower salt concentrations. Linear extrapolation of the conductance to a salt concentration of zero yields a conductance much greater than the expected value of zero. The extrapolated zero salt concentration is 9.4 pS for the high-conductance-type channel and 6.2 pS for the low-conductance-type channel. Therefore, the relationship of conductance to salt concentration appears to be nonlinear at salt concentrations below 140 mM.

Flickering-Type Closings Are Short-Lived. Flickering-type closings punctuate the long-lived openings of both the low- and high-conductance channels (Figure 3b). Since the duration of flickering-type closings tends to increase with the amplitude of these events (Figure 6), the closings are most likely unresolved by our recording system. The distribution of flicker-

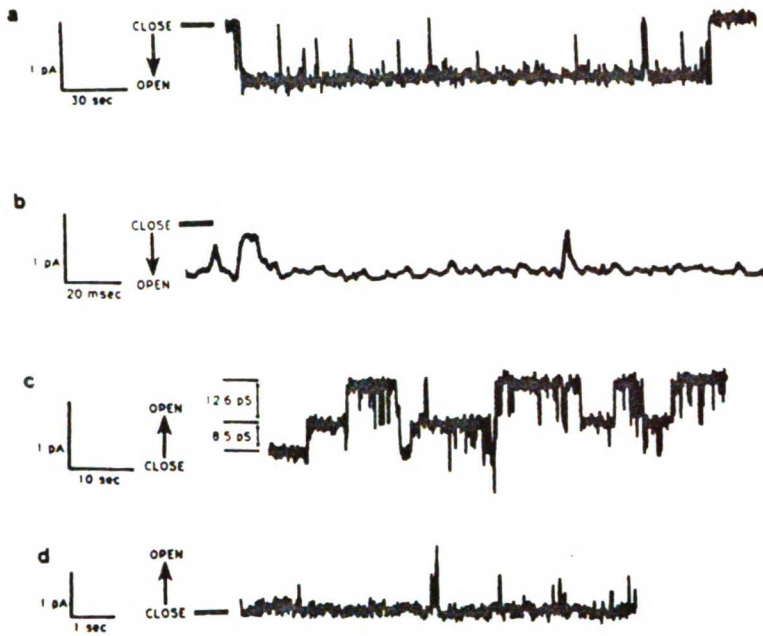

FIGURE 3: (a) Single-channel currents resulting from the MA-β peptide in symmetrical 500 mM NaCl, 1 mM $CaCl_2$, and 10 mM HEPES, pH 7.2, at a holding potential of +94 mV. The downward deflection represents an opening of a low-conductance channel which remains open for approximately 4 min. Flickering-type closings are evident throughout the opening as spiky, upward deflections. The horizontal bar indicates the current level without any channels present in the membrane. For purposes of display, the trace was digitized and plotted at 10 ms/point. (b) Portion of the single-channel current from (a) is shown at a greater time resolution. The horizontal bar indicates the current level of the fully closed state. Four flickering-type closings are evident. For purposes of display, the trace was digitized and plotted at 1 ms/point. (c) Multiple open channels formed by the MA-β peptide in symmetrical 500 mM NaCl, 1 mM $CaCl_2$, and 10 mM HEPES, pH 7.2, at a holding potential of −50 mV. Upward deflections correspond to opening events, and spiky, downward deflections correspond to flickering-type closings. The patch, which contains at least three channels, contains both a high-conductance (12.5 pS) and a low-conductance channel (8.6 pS). The current level without any channels present is not shown. For purposes of display, the trace was digitized and plotted at 5 ms/point. (d) Erratic increases in current caused by the AL peptide in symmetrical 1000 mM NaCl, 1 mM $CaCl_2$, and 10 mM HEPES, pH 7.3, at a holding potential of −124 mV. Upward deflections indicate opening events. The bar indicates the current level without any channels present in the membrane. For purposes of display, the trace was digitized and plotted at 1 ms/point.

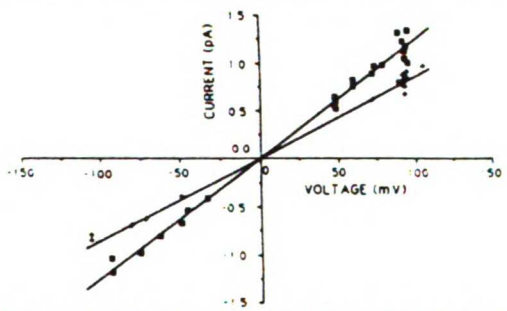

FIGURE 4: Current–voltage relationship of the MA-β peptide recorded in symmetrical 500 mM NaCl, 1 mM $CaCl_2$, and 10 mM HEPES, pH 7.2. (⊟) corresponds to the high-conductance channel, and (+) corresponds to the low-conductance channel. Each point represents an observation of a single open channel, and current amplitudes were determined from amplitude histograms. The plot includes data from nine different membranes.

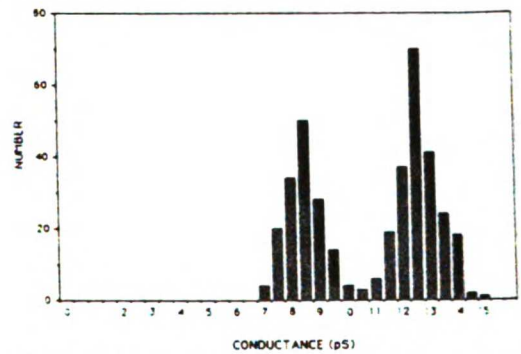

FIGURE 5: Histogram of the magnitude of opening and closing transitions between conductance levels. The step size of transitions was determined from current amplitude histograms. Sixteen membrane patches contributed to this analysis, at potentials ranging from +105 to −105 mV. All recordings were carried out with symmetrical 500 mM NaCl, 1 mM $CaCl_2$, and 10 mM HEPES, pH 7.2.

ing-type closing durations can be fitted by a single exponential with a time constant of 1.4 ms (Figure 7a), which is at the limit of our recording system and probably represents this limit rather than the kinetics of the channel. As indicated by the resolution limit of our recording system, the lifetime of the flickering-type closings appears to be 1 ms or less. The duration that the channel exists in the fully open state uninterrupted by flickering-type closings can be fitted by a single exponential with a much longer time constant of 225 ms (Figure 7b). Therefore, the fully open state is more stable than the flickering-type closed states by a factor of at least 160.

Since the flickering-type closings may have arisen from a blockade of the ion channel caused by Ca^{2+} present throughout these experiments, the concentration of Ca^{2+} was varied from 0 to 50 mM while the NaCl concentration was held constant

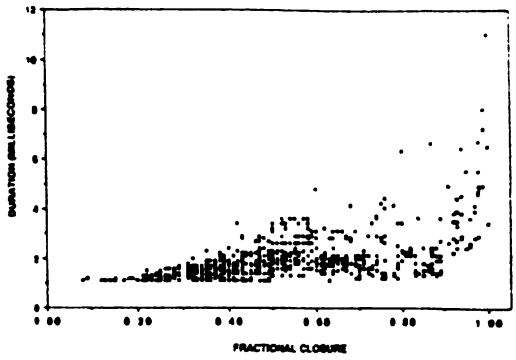

FIGURE 6: Scatter plot of the amplitude of flickering-type closings versus the duration of those events. The amplitude of closing is expressed as a fraction of full closure with 1.0 representing full closure. Flickering-type closing events were identified and analyzed by using the programs C-Clamp and C-Crunch (Indec, Sunnyvale, CA). Only flickering-type closings whose duration was 1 ms or greater and whose amplitude was at least twice the root-mean-square deviation of the full open channel current were analyzed. One low- and two high-conductance channels, which were recorded in symmetrical 500 mM NaCl, 1 mM $CaCl_2$, and 10 mM HEPES, pH 7.2, at voltages between +95 and −85 mV, were used for this analysis.

at 500 mM. The number and frequency of the flickering-type closures were independent of Ca^{2+} concentration (data not shown). When EDTA and EGTA were added to the bath to remove trace amounts of Ca^{2+}, the membrane seal failed to form. Changes in buffer from HEPES to Tris or dimethylglutarate and changes in pH from 7.2 to 4.0 did not alter the number or frequency of partial or full closures (data not shown). These changes in Ca^{2+} concentration, buffer, and pH did not affect the conductance of the two types of channel.

Discussion

A peptide corresponding to the MA segment of the β-subunit of *Torpedo californica* AChR forms discrete-conductance ion channels. The β-subunit's MA segment was selected since it has the most pronounced amphipathic α-helical periodicity of any of the other subunit's MA segments (Finer-Moore & Stroud, 1984). The MA-β channels do not mimic the electrophysiological properties of the native AChR. While the *T. californica* AChR has a conductance of 47 pS in 500 mM NaCl and 0.5 mM $CaCl_2$ (Montal et al., 1986), the MA-β peptide forms two discrete-conductance channels of 8.6 and 12.5 pS in 500 mM NaCl and 1.0 mM $CaCl_2$. In addition, the native AChR is not observed to undergo the flickering-type closings found for MA-β. The most striking difference between the native AChR and MA-β is that the open time for the AChR is a few milliseconds and for MA-β is on the order of minutes. Thus, the ion flux through the MA-β peptide channel is lower than through the native AChR, but the open peptide channel is much more stable than the open native AChR channel.

A 23 amino acid peptide (M2-δ) corresponding to the M2 segment of the δ-subunit of *T. californica* AChR has also been found to form ion channels (Figure 1b, Table I) (Oiki et al., 1988a). We synthesized a peptide (M2-α) corresponding to the M2 segment of the α-subunit of *T. californica* AChR (residues 256–283), but it proved to be insoluble in a variety of solvents and could not be purified or reliably assayed for ion channel formation. M2-α's insolubility may result from the fact that 18 of its 27 amino acids are hydrophobic, while only 13 of the soluble M2-δ peptide's 23 amino acids are hydrophobic. In artificial phospholipid bilayers, the M2-δ peptide forms a continuum of conducting species that range in conductance from 5 to 65 pS; the most frequently observed conducting species has a conductance of 10 pS. Somewhat greater than 10% of all openings have a conductance of 40 pS, which is similar to the conductance of the native AChR. The mean open time of these channles is on the order of milliseconds, within the same range as the native AChR. The continuum of conductance states found for M2-δ contrast with the discrete conductance states found for MA-β.

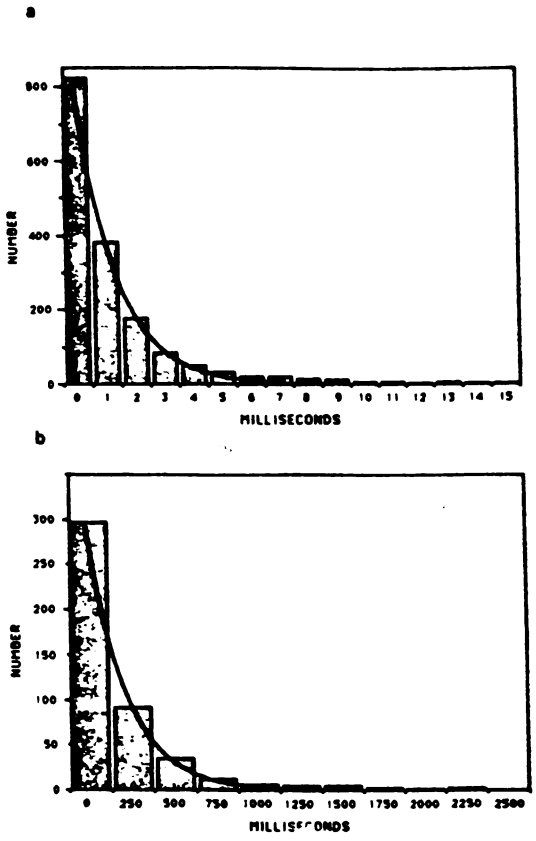

FIGURE 7: (a) Histogram of the duration of flickering-type closings is fitted with a single exponential with a time constant equal to 1.4 ms. Twelve independent channels, which were recorded in symmetrical 500 mM NaCl, 1 mM $CaCl_2$, and 10 mM HEPES, pH 7.2, at voltages between +105 and −105 mV, were used for this analysis. (b) Histogram of the duration that the channel remains in the fully open state uninterrupted by flickering-type closings is fitted with a single exponential with a time constant equal to 225 ms. One low- and two high-conductance channels, which were recorded in symmetrical 500 mM NaCl, 1 mM $CaCl_2$, and 10 mM HEPES, pH 7.2, at voltages between +94 and −85 mV, were used for this analysis.

The M2-δ ion channels are functionally similar to ion channels formed by a 22 amino acid peptide derived from a segment of the voltage-gated sodium channel (Table I) (Oiki et al., 1988b). Like M2-δ peptide, the sodium-channel peptide produces a continuum of conducting species. These range from 5 to 60 pS, and the major species has a conductance of 15–25 pS, which includes the 20-pS conductance of the native voltage-gated sodium channel. However, the sodium channel peptide produces channels which mimic the conductance of the native AChR as frequently as the AChR-derived M2-δ peptide. Thus, neither M2-δ nor the sodium channel peptide exclusively mimics the functional properties of the protein ion

channel from which it is derived.

A peptide composed of a repeat of leucines and serines has also been found to form ion channels in artificial phospholipid bilayers (Lear et al., 1988) (Table I). This 21 amino acid peptide, composed of 3 repeats of the heptamer LSSLLSL, is designed to form an amphipathic α-helix capable of spanning the phospholipid bilayer and is not mimetic of any known native channel. Like the MA-β peptide channel, the leucine-serine repeat peptide forms a discrete-conductance ion channel, having a conductance of 70 pS in 500 mM KCl and an open time in the millisecond range. In contrast to the 21 amino acid triad repeat peptide, a 14-amino acid peptide composed of 2 of the same heptamer repeats does not form ion channels but gives rise to erratic increases in membrane conductance. It is probable that the dyad repeat peptide is not of sufficient length to span the bilayer as an α-helix and therefore acts as a chaotropic agent, as does the AL peptide.

These synthetic peptides are reminiscent of the naturally occurring peptides that insert into membranes and form ion channels, such as alamethicin (Hall et al., 1984) and gramicidin A (Finkelstein & Andersen, 1981). Alamethicin, a 20 amino acid antibiotic which contains the unusual amino acid α-aminoisobutyric acid, forms discrete, voltage-dependent ion channels (Table I). These channels have a number of conductance states in the nanosiemen range and open lifetimes in the millisecond range (Vodyanoy et al., 1982). On the basis of structural and functional studies, the various conductance states of the alamethicin channel are thought to be formed by various aggregates of mostly α-helical monomers (Fox & Richards, 1982; Cascio & Wallace, 1988). The number of alamethicin monomers per channel seems to vary between 6 and 12. Gramicidin A, a 15 amino acid antibiotic, bears less resemblance to the synthetic peptides than alamethicin since it is composed of alternating L- and D-amino acids. Gramicidin A forms discrete ion channels, which have a conductance of approximately 10 pS in 500 mM NaCl and open times in the millisecond to second range (Finkelstein & Andersen, 1981). The gramicidin A channels are not formed by α-helices but instead by two $\beta^{6,3}$-helical monomers arranged amino terminus to amino terminus (Arseniev et al., 1985), a structure not likely to be found in proteins.

By analogy to alamethicin, the MA-β peptide ion channel is most probably formed by a multimeric association of α-helical peptides. The MA-β sequence is predicted to form an α-helix (Finer-Moore & Stroud, 1984) and as such would be 4.0 nm in length and capable of spanning the lipid bilayer. A pentamer of these α-helices would create a channel with a radius of 0.4 nm, a size sufficient to allow the passage of a Na^+ ion with one shell of water, which in total has a radius of 0.32 nm (Stroud & Finer-Moore, 1985). If the channel were indeed formed by multimers, then the two conductance types may reflect a difference in the multimeric state of the peptide. For example, the high-conductance channel may be formed by a hexamer and the low-conductance channel by a pentamer of peptides. The association state of the peptide could not be easily evaluated in our recording system, because only a narrow range of peptide concentrations could be successfully tested for ion channel formation. The long open times of the channel, which range from seconds to minutes, may result from favorable electrostatic interactions among the large number of charges located within the channel's interior. Among the aforementioned peptides capable of forming ion channels, MA-β peptide possesses the greatest number of charged residues: three lysines and four aspartates or glutamates. Closure of the ion channel may result from the exit of the peptide multimers from the membrane, conformational change within the multimers to a nonconducting state, or dissociation of the multimers into nonconducting monomers or oligomers.

Our data suggest that ion channel forming peptides can be grouped into at least three general classes: discrete-conductance channels, such as MA-β, the triad leucine-serine repeat peptide, and alamethicin; continuous-conductance channels, such as M2-δ and the sodium channel peptide; and membrane disruptors, such as AL and the dyad leucine-serine repeat peptide (Table I). The discrete-conductance channels, such as MA-β and the triad leucine-serine repeat peptide, have in common marked amphipathic α-helical periodicities while the two continuous-conductance channels have the weakest amphipathic α-helical periodicities of the peptides examined. Alamethicin, a discrete-conductance channel, has an intermediate amphipathic α-helical periodicity, perhaps because it is not α-helical for its entire length (Fox & Richards, 1982). Like the discrete-conductance channels, the two membrane disruptors possess notable amphipathic α-helical periodicity but appear to be too short to span the membrane as α-helices.

Although peptide ion channels fail to mimic the action of the protein ion channels from which they are derived, they are among the best examples of easily alterable ion channel formers. Along with alamethicin (Menestrina et al., 1986) and gramicidin A (Durkin et al., 1990), they present a tractable system in which to examine the relationship between sequence composition and ion channel properties.

ACKNOWLEDGMENTS

We thank Dr. A. James Hudspeth and Dr. Juan Korenbrot for their assistance and the generous use of their laboratories. We also thank Dr. William M. Roberts and Dr. Fernán Jaramillo for the use of their computer programs, Richard A. Jacobs for technical assistance, and Dr. A. J. Hudspeth, Dr. Michael J. Shuster, Dr. Alexander Kamb, and Stephanie Mel for critical reading of the manuscript.

REFERENCES

Arseniev, A. S., Barsukov, I. L., Bystrov, V. F., Lomize, A. L., & Ovchinnikov, Y. A. (1985) *FEBS Lett. 186*, 168–174.

Cascio, M., & Wallace, B. A. (1988) *Proteins: Struct., Funct., Genet. 4*, 89–98.

Coronado, R., & Latorre, R. (1983) *Biophys. J. 43*, 231–236.

Durkin, J. T., Koeppe, R.E., II, & Andersen, O. S. (1990) *J. Mol. Biol. 211*, 221–234.

Eisenberg, D., Weiss, P., Terwilliger, T., & Wilcox, W. (1982) *Faraday Symp. Chem. Soc. 17*, 109–120.

Finer-Moore, J., & Stroud, R. M. (1984) *Proc. Natl. Acad. Sci. U.S.A. 81*, 155–159.

Finkelstein, A., & Andersen, O. S (1981) *J. Membr. Biol. 59*, 155–171.

Fox, R. O., & Richards, F. M. (1982) *Nature 300*, 325–330.

Giraudat, J., Dennis, M., Heidmann, T., Haumont, P.-Y., Lederer, F., & Changeux, J.-P. (1987) *Biochemistry 26*, 2410–2418.

Grenningloh, G., Rientiz, A., Schmitt, B., Methfessel, C., Zensen, M., Beyreuther, K., Gundelfinger, E. D., & Betz, H. (1987) *Nature 238*, 215–220.

Hall, J. E., Vodyanov, I., Balasubramanian, T. M., & Marshall, G. R. (1984) *Biophys. J. 45*, 233–247.

Hille, B. (1984) *Ionic Channels of Excitable Membranes*, Sinauer Associates, Inc., Sunderland, MA.

Imoto, K., Busch, C., Sakmann, B., Mishina, M., Konno, T., Nakai, J., Bujo, H., Mori, Y., Fukuda, K., & Numa, S. (1988) *Nature 335*, 645–648.

Kagawa, Y., & Racker, E. (1971) *J. Biol. Chem. 246*, 5477–5487.

Kistler, J., Stroud, R. M., Klymkowsky, M. W., Lalancette, R. A., & Fairclough, R. H. (1982) *Biophys. J. 34*, 371–383.

Lear, J. D., Wasserman, Z. R., & DeGrado, W. F. (1988) *Science 240*, 1177–1181.

Leonard, R. J., Labarca, C. G., Charnet, P., Davidson, N., & Lester, H. A. (1988) *Science 242*, 1578–1581.

Menestrina, G., Voges, K.-P., Jung, G., & Boheim, G. (1986) *J. Membr. Biol. 93*, 111–132.

Mitra, A. K., McCarthy, M. P., & Stroud, R. M. (1989) *J. Cell Biol. 109*, 755–774.

Montal, M., Anholt, R., & Labarca, P. (1986) in *Ion Channel Reconstitution* (Miller, C., Ed.) pp 157–204, Plenum Press, New York.

Noda, M., Takahashi, H., Tanabe, T., Mitsuyoshi, T., Kikyotani, S., Furutani, Y., Hirose, T., Takashima, H., Inayama, S., Miyata, T., & Numa, S. (1983) *Nature 302*, 528–532.

Oberthür, W., Muhn, P., Baumann, H., Lottspeich, F., Wittmann-Leibold, B., & Hucho, F. (1986) *EMBO J. 5*, 1815–1819.

Oiki, S., Danho, W., Madison, V., & Montal, M. (1988a) *Proc. Natl. Acad. Sci. U.S.A. 85*, 8703–8707.

Oiki, S., Danho, W., & Montal, M. (1988b) *Proc. Natl. Acad. Sci. U.S.A. 85*, 2393–2397.

Ross, M., Klymkowsky, M. W., Agard, D. A., & Stroud, R. M. (1977) *J. Mol. Biol. 116*, 635–659.

Schofield, P. R., Darlison, M., Fujita, N., Burt, D. R., Stephenson, F. A., Rodriguez, H., Rhee, L. M., Ramachandran, J., Reale, V., Glencorse, T. A., Seeburg, P. H., & Barnard, E. A. (1987) *Nature 328*, 221–227.

Stroud, R. M., & Finer-Moore, J. (1985) *Annu. Rev. Cell Biol. 1*, 317–351.

Suarez-Isla, B. A., Wan, K., Lindstrom, J., & Montal, M. (1983) *Biochemistry 22*, 2319–2323.

Vodyanoy, I., Hall, J. E., Balasubramanian, T. M., & Marshall, G. R. (1982) *Biochim. Biophys. Acta 684*, 53–58.

CHAPTER 2
A CARBOXY-TERMINAL FRAGMENT OF COLICIN Ia FORMS ION CHANNELS

Partho Ghosh, Stephanie F. Mel[#], and Robert M. Stroud[+]

Departments of Biochemistry and Biophysics and Experimental Pathology[#]
University of California, San Francisco
San Francisco, California 94143-0448

[+]Author to whom correspondence should be addressed

Running Title: Ion channel-forming domain of colicin Ia

SUMMARY

A carboxy-terminal, 18 kD fragment of colicin Ia, a bacterial toxin, forms ion channels in artificial phospholipid bilayers. This fragment, which comprises a quarter of the intact 70 kD molecule, is resistant to extensive protease digestion and probably constitutes a structural domain of the protein. The ion channels formed by the 18 kD fragment are functionally heterogeneous, having conductances that range from 15 to 30 pS at positive voltages and from 70 to 250 pS at negative voltages, and open lifetimes that range from at least 25 milliseconds to 5 seconds. In contrast, ion channels formed by whole colicin Ia open only at negative voltages, at which their conductances range from 6 to 30 pS, and their open lifetimes range from 1 second to 3 minutes. Additionally, the open state of the 18 kD fragment channel is characterized by noisy fluctuations in current, while the open state of the whole molecule ion channel is often marked by numerous, stable sub-conductance states. Since the properties of the fragment channel differ substantially from those of the whole molecule channel, we suggest that portions of the molecule outside of the 18 kD fragment are involved in forming the whole molecule ion channel.

INTRODUCTION

Ion channel proteins are significant transducers of signals across membranes. In order to understand the structural basis for

ion channel formation and function, we have studied the bacterial toxin colicin Ia, a member of the ion channel-forming family of colicins. This family includes colicins A, B, E1, Ib, K and N as well (for review see Cramer, et al., 1990; Pattus, et al., 1990). The colicins are plasmid-encoded, soluble proteins of 42 to 70 kD which are synthesized upon stress during the SOS response (Morlon, et al., 1983; Waleh & Johnson, 1985; Mankovich, Hsu & Konisky, 1986; Salles, Weisemann & Weinstock, 1987). These proteins are secreted into the media, bind to an outer membrane receptor of target bacteria, and translocate across the periplasmic space to the inner plasma membrane, where they form lethal, transmembrane ion channels. Colicin ion channels are voltage-gated and relatively non-selective, as determined by recordings from artificial membranes (Schein, Kagan & Finkelstein, 1978; Weaver, et al., 1981; Seta, et al., 1983; Raymond, Slatin & Finkelstein, 1985).

Proteolytic digestion (Carmen Martinez, Lazdunski & Pattus, 1983) and genetic truncation (Baty, et al., 1988; Baty, et al., 1990) of colicin A have identified the carboxy-terminal third of the protein as the ion channel-forming region. Similarly, proteolytic cleavage of colicin E1 has shown that the carboxy-terminal third of colicin E1 is responsible for forming ion channels (Ohno-Iwashita & Imahori, 1982). The functional properties of the ion channel-forming domains of colicins A and E1 are generally similar to those of each respective whole molecule, although some minor differences do exist in voltage-dependence, gating kinetics, and ion selectivities (Carmen Martinez,

et al., 1983; Cleveland, et al., 1983). These functional ion channel-forming regions appear to be equivalent to structural domains. The x-ray crystal structure of the ion channel-forming portion of colicin A reveals that it is a compact bundle of 10 α–helices (Parker, et al., 1989; Parker, et al., 1990), and nuclear magnetic resonance (NMR) shows that the ion channel-forming portion of colicin E1 is structurally similar to the colicin A fragment (Wormald, et al., 1990).

We asked whether a carboxy-terminal portion of the 70 kD protein colicin Ia is also capable of forming ion channels. We report that a tryptic, carboxy-terminal fragment of colicin Ia does form ion channels, but that these channels differ substantially from those formed by intact colicin Ia. These results are discussed in the context of other channel-forming colicins and their channel-forming fragments.

MATERIALS AND METHODS

Probing the structure of colicin Ia with trypsin and V8. Colicin Ia was expressed and purified (Mel & Stroud, 1992) from plasmid pJK5 in *E. coli* strain 294 (Weaver, Redborg & Konisky, 1981). The purified molecule was digested at 37° C with bovine trypsin (Worthington) at a 1:3 trypsin:colicin Ia molar ratio, with colicin Ia at a concentration of 270 μM in 50 mM NaCl, 20 mM citrate buffer, pH 5.2. The reaction was stopped by the addition of leupeptin to a final concentration of 90 μM.

For digestion with *S. aureus* V8 protease (Endoproteinase Glu-C, Boehringer Mannheim), the reaction was carried out at 37° C at a V8:colicin Ia molar ratio of 1:3, with colicin Ia at a concentration of 44 μM in 50 mM phosphate buffer, pH 7.8, and 2.4 M urea. The products of both reactions were examined by SDS-PAGE (Laemmli, 1970).

Purification of fragments. Purified colicin Ia was digested with trypsin as above, except at a lower trypsin:colicin Ia molar ratio of 1:30. The products of the digest were purified by size-exclusion HPLC on two, tandem Biosil TSK 250 columns (each 21.5 mm x 60 cm), which had been equilibrated with 50 mM NaCl, 20 mM citrate buffer, pH 5.2. Three resolved fractions, which eluted at 117, 141, and 160 minutes at a column flow rate of 2 ml/min, were collected and subjected to amino-terminal sequencing and relative molecular weight determination by SDS-PAGE. Only the leading edge of the peak eluting at 160 minutes was collected, since the trailing edge of this peak overlaps with another peak.

Formation of Artificial Phospholipid Bilayers. Artificial phospholipid bilayers were formed on the tip of tight-seal pipets (Coronado & Latorre, 1983; Suarez-Isla, et al., 1983) as described in Ghosh & Stroud (1991) using soybean asolectin (Associated Concentrates) which had been purified (Kagawa & Racker, 1971). This procedure yielded membrane-sealed tips having a resistance of 5-100 GΩ with

a success rate of 80-90%. Colicin Ia and the tryptic fragments were added to the unstirred, 2 ml bath solution containing the membrane-sealed tip to a final concentration ranging from 0.03-145 μg/ml. Ion channels typically appeared after 10 to 20 minutes after the introduction of the protein into the bath solution.

Channel Recordings. A voltage-clamp amplifier (EPC-5, List Electronics) was used to set the transmembrane potential and to measure ionic currents. Ground potential was defined as that of the bath, so the reported potentials represent those of the trans compartment; the cis compartment is defined as the compartment to which protein was added. The sign convention is such that current into the pipet (from cis to trans) is defined as positive and shown as an upward deflection. Ion channels were recorded with cis and trans compartments containing symmetrical solutions of either 500 mM or 1000 mM NaCl and 1 mM $CaCl_2$, 10 mM dimethylglutarate, pH 4.0. Current and voltage records were recorded on chart paper with a Gould 220 brush recorder resulting in 40 Hz filtering of data.

RESULTS

The carboxy-terminal quarter of colicin Ia is resistant to proteolysis. Tryptic digestion of colicin Ia yields two major products, a protease-resistant fragment of M_r 18.0 ± 0.4 kD (n=7) and a less resistant fragment of M_r 34.1 ± 1.0 kD (n=6) (Figure 1a). The 34 kD fragment disappears after two hours of digestion at 37° C at a trypsin:colicin Ia

molar ratio of 1:3, while the 18 kD fragment persists for at least 4 hours. The amino-terminus of the 34 kD fragment is residue 7, having been cleaved at arginine 6, as determined by amino-terminal sequencing. Its carboxy-terminus probably extends to arginine 313, as determined from its relative molecular weight and the specificity of trypsin for lysines and arginines. However, given the errors in determining the relative molecular weight, it is possible that either arginine 299 or arginine 313 could be the carboxy-terminus of the 34 kD fragment. The 18 kD fragment begins at aspartate 451 and likely extends to the carboxy terminus of the intact molecule, isoleucine 626. However, the fragment may be shorter, having been cleaved at either arginine 619 or lysine 622. Even with the uncertainty in the carboxy-terminii of these fragments, it is clear that the 34 kD fragment constitutes the amino-terminal half of colicin Ia while the 18 kD fragment constitutes the carboxy-terminal quarter.

The structural stability of the carboxy-terminal quarter is confirmed by a more rigorous digest in the presence of 2.4 M urea using V8 (Figure 1b). After 5 minutes of digestion at 37° C at a V8:colicin Ia molar ratio of 1:3, only a 20.4 ± 0.2 kD M_r (n=4) fragment as well as several lower molecular weight fragments remain. The 20 kD fragment, whose amino-terminus is residue 446 and whose carboxy-terminus probably extends to the carboxy-terminus of intact colicin Ia, remains uncleaved for at least 2 hours. The 20 kD V8 fragment is longer by 6 residues at its amino-terminal

end and probably by 7 residues at its carboxy-terminal end than the 18 kD tryptic fragment. Therefore, as determined from tryptic and V8 proteolysis, the carboxy-terminal quarter of colicin Ia appears to constitute a stable, structural domain.

The 18 kD colicin Ia fragment forms ion channels. In order to determine whether the carboxy-terminal quarter of colicin Ia possesses ion channel-forming activity, the 18 kD tryptic fragment was purified by size-exclusion HPLC (Figures 2a and b) and assayed for ion channel-forming activity by single channel recording techniques. The addition of the 18 kD, carboxy-terminal fragment to artificial phospholipid bilayers results in the appearance of ion channels which are characterized by noisy open states (Figures 3a, b, and c). The current flowing through these channels is not stable, but instead fluctuates at a rate greater than the resolution limit of our recording system, 25 milliseconds. These fluctuations can be as great as the open channel current. Furthermore, ion channels formed by the 18 kD fragment are functionally heterogeneous such that a range of conductance rather than a single conductance value is observed. The range of conductances is dependent on the polarity of the voltage. At positive voltages, the conductance ranges from 15 to 30 pS (Figure 3a) in 500 mM NaCl, pH 4.0, as determined from 17 different membranes and 153 channels. However, at negative voltages, the conductance is higher, ranging from 70 to 250 pS (Figures 3b and c), as determined from 21 different membranes and

204 channels. Infrequently, channels of much smaller conductance, approximately 10 pS, are observed at negative voltages (Figure 3c). The open lifetimes of these fragment channels range from at least 25 milliseconds to approximately 700 milliseconds at positive voltages and from 25 milliseconds to approximately 5 seconds at negative voltages (Figures 3a, b, and c).

To determine whether these ion channels result uniquely from the action of the 18 kD fragment and to determine whether other portions of the molecule are capable of forming ion channels, the amino-terminal 34 kD fragment was also assayed for ion channel-forming activity. This fragment was generated by the same tryptic digest yielding the 18 kD fragment and purified identically to the 18 kD fragment (Figures 2a and b). In contrast to the 18 kD fragment, the 34 kD fragment does not form detectable ion channels, those greater than 1 pS, within the 6 hour duration of an experiment (data not shown). Therefore, it appears that only the carboxy-terminal quarter of colicin Ia is required to form ion channels.

Channels formed by the 18 kD fragment are dissimilar to channels formed by whole colicin Ia. Ion channels formed by the 18 kD fragment, however, differ considerably from those formed by whole colicin Ia. As determined from 10 different membranes and 28 different channels, the conductance of whole colicin Ia at negative voltages in 500 mM NaCl, pH 4.0 ranges from 6 to 30 pS (Figures 4a and b), approximately 10-fold less than that for the 18 kD fragment

at negative voltages. A single conductance value is difficult to assign to these channels, since a variety of conductance states are found (Figures 4a and b). Some of these are sub-conductance states of the same channel rather than separate conductance states of a number of channels. This was determined from the observation that closure to the zero current level often occurs from a state other than the lowest conductance state. One channel was observed to vary among several states and then to close from the second largest sub-conductance state (Figure 4b); the lifetime of each of these sub-conductance states is on the order of seconds. The open lifetime of the whole colicin Ia channel ranges from 1 second to 3 minutes, contrasting with the much shorter lifetimes of the 18 kD fragment.

In further contrast, the opening of the colicin Ia channel but not of the 18 kD fragment is dependent on voltage. Membranes in which several whole colicin Ia channels are active show that the channel conducts current only at negative voltages (Figure 5a and 5b). Whole colicin Ia channels close at positive voltages but reversibly re-open at negative voltages. In contrast, the 18 kD fragment conducts ions at either positive or negative voltages (Figures 3a, b, and c), although its conductance is diminished at positive voltages.

DISCUSSION

We have found from proteolytic digestion and single channel recordings that the carboxy-terminus of colicin Ia is capable of

forming ion channels, as are the carboxy-terminal portions of colicins A and E1. However, in contrast to colicins A and E1, the ion channel properties of this colicin Ia carboxy-terminal fragment differ greatly from those of the whole molecule.

The ion channel properties found in this and other studies (Bullock & Cohen, 1986; Nogueira & Varanda, 1988) for whole colicin Ia are generally similar to those found for whole A and E1. In comparison to the range of 6 to 30 pS found for colicin Ia in 500 mM NaCl, pH 4.0, colicin A has a conductance of 13 pS in 1 M KCl, pH 6.2 (Carmen Martinez, et al., 1983), and colicin E1 has a conductance of 21 pS in 1 M NaCl, pH 6 (Bullock, et al., 1983). The recordings in this study were carried out at pH 4 since colicins insert preferentially into membranes at pH values ≤ 4 (Pattus, et al., 1983; Davidson, et al., 1984; Mel & Stroud, 1992). The finding that the whole colicin Ia channel can adopt a number of sub-conductance states with lifetimes in the range of seconds has also been noted for colicin E1 (Raymond, et al., 1986). In general, channels formed by whole colicins A, E1, and Ia have similar conductances, a dependence on negative voltage for opening, and open lifetimes in the range of seconds to minutes.

However, unlike colicins A and E1, colicin Ia's channel-forming fragment has ion channel properties which differ markedly from those of the whole molecule. The single channel conductance of the 18 kD fragment is 10-fold greater at negative voltages than that of the whole molecule, and the open lifetimes are much shorter. Therefore, although the flux of ions through the fragment channel is

greater than through the whole molecule channel, the open fragment channel is much less stable than the open whole molecule channel. In parallel with the reduced stability, the large fluctuations of current through the fragment channel may indicate of greater conformational flexibility in the open state of the fragment channel than of the whole molecule channel (Sigworth, 1985). The gating of the fragment ion channel also differs from that of the whole molecule. While the whole molecule ion channel closes at positive voltages, the 18 kD fragment ion channel continues to conduct current, although the magnitude of its conductance is diminished by at least 2-fold.

It is possible that these differences arise from an alteration in the mechanism of ion channel formation. While whole colicin Ia probably forms channels as a monomer by analogy to colicin E1 (Bruggemann & Kayalar, 1986; Peterson & Cramer, 1987; Slatin, 1988; Levinthal, et al., 1991), it is possible that the 18 kD fragment forms channels as an oligomer. Peptides with sequences capable of forming amphipathic α–helices have been shown to form ion channels most likely as oligomers (Lear, Wasserman & DeGrado, 1988; Oiki, et al., 1988; Oiki, Danho & Montal, 1988; Ghosh & Stroud, 1991), and the 18 kD fragment contains such sequences. Our experiments, however, do not allow us to distinguish the association state of the channel, since addition of too few molecules leads to no channel formation within the 6 hours of an experiment and addition of too many molecules leads to lysis of the membrane.

A more likely possibility is that the differences between the 18 kD fragment and the whole molecule channel indicate that portions of the protein outside this ion channel-forming fragment are involved in forming the whole molecule channel. Studies with colicin A truncation mutants (Frenette, et al., 1989) and colicin A-E1 fusion proteins (Benedetti, et al., 1991) indicate that the colicin A channel-forming domain interacts with the middle third of the protein, the receptor-binding domain. Analogously, portions amino-terminal to the colicin Ia 18 kD fragment may interact with this channel-forming domain and may be necessary to form the whole colicin Ia channel. These portions may confer stability to the open ion channel, perhaps by anchoring it in the membrane, and may also be involved in some aspects of the gating of the whole molecule.

Structurally, the 18 kD fragment of colicin Ia probably constitutes a stable core of the protein as seen from its protease resistance, and is probably similar to the compact, structural domain of the colicin A channel-forming fragment (Parker, et al., 1989; Parker, et al., 1990). The colicin A fragment is composed of 10 α-helices arranged in a three-layer bundle, with helices 8 and 9 forming the hydrophobic core. The channel-forming fragment of colicin E1 as determined by NMR is consistent with this structure, except that helices 9 and 10 are slightly rearranged relative to colicin A (Wormald, et al., 1990). The channel-forming colicin Ia fragment is slightly shorter than the colicin A fragment but about the same size as the colicin E1 fragment. By sequence comparison, the amino-

terminus of the 18 kD fragment corresponds to helix 1 of the colicin A fragment without the first 7 residues; its likely carboxy-terminus at residue 626 corresponds to the colicin A fragment without its last 3 residues. Therefore, the colicin Ia fragment is probably structurally similar to both the colicin A and E1 fragments, although confirmation of this awaits the x-ray crystal structure of colicin Ia (see Chapter 3).

The marked difference in functional properties between the 18 kD fragment and the colicin A and E1 fragments then likely arise from small, specific differences in structure arising from differences in sequence. However, it is also possible that although the soluble structures of these fragments may be similar, the membrane-inserted structures could vary considerably from each other. The channel-forming domains of the colicins share little sequence identity, about 25-30%, but have in common sequences that are capable of forming amphipathic α–helices and a hydrophobic stretch of about 35 amino acids. Since their secondary and tertiary structure are likely to be similar but their ion channel properties differ, the channel-forming domains of these colicins provide a useful way to identify sequence elements responsible for specific ion channel properties.

ACKNOWLEDGEMENTS

This work was supported by National Institutes of Health Grant GM24485 (to R.M.S.). P.G. is the recipient of an NSF Predoctoral

Fellowship and was partially supported by a grant from the Lucille P. Markey Charitable Trust. S.F.M. is the recipient of a Claypole Fellowship and a U.C.S.F. Mentorship Award. We thank Jordan Konisky for plasmid pJK5, A. J. Hudspeth for advice and the use of his lab for carrying out channel recordings, and Larry Miercke for assistance in HPLC purification. We also thank Juan Korenbrot, Michael Shuster, and Michael Wiener for comments on the manuscript.

REFERENCES

Baty, D., Frenette, M., Lloubes, R., Geli, V., Howard, S. P., Pattus, F., Lazdunski, C. 1988. Functional domains of colicin A. *Mol. Microbiol.* **2**:807-811

Baty, D., Lakey, J., Pattus, F., Lazdunski, C. 1990. A 136-amino-acid-residue COOH-terminal fragment of colicin A is endowed with ionophoric activity. *Eur. J. Biochem.* **189**:409-413

Benedetti, H., Frenette, M., Baty, D., Knibiehler, M., Pattus, F., Lazdunski, C. 1991. Individual domains of colicins confer specificity in colicin uptake, in pore-properties and in immunity requirement. *J. Mol. Biol.* **217**:429-439

Bruggemann, E. P., Kayalar, C. 1986. Determination of the molecularity of the colicin E1 channel by stopped-flow ion flux kinetics. *Proc. Nat. Acad. Sci. USA* **83**:4273-4276

Bullock, J. O., Cohen, F. S. 1986. Octylglucoside promotes incorporation of channels into neutral planar phospholipid bilayers. Studies with colicin Ia. *Biochim. Biophys. Acta* **856**:101-108

Bullock, J. O., Cohen, F. S., Dankert, J. R., Cramer, W. A. 1983. Comparison of the macroscopic and single channel conductance

properties of colicin E1 and its COOH-terminal tryptic peptide. *J. Biol. Chem.* **258:**9908-9912

Carmen Martinez, M., Lazdunski, C., Pattus, F. 1983. Isolation, molecular and functional properties of the C-terminal domain of colicin A. *EMBO J.* **2:**1501-1507

Cleveland, M. v., Slatin, S., Finkelstein, A., Levinthal, C. 1983. Structure-function relationships for a voltage-dependent ion channel: Properties of COOH-terminal fragments of colicin E1. *Proc. Nat. Acad. Sci. USA* **80:**3706-3710

Coronado, R., Latorre, R. 1983. Phospholipid bilayers made from monolayers on patch-clamp pipettes. *Biophys. J.* **43:**231-236

Cramer, W. A., Cohen, F. S., Merrill, A. R., Song, H. Y. 1990. Structure and dynamics of the colicin E1 channel. *Mol. Microbiol.* **4:**519-526

Davidson, V. L., Cramer, W. A., Bishop, L. J., Brunden, K. R. 1984. Dependence of the activity of colicin E1 in artificial membrane vesicles on pH, membrane potential, and vesicle size. *J. Biol. Chem.* **259:**594-600

Frenette, M., Knibiehler, M., Baty, D., Geli, V., Pattus, F., Verger, R., Lazdunski, C. 1989. Interaction of colicin A domains with

phospholipid monolayers and liposomes: Relevance to the mechanism of action. *Biochemistry* **28**:2509-2514

Ghosh, P., Stroud, R. M. 1991. Ion channels formed by a highly charged peptide. *Biochemistry* **30**:3551-3557

Kagawa, Y., Racker, E. 1971. Partial resolution of the enzymes catalyzing oxidative phosphorylation. *J. Biol. Chem.* **246**:5477-5487

Laemmli, U. K. 1970. Cleavage of structural proteins during the assembly of the head of bacteriophage T4. *Nature* **227**:680-685

Lear, J. D., Wasserman, Z. R., DeGrado, W. F. 1988. Synthetic amphiphilic peptide models for protein ion channels. *Science* **240**:1177-1181

Levinthal, F., Todd, A. P., Hubbell, W. L., Levinthal, C. 1991. A single tryptic fragment of colicin E1 can form an ion channel: Stoichiometry confirms kinetics. *Proteins* **11**:254-262

Mankovich, J. A., Hsu, C., Konisky, J. 1986. DNA and amino acid sequence analysis of structural and immunity genes of colicins Ia and Ib. *J. Bacteriol.* **168**:228-236

Mel, S., Stroud, R. M. 1992. Colicin Ia inserts into negatively charged membranes at low pH with a tertiary but little secondary structural change. *Biochemistry*, submitted

Morlon, J., Lloubes, R., Varenne, S., Chartier, M., Lazdunski, C. 1983. Complete nucleotide sequence of the structural gene for colicin A, a gene translated at non-uniform rate. *J. Mol. Biol.* **170**:271-285

Nogueira, R. A., Varanda, W. A. 1988. Gating properties of channels formed by colicin Ia in planar lipid bilayer membranes. *J. Membr. Biol.* **105**:143-153

Ohno-Iwashita, Y., Imahori, K. 1982. Assignment of the functional loci in the colicin E1 molecule by characterization of its proteolytic fragments. *J. Biol. Chem.* **257**:6446-6451

Oiki, S., Danho, W., Madison, V., Montal, M. 1988. M2, a candidate for the structure lining the ionic channel of the nicotinic cholinergic receptor. *Proc. Nat. Acad. Sci. USA* **85**:8703-8707

Oiki, S., Danho, W., Montal, M. 1988. Channel protein engineering: Synthetic 22-mer peptide from the primary structure of the voltage-sensitive sodium channel forms ionic channels in lipid bilayers. *Proc. Nat. Acad. Sci. USA* **85**:2393-2397

Parker, M. W., Pattus, F., Tucker, A. D., Tsernoglou, D. 1989. Structure of the membrane-pore-forming fragment of colicin A. *Nature* **337**:93-96

Parker, M. W., Tucker, A. D., Tsernoglou, D., Pattus, F. 1990. Insights into membrane insertion based on studies of colicins. *Trends Biochem. Sci.* **15**:126-129

Pattus, F., Martinez, M. C., Dargent, B., Cavard, D., Verger, R., Lazdunski, C. 1983. Interaction of colicin A with phospholipid monolayers and liposomes. *Biochemistry* **22**:5698-5703

Pattus, F., Massotte, D., Wilmsen, H. U., Lakey, J., Tsernoglou, D., Tucker, A., Parker, M. W. 1990. Colicins: Prokaryotic killer-pores. *Experientia* **46**:180-192

Peterson, A. A., Cramer, W. 1987. Voltage-dependent, monomeric channel activity of colicin E1 in artificial membrane vesicles. *J. Membr. Biol.* **99**:197-204

Raymond, L., Slatin, S. L., Finkelstein, A. 1985. Channels formed by colicin E1 in planar lipid bilayers are large and exhibit pH-dependent ion selectivity. *J. Membr. Biol.* **84**:173-181

Raymond, L., Slatin, S. L., Finkelstein, A., Liu, Q., Levinthal, C. 1986. Gating of a voltage-dependent channel (colicin E1) in planar lipid bilayers: translocation of regions outside the channel-forming domain. *J. Membr. Biol.* **92:**255-268

Salles, B., Weisemann, J. M., Weinstock, G. M. 1987. Temporal control of colicin E1 induction. *J. Bacteriol.* **169:**5028-5034

Schein, S. J., Kagan, B. L., Finkelstein, A. 1978. Colicin K acts by forming voltage-dependent channels in phospholipid bilayer membranes. *Nature* **276:**159-163

Seta, P., d'Epenoux, B., Sandeaux, R., Pattus, F., Lazdunski, C., Gavach, C. 1983. Voltage and time dependence of the conductance of planar lipid bilayers doped with colicin A. *Biochem. Biophys. Res. Commun.* **113:**765-771

Sigworth, F. J. 1985. Open channel noise. *Biophys. J.* **47:**709-720

Slatin, S. L. 1988. Colicin E1 in planar lipid bilayers. *Int. J. Biochem.* **20:**737-744

Suarez-Isla, B. A., Wan, K., Lindstrom, J., Montal, M. 1983. Single-channel recordings from purified acetylcholine receptors

reconstituted in bilayers formed at the tip of patch pipets. *Biochemistry* **22:**2319-2323

Waleh, N. S., Johnson, P. H. 1985. Structural and functional organization of the colicin E1 operon. *Proc. Nat. Acad. Sci. USA* **82:**8389-8393

Weaver, C. A., Kagan, B. L., Finkelstein, A., Konisky, J. 1981. Mode of action of colicin Ib. *Biochim. Biophys. Acta* **645:**137-142

Weaver, C. A., Redborg, H., Konisky, J. 1981. Plasmid-determined immunity of *Escherichia coli* K-12 to colicin Ia Is mediated by a plasmid-encoded membrane protein. *J. Bacteriol.* **148:**817-828

Wormald, M. R., Merrill, A. R., Cramer, W. A., Williams, R. J. P. 1990. Solution NMR studies of colicin E1 C-terminal thermolytic peptide: Structural comparison with colicin A and the effects of pH changes. *Eur. J. Biochem.* **191:**155-161

FIGURE LEGENDS

Figure 1. Proteolytic digestion of colicin Ia. (a) 14% SDS-PAGE of tryptic digest of colicin Ia. Colicin Ia was digested with trypsin at a trypsin:colicin Ia molar ratio of 1:3 with colicin at 270 μM at 37° C, and time points were collected as indicated on the figure. The 18 kD colicin Ia fragment, whose amino-terminus is residue 451, persists for 4 hours, while the 34 kD fragment, whose amino-terminus is residue 7, persists for 1 hour. The band at 28 kD corresponds to trypsin. (b) 16% SDS-PAGE of V8 digest of colicin Ia in 2.4 M urea. Colicin Ia was digested with V8 at a V8:colicin Ia molar ratio of 1:3 with colicin Ia at 44 μM at 37° C, and time points were collected as indicated on the figure. A 20 kD fragment, whose amino-terminus is residue 446, and several lower molecular weight fragments persist through 2 hours of digestion.

Figure 2. Tryptic digestion and purification of 34 and 18 kD fragments. (a) Size exclusion HPLC of tryptic digest of colicin Ia. The extent of the fractions collected are indicated by shading. Digestion conditions were as in the legend to Figure 1a except that the trypsin:colicin Ia molar ratio was 1:30. The digest was stopped at 4 hours, and the products were applied to two, tandem Biosil TSK 250 columns at a flow rate of 2 ml/min. The peaks eluting are: Peak 1, colicin Ia at 117 minutes; Peak 2, 34 kD fragment at 141 minutes;

and Peak 3, 18 kD fragment at 160 minutes. (b) 16% SDS-PAGE of peak fractions from size exclusion HPLC. Lane 1 contains Peak 1, 117 minutes; lane 2 contains Peak 2, 141 minutes; and lane 3 contains Peak 3, 160 minutes.

Figure 3. 18 kD fragment ion channels. The three traces are from three different membranes. (a) Single channel currents resulting from the 18 kD fragment in symmetrical 500 mM NaCl, 1 mM $CaCl_2$, 10 mM dimethylglutarate, pH 4.0, at a holding potential of +78 mV. The horizontal bar represents the closed state of the channel, and the downward deflections indicate opening of the channel. The conductances of these channels range from 15 to 30 pS and their open times range from 25 to 400 milliseconds. (b) Single channel currents resulting from the 18 kD fragment in the same conditions as in 4a, except that the holding potential is -55 mV. The conductance of these channels is approximately 100 pS and their open times range from approximately 200 milliseconds to 4 seconds. Large fluctuations in current flowing through the open channel are evident. (c) Single channel currents resulting from the 18 kD fragment in the same conditions as in 4a, except that the holding potential is -45 mV. The channels displayed range between approximately 60 pS and 180 pS, although smaller channels of 10 pS are evident.

Figure 4. Whole colicin Ia channels. The two traces are from two different membranes. (a) Single channel currents resulting from

whole colicin Ia in symmetrical 500 mM NaCl, 1 mM $CaCl_2$, 10 mM dimethylglutarate, pH 4.0, at a holding potential of -93 mV. The current was filtered at 10 Hz with an 8-pole Butterworth filter resulting in the low current noise level in this trace. The horizontal bar represents the closed state of the channel, and upward deflections represent channel openings. At the beginning of the record, the closure of a previously open channel is followed by the opening of another channel or the same channel to a sub-conductance state. Various conductance states are evident with the lowest conductance state being 11 pS. (b) Single channel currents resulting from whole colicin Ia in the same conditions as the legend to Figure 4a, except that the holding potential is -80 mV. A previously open channel transits through various sub-conductance states and finally closes from the second largest sub-conductance state, which is 25 pS.

Figure 5. Whole colicin Ia opens only at negative voltages. The two traces are from the same membrane. (a) Single channel currents resulting from whole colicin Ia in symmetrical 1 M NaCl, 1 mM $CaCl_2$, 10 mM dimethylglutarate, pH 4.0. The voltage was ramped between +75 mV and -80 mV. About 5 to 20 channels are open, resulting in a peak total conductance of 140 pS at -80 mV. Upward deflections at negative voltages, which represent channel openings, are evident. The current at positive voltages is saturated, and therefore an off-set to the amplifier was applied in (b), shown at the arrow. Here,

current at positive voltages is no longer saturated, although current at negative voltages is partially saturated. This record shows that no channel activity is found at positive voltages while upward deflections, indicative of channel openings, are still found at negative voltages.

FIGURE 1a

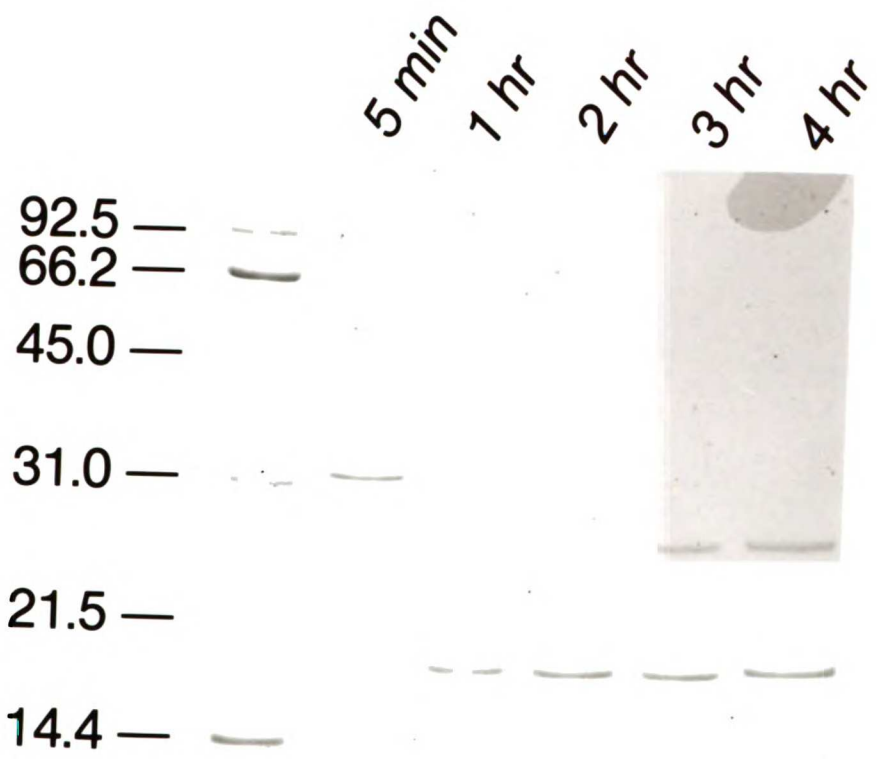

FIGURE 1b

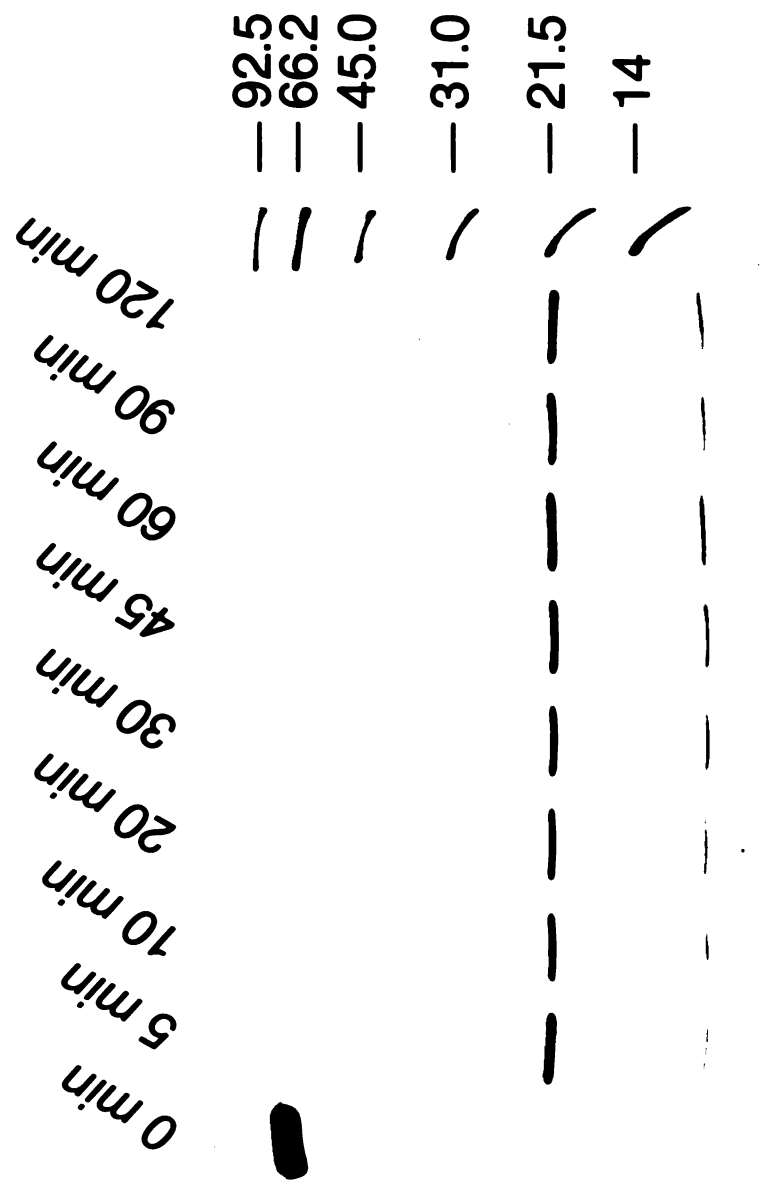
92.5
66.2
45.0
31.0
21.5
14
0 min
5 min
10 min
20 min
30 min
45 min
60 min
90 min
120 min

FIGURE 2a

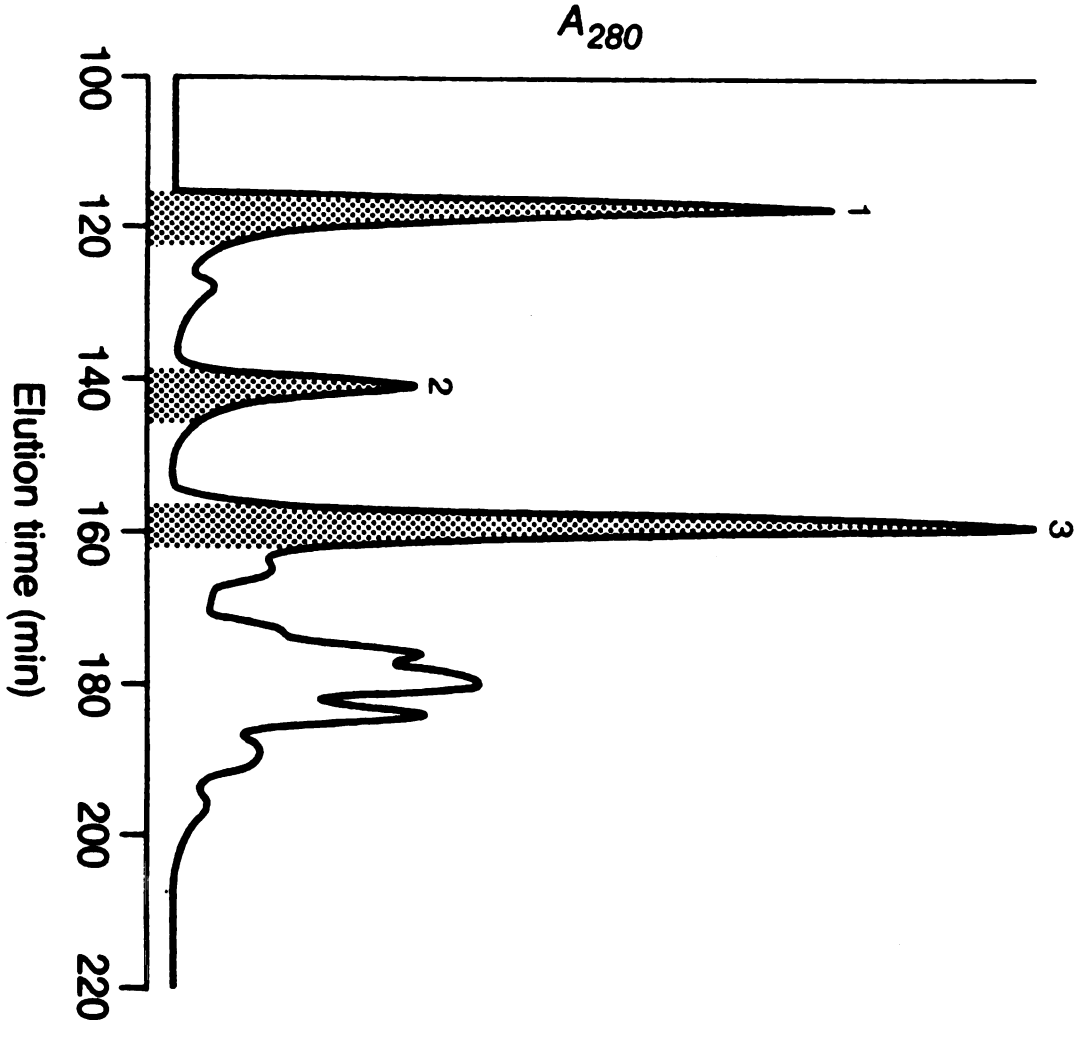

FIGURE 2b

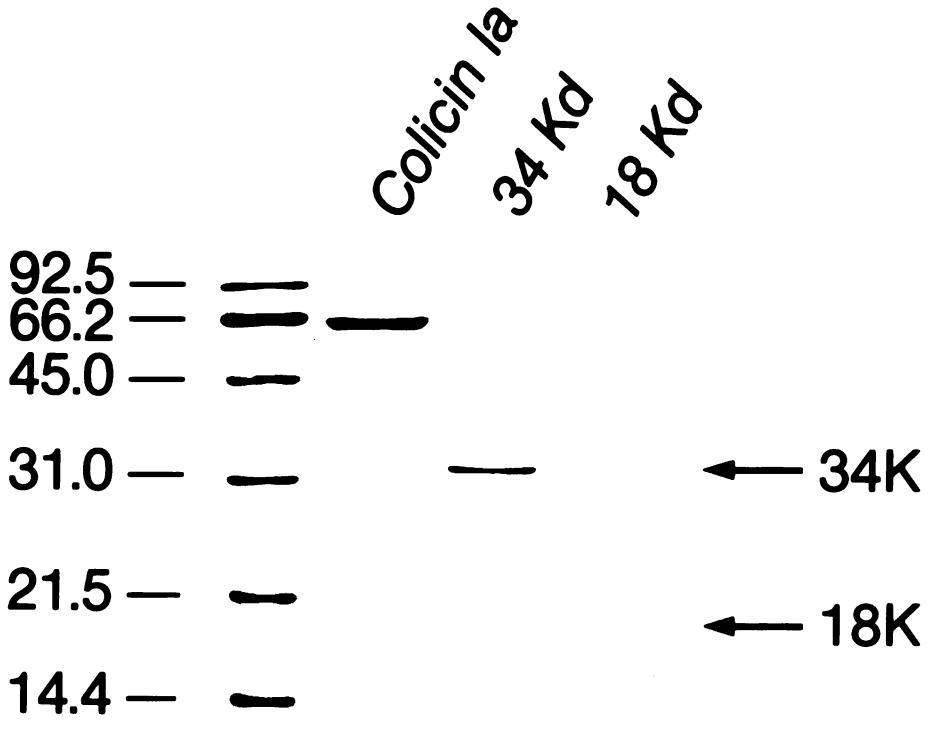

FIGURES 3a, b , and c

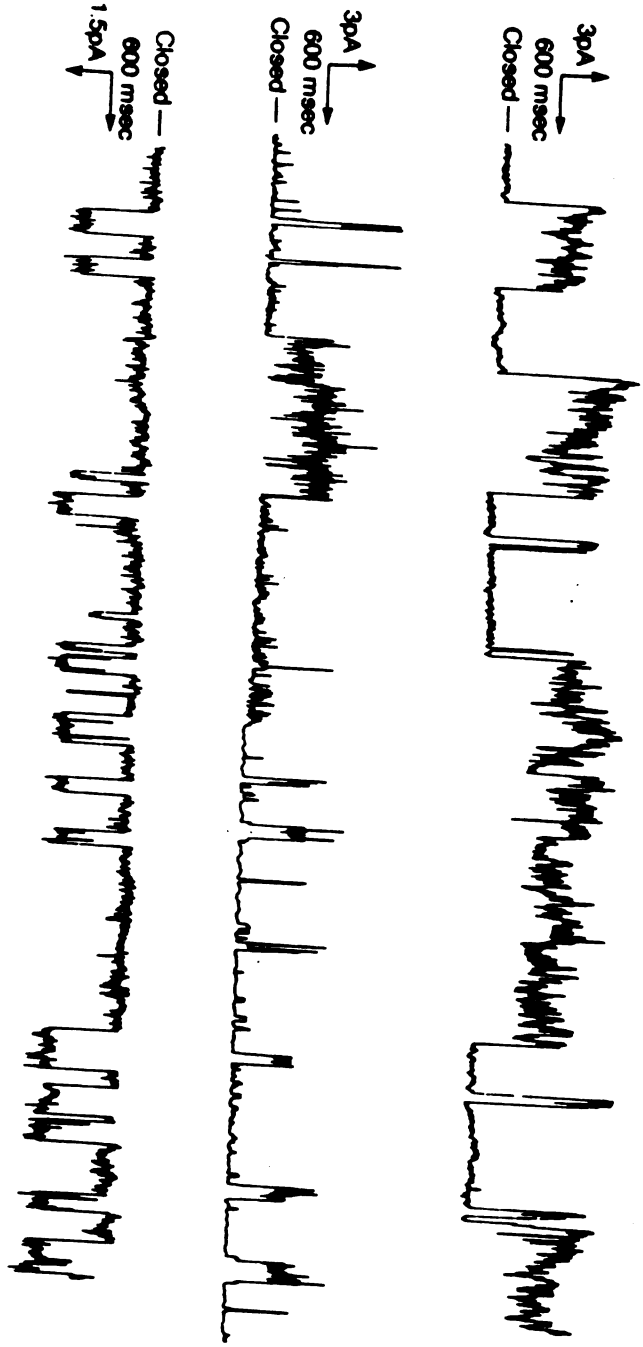

FIGURES 4a and b

FIGURES 5a and b

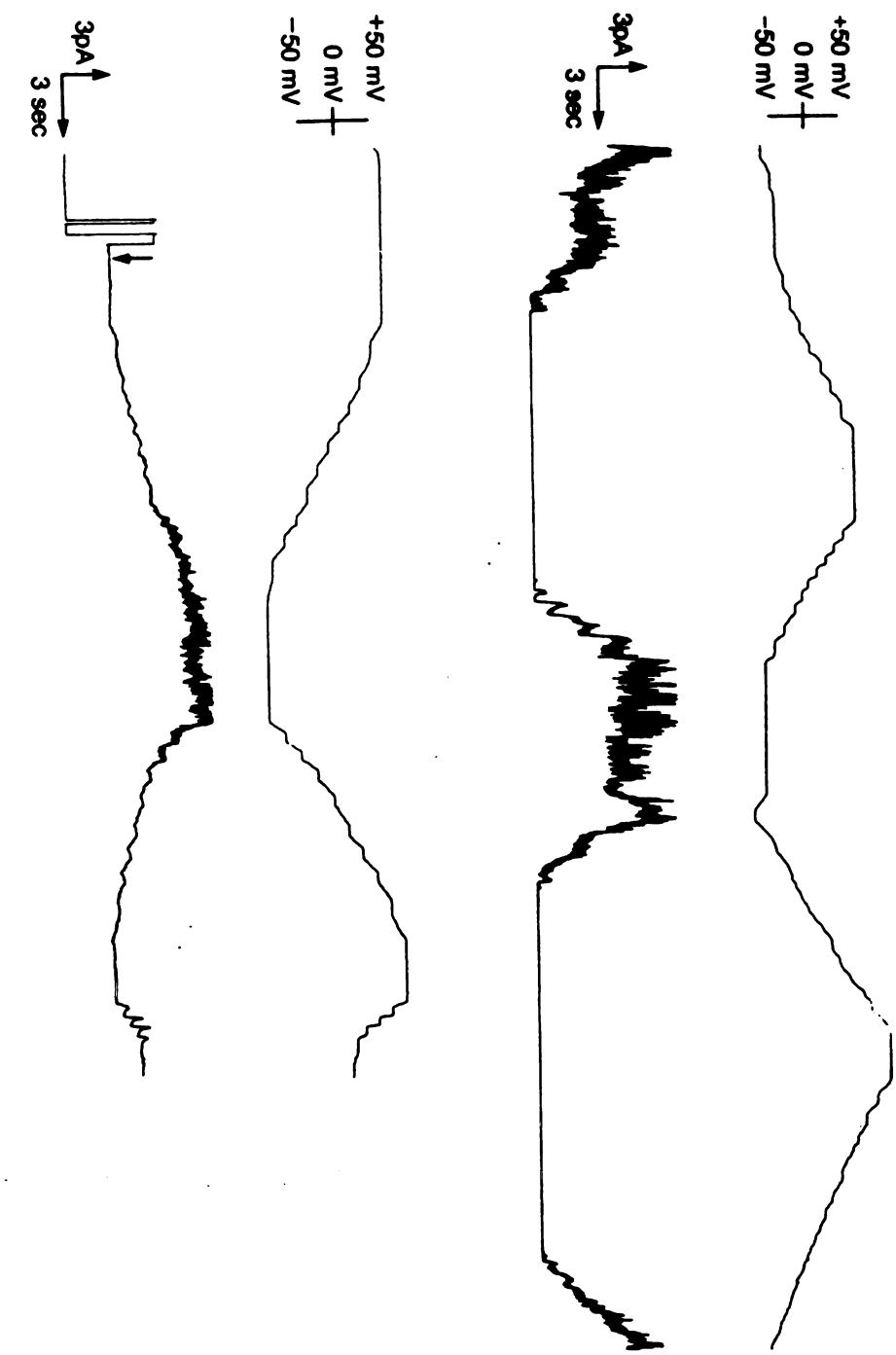

Chapter 3

THE STRUCTURE OF COLICIN Ia

Abstract

The 3.4 Å x-ray crystal structure of the ion channel-forming toxin colicin Ia has been solved by multiple isomorphous replacement (MIR) techniques, using five heavy atom derivatives. Four of these are derivatives of the wild-type molecule, while one is a mercurial derivative of a serine to cysteine (S171C) site-directed mutant. The molecule packs in the unit cell such that large solvent channels run throughout the crystal. The molecule itself is "Y"-shaped, with the two arms of the "Y" formed by α-helical bundles and the stalk of the "Y" formed by five α-helices which are ~70 Å long. One of the arms appears to correspond to the ion channel-forming domain of colicin A (Parker, et al., 1989; Parker, et al., 1990) and is likely to be the ion channel-forming domain of colicin Ia (see Chapter 2). The other arm of the "Y" contains S171C and therefore likely corresponds to the end of the translocation domain or the beginning of the receptor-binding domain. The molecule is modelled as 28 α-helical fragments containing 482 residues. Recently collected data to 2.8 Å will likely result in the assignment of sequence to this poly-alanine model.

Introduction

The channel-forming colicins, a family of bacteriocins which includes colicins A, B, E1, K, Ia, Ib, and N, can exist as either soluble or as transmembrane proteins. The colicins are bacterial, plasmid-

encoded, cytoplasmic proteins that are synthesized and released from the cell during the SOS response (Morlon, et al., 1983; Waleh & Johnson, 1985; Mankovich, et al., 1986; Salles, et al., 1987). They bind to an outer membrane receptor of target bacteria and translocate across the periplasmic space to the inner plasma membrane, where they form lethal, transmembrane ion channels. Colicin ion channels are voltage-gated and relatively non-selective (Schein, et al., 1978).

In order to understand the mechanism of insertion into membranes and subsequent formation of ion channels, the soluble form of colicin Ia has been crystallized and its x-ray structure has been solved to 3.4 Å by multiple isomorphous replacement (MIR) techniques. A total of five derivatives were used for phasing, 4 of wild-type colicin Ia and 1 of a site-directed serine to cysteine mutant (S171C). Higher resolution data to 2.8 Å from flash-frozen crystals have been collected, and phases for these data were calculated based on the 3.4 Å map and structure. In this chapter methods and results of diffraction data collection and processing, site-directed mutagenesis, and phasing are presented.

Crystallization of colicin Ia

Crystals of colicin Ia were grown in 2-3 days by vapor diffusion at 25° C from purified protein (Mel, 1992), which was expressed from plasmid pJK5 in *E. coli* 294 (JK365) (Weaver, et al., 1981). Typically, 6 µl of 2-3 mg/ml purified protein (in 50 mM NaCl,

20 mM citrate buffer, pH 5.2) were added to 4 µl of precipitant solution (1.06-1.10 M $(NH_4)_2SO_4$, 200 mM NaCl, 20 mM citrate buffer, pH 5.2) on a silanated cover slip, which was inverted and placed over a well (Linbro 24 well tissue culture plate) containing 1 ml of precipitant solution. The cover slip was sealed to the well using vacuum grease. Although most crystallization drops yielded aggregates, 10% of drops yield usable plate-like crystals, whose typical dimensions are 1 x 0.3 x 0.05 mm (Figure 1).

Space group

Crystals of colicin Ia belong to the centered, orthorhombic space group $C222_1$ (Choe, 1987), with unit cell dimensions a = 66.0 Å, b = 176.2 Å, c = 290.2 Å, and $\alpha = \beta = \gamma = 90°$. The asymmetric unit contains a monomer of colicin Ia, and the crystal contains 79% solvent, as determined by quantitating the amount of protein in a crystal whose volume had been measured (Choe, 1987).

Crystal Preparation

Crystals, which were mounted in 1 mm glass capillaries (Glas, Germany) with their longest axis (c*) parallel to the capillary axis, were left somewhat wet, since removing all of the solution surrounding the crystal results in cracking.

Data Collection

Colicin Ia crystals are extremely sensitive to radiation, diffracting to no more than 6 Å using a rotating-anode source of x-rays (Phillips, 1985). Therefore, data sets were collected to 3.4 Å using the intense x-rays of synchrotron sources by the oscillation method (Enraf-Nonius camera) (Arndt, et al., 1973; Arndt & Wonacott, 1977; Winkler, et al., 1979; Harrison, et al., 1985). However, even 1 or 2 exposures at the synchrotron of approximately 1 minute each results in severe radiation damage, evidenced by loss of diffraction beyond 4-5 Å. Thus, for data collection, each exposure was taken from a fresh portion of the crystal. That is, after each exposure, the crystal was translated along the oscillation axis of the camera by the size of the beam, typically collimated to 0.2-0.3 mm. Since 3° oscillations were typically taken for the native data and since 90° of unique data are required for $C222_1$, at least 30 exposures and 6 crystals were necessary. For derivative data (see below, Heavy Atom data collection), each oscillation comprised 4°, and therefore fewer exposures and fewer crystals were necessary.

In order to collect non-overlapping portions of reciprocal space from successive crystals, the orientation of each crystal was determined from a 1-2° oscillation recorded on Polaroid film and the rotation axis (ϕ) was adjusted based on the determined orientation. To randomly sample the missing cone of data along the rotation axis, c* was purposefully left misaligned along ϕ. Since orientations determined from the Polaroid are approximations, usually more than 90° of data were collected to ensure completion of the data set.

Native data on film

A native data set was collected on CEA Reflex 25 film (Morimoto & Uyeda, 1963; Arndt, et al., 1977) using packs consisting of 3 films at LURE-DCI (λ=1.42 Å and 1.35 Å)[1] (Fourme & Kahn, 1985) and at the Stanford Synchrotron Radiation Laboratory (SSRL) (λ=1.54 Å). Each exposure at LURE constituted 3° of oscillation and at SSRL constituted 4° of oscillation. When data were collected at the short 1.08 Å wavelength, individual films in the pack were separated by 5 pieces of aluminum foil in order to provide sufficient attenuation. Films were developed by standard means: 3 minutes in developer, 30 seconds in stop bath (4% CH_3COOH), and 5 minutes in fixer solution, with 10 to 20 minutes of washing in H_2O, followed by drying with heated air.

Native data on storage phosphor plates

Native data were also collected on storage phosphor plates (Sonoda, et al., 1983; Miyahara, et al., 1986; Whitting, et al., 1988) once these were installed at the Cornell High Energy Synchrotron Source (CHESS) and at SSRL. At CHESS, data were collected at stations A1 (λ=1.565 Å) and F1 (λ=0.91 Å) on Kodak plates and scanned at a 100 μm raster with a gain setting of 3x or 10x using a Kodak scanner. At SSRL, data were collected at station 7-1 (λ=1.08 Å) on MAR plates and scanned at a 150 μm raster with the MAR scanner.

---

[1] C. Wolberger, personal communication.

Film Scanning and non-linearity correction

Films were scanned at a 50 μm raster with a PDS Microdensitometer (Perkin-Elmer) (Wooster, 1964; Arndt, et al., 1968; Elder, 1985), which outputs data on a 12-bit scale (0 to 4096) in CCP4 (1979) map format.

A film non-linearity correction was experimentally determined from intensities recorded on CEA Reflex 25 film for varying exposure times (Figure 2). For this determination, the direct beam from CuKα x-rays generated by a Rigaku rotating-anode source was attenuated with copper shims and recorded on CEA Reflex 25 film. The film was placed in a cassette that was mounted with an x- and y-translation device and therefore could be translated in directions orthogonal to the beam. Exposures were taken on different portions of the same film for varying amounts of time, some of which purposefully saturated the film. The film was scanned and a film non-linearity correction was determined with a cubic polynomial, least-squares fit using LINEAR[2].

Data Processing and Reduction

Data recorded on film and Kodak phosphor plate images were indexed and integrated using a version of DENZO[3] which was modified to accept CCP4 map files and 12-bit data. Data in Kodak

---

[2]E. Westbrook, personal communication.
[3]Z. Otwinowski, personal communication.

and MAR image plate format were converted to CCP4 format, with KODAK_TO_IMAGE (PG)[4] and MAR_TO_IMAGE (PG) respectively, for compatibility with the modified version of DENZO and for graphical display using PRISM (Chen, et al., 1990). DENZO was further modified, with the help of Hans Chen, such that predicted and observed diffraction data could be displayed on the Parallax 1280 graphics system (Chen, et al., 1990). For MAR image plate data, a version of DENZO[5] which accepts MAR format and refines MAR radial and angular offsets was used. In order to index and integrate data with DENZO, an initial orientation matrix was determined by hand and improved by interactive graphics and refinement. A typical refinement protocol is shown in Figure 3.

In order to correct for polarization of the synchrotron beam (Azaroff, 1955; Kahn, et al., 1982), the polarizations experimentally determined for LURE and CHESS (horizontally polarized 90.3% and 67.0% respectively) were used in DENZO. Since the polarization of the beam at SSRL has not been measured, it was set in DENZO to 98% horizontal polarization, as was estimated by finding the minimum in R_{symm}[6] as a function of polarization (Figure 4a). A similar analysis with LURE data indicated that the experimentally determined LURE polarization lies within a broad minimum of the R_{symm} (Figure 4b).

---

[4]"PG" indicates that the program was written by the author of this thesis.

[5]P. Phizackerley, personal communication.

[6]$R_{symm} = \frac{\sum_h \sum_i |I_{h,i} - I_h|}{\sum_h \sum_i I_{h,i}}$, where I_h is the mean intensity for a reflection and $I_{h,i}$ are the individual observations of that reflection.

Once indexed and integrated, data were scaled and reduced. For data from film packs, individual films were first scaled (Matthews, et al., 1972) and averaged using PATCH2[7], a modified version of PROTIN (CCP4), in which the Lorentz and polarization corrections have been disabled since DENZO itself applies these corrections. Scale factors between films in film packs were approximately 2-3; with the shorter 1.08 Å wavelength and with aluminum foil attenuation, the scale factor was approximately 4. Reflections that were found on B and C films but not found on the A film because of slight differences in refined orientation parameters were eliminated using EXCLUDE (PG). Diffraction data from scaled film packs or individual image plates were then scaled using ROTAVATA/AGROVATA (CCP4) (Fox & Holmes, 1966).

Throughout, profile-fit (Rossmann, et al., 1979) instead of summed intensities were used. Using summation rather than profile-fitting leads to 2-3% higher R_{symm}'s. After scaling, data were post-refined (Winkler, et al., 1979) using POSTREF (CCP4), which resulted in adjustment of the mosaicity from an initial 0.4° set in DENZO to 0.6-0.8°. For cryocrystal data (see below, Cryocrystallography), the mosaicity was initially set to 0.2° and refined to 0.25-0.35°. After post-refinement, data were scaled once more with ROTAVATA/AGROVATA and then truncated by the method of French and Wilson (French & Wilson, 1978) with TRUNCATE (CCP4).

---

[7]Jenkins, personal communication.

Native data sets

Native film data (Table I) were collected from a total of 11 crystals, 6 at LURE and 5 at SSRL, resulting in 40 3° oscillations. Data were initially collected at LURE[8] but constituted only half of the unique data; data constituting the missing half were later collected at SSRL. Since some of these films have high backgrounds, weak, middle to high resolution reflections (3.4-5 Å) from these films were not included in the data set. Furthermore, stringent rejection criteria were applied for reflections having multiple observations: for reflections with at least 3 observations, those observations greater than 2σ from the mean intensity were continually rejected, until 90% of the initial observations had been rejected or at least 2 observations remained (SDFMON=2, LFLAG2=0, LFLAGN=3, LFLAGP=90 in ROTAVATA/AGROVATA). This resulted in 14% of observations being excluded. Reflections that were greater than 90% partial after post-refinement were scaled and included in the data set. The processed data seta is 3-fold redundant and has an R_{symm} of 12.7% for 12,375 reflections. The unit cell parameters for the native film data refined to a=66.00 ±0.17 Å, b=176.23 ± 0.30 Å, c=290.20 ±0.57 Å.

Native image plate data (Table II) were collected from a total of 10 crystals at CHESS and comprised 47 3° oscillations. The rejection criteria used for image plate data were less stringent than

---

[8]C. Wolberger, personal communication.

those for film data: for reflections with at least 3 observations, those observations greater than 3σ from the mean intensity were continually rejected, until 50% of the initial observations had been rejected or at least 2 observations remained (SDFMON=3, LFLAG2=0, LFLAGN=3, LFLAGP=50 in ROTAVATA/AGROVATA). This resulted in rejection of 2% of observations. Only full reflections were reduced, since scaling post-refined, partial reflections (partialities ≥ 70-90%) increased the R_{symm} by approximately 1-3% and resulted in only 100-200 additional, unique reflections. The data set is 4-fold redundant and has an R_{symm} of 12.7% for 22,777 reflections. The unit cell parameters for the image plate data refined to a=66.02 ± 0.29 Å, b=176.23 ±0.77 Å, c=290.39 ± 0.53 Å, very similar to the film data.

For comparison, if the less stringent rejection criteria applied to image plate data are applied to the film data and if reflections are not excluded based on resolution, then only 1% of observations are rejected and the R_{symm} rises to 30% for 24,261 reflections for the film data (Table III); the redundancy also increases to 4-fold. As for image plate data, only full reflections were processed for this comparison. As the high R_{symm} shows, the film data are poorly measured in comparison to the image plate data, probably resulting from the high background level on film caused by chemical fog.

Cryocrystal data to 2.8 Å (see below, Cryocrystallography; Table IV) were collected on MAR image plates from 1 crystal and constituted 45 3° oscillations. These data were processed identically

to the Kodak image plate data, resulting in rejection of 1% of observations. The data set is 4-fold redundant and has an R_{symm} of 7.7% for 34,076 reflections. The unit cell parameters for these data refined to a=65.42 ±0.07 Å, b=175.09 ± 0.49 Å, c=285.51 ±0.37 Å. The major difference in unit cell dimensions between room temperature and flash-frozen data is in the c axis, which shrinks by 1.6%.

Cryocrystallography

In order to reduce the effects of radiation damage, crystals were frozen to ~100 K prior to data collection. In the first attempt at freezing, crystals were placed on small, glass micro-spatulas and plunged into liquid C_2H_6 and then into liquid N_2 (Hope, 1988; Hope, et al., 1989), and placed in a stream of N_2 gas cooled by a boil-off system. This method usually requires placing the crystal in a drop of oil, but this proved to be impossible for colicin Ia crystals, since they failed to enter the drop and curved away from the oil surface. In ~20 attempts at the synchrotron, frozen crystals of colicin Ia were found to be disordered; lattice lines were superimposed at random angles, as if the crystal had frozen in a number of mosaic blocks. Diffraction from ice was also readily apparent. One attempt in the laboratory resulted in frozen crystals with no apparent disorder, but diffraction did not extend beyond 6 Å[9].

---

[9]C. Wolberger and T. Earnest, personal communication.

A second attempt was made using glycerol to protect against ice formation and a small, wire loop containing a thin film of liquid to mount the crystal (Teng, 1990). Crystals were first soaked in 30:70 v/v glycerol in crystal stabilizing buffer (1.1 M $(NH_4)_2SO_4$, 0.2 M NaCl, 0.02 M citrate buffer, pH 5.2) for 10-15 minutes. The loop, made of 100 mm diameter nichrome wire, was approximately 2 mm in diameter and was used to gather the crystal from the glycerol soak. The drop, which then held the crystal in the loop, was thinned to a film by aspiration, and within 10 seconds of thinning the crystal was flash-frozen in a stream of N_2 gas cooled to ~100 K using a flow-through system. This method proved to be successful and diffraction data from frozen crystals were collected to 2.8 Å at SSRL station 7-1 (λ=1.08 Å) on MAR image plates. Diffraction appeared to extend beyond 2.8 Å, but the image plate could not be placed closer to the crystal to record higher orders because of the resulting loss in resolution along c*. Using a rotating-anode instead of a synchrotron source of x-rays and R-axis image plates, diffraction from a flash-frozen crystal appears to extend to at least 3.0 Å.

Since orientations in which the loop impinges on the direct or diffracted beam cannot be collected without systematic error, data sets collected by this method are missing a small portion of unique data. Since the colicin Ia crystals collected by this method were oriented in the loop with a* orthogonal to the loop axis, all the cryocrystal sets have a common, overlapping missing cone of data.

Three native cryo-data sets were collected to 2.8 Å from flash-frozen crystals. One of the native data sets was collected from a single, strongly diffracting crystal, and the other two were collected from a second, less strongly diffracting crystal. The unit cell dimensions of all three agree within experimental error, and they have R_{scale}[10]'s of 10-14%. The data set from the strongly diffracting crystal has the lowest R_{symm}, 7.7%; merging it prior to reduction with the other native cryo-data sets increases the R_{symm} to 12.5% (to 2.8 Å) and adds only 829 unique reflections. Thus, the data from the strongly diffracting crystal were used exclusively as the native, cryocrystal set (Table IV).

Wilson Plots

The Wilson B-factor (Wilson, 1949) for both native film and image plate data is 76 $Å^2$ (Figure 5), as determined from a Wilson plot using data between 5.0 and 3.4 Å (calculated with WILSONPLOT[11]). It is 55 $Å^2$ for the cryocrystal, using data between 3.4 and 2.95 Å (Figure 5). The unusually high Wilson B-factor for this flash-frozen crystal indicates the high amount of spatial and lattice disorder inherent in these crystals.

Wilson plots were also used to place data on an absolute scale, whose accuracy was checked by simulation of heavy atom binding.

---

[10] $R_{scale} = \frac{\sum |F_1 - F_2|}{\sum F_1}$, where F_1 is the amplitude for one data set and F_2 is the amplitude for a second data set.

[11] E. Fauman, personal communication.

Native amplitudes, which were placed on an absolute scale, were assigned random phases using RANDPHASE (PG); they were added vectorially to structure factors calculated with GENSFC (CCP4) for a single atom with a given number of electrons (e.g., 80). The simulated, derivative amplitudes (F_{ph}'s) were scaled to the observed, native amplitudes (F_p's) using local scaling (Matthews & Czerwinski, 1975) and the differences between the two (R_{der}[12]) were checked for agreement with the predicted value (Crick & Magdoff, 1956).

Ab initio phasing

During the process of obtaining experimental phases, two different methods of *ab initio* phasing methods were also investigated.

First, since colicin Ia was found to be highly α-helical (66%) (Mel & Stroud, 1992), origin-removed self-Patterson maps (Stout & Jensen, 1989) were computed to determine the direction of α-helical axes. Peaks at 5 and 10 Å were identified but were not well-resolved from noise. Because of the lack of confidence in these peaks, phasing on a small number of oriented α-helices was not pursued. Inspection of the structure (see below, Description of Structure) shows that the α-helical axes in colicin Ia adopt a number

---

[12] $R_{der} = \frac{\sum |F_p - F_{ph}|}{\sum F_p}$, where F_p is the native amplitude and F_{ph} is the derivative amplitude.

of different directions, indicating that this method would have been unlikely to yield useful phases.

Second, a Monte Carlo approach to phasing low resolution reflections (Subbiah, 1991), in which point atoms are moved at random as a correlation coefficient between observed and calculated amplitudes is followed, was attempted using SUBBIAH5[13]. This method resulted in correct solutions in 10% of runs, as determined by comparison against electron micrographic images of the crystal (Choe, 1987). If a condensation requirement was not imposed, the method failed to yield correct solutions, possibly because extremely low resolution reflections (<20 Å) are missing from the data set[14]. This phasing method was not pursued, since tests showed that it correctly phased only the first several orders[15].

Heavy-atom Data

Phases for colicin Ia were determined experimentally by standard multiple, isomorphous derivatization methods (Green, et al., 1954; Blundell & Johnson, 1976; Petsko, 1985).

Heavy atoms solutions were prepared as 100 mM or saturated stock solutions in H_2O, except for non-polar heavy atom compounds (for example, C_2H_5HgCl) which were dissolved in ethanol or isopropanol. Crystals were soaked for 30 hours to 3 weeks in a well (Linbro Tissue Culture 24 well plate 1.7 X 1.6 cm) containing 1 ml of

---

[13]C. Bystroff, personal communication.
[14]Subbiah, personal communication.
[15]C. Bystroff, personal communication.

stabilizing buffer (1.1 M $(NH_4)_2SO_4$, 200 mM NaCl, and 20 mM citrate buffer, pH 5.2) and the appropriate concentration of heavy atom (Tables V, VI). Several soaks were also carried out in unbuffered solutions (Table VI), since citrate often chelates heavy atoms (Blundell & Johnson, 1976). Furthermore, 1.1 M $(NH_4)_2SO_4$ was replaced by 1.1 M Na_2SO_4 in certain soaks (Table VI) because of the susceptibility of certain metals (Class b) to $(NH_4)_2SO_4$ (Blundell & Johnson, 1976).

Heavy atom soak conditions were initially assayed to 6 Å using focused (Phillips & Rayment, 1985) CuKαx-rays produced from a rotating-anode Rigaku generator. Data were collected on a Siemens area detector (Durbin, et al., 1986) with a frame size of 0.25° and a time per frame of 15 minutes. These data could not be processed using XENGEN (Howard & al, 1987), probably because of inaccurate spot profiles calculated from weakly diffracting colicin Ia. Indicative of the processing problem, XENGEN assigns an intensity to sigma (I/σ) ratio of 3 to reflections that are systematically absent. The program BUDDHA (Blum, et al., 1987), in which masks for spot calculation are defined by the user, was used instead and eliminated the processing problem. Since colicin Ia crystals are highly mosaic (0.6-0.8°), the large mask size was used in BUDDHA.

A total of 27 conditions were assayed, and a total of 23 data sets were collected (Table V). In order to minimize systematic data collection differences, several native data sets were also collected on

the Siemens area detector for comparison with the derivative data. Several possible derivatives were identified by large differences between native and locally scaled, derivative amplitudes (R_{der}), including 0.5 mM TlK_3Cl_6 and 0.1 mM Nb_6Cl_{14}, conditions which both proved useful for forming isomorphous derivatives (see below, Phasing of colicin Ia). Other promising derivatives were 1 and 10 mM $PtCl_4$, 1% saturated K_2PtI_6 and K_2PtBr_6, 0.1 mM terpyridine Pt(II) Cl, and 10 mM Na_3IrCl_6. Two of these conditions, 0.1 mM Nb_6Cl_{14} and10 mM Na_3IrCl_6, produced colored crystals, indicative of heavy atom binding.

Rationale for mutagenesis

Due to the lack of initial success in finding suitable isomorphous derivatives (see below, Phasing of colicin Ia), 10 serine to cysteine mutants were created by site-directed mutagenesis for subsequent mercurial derivatization, a method which had proved successful in several cases (Hatfull, et al., 1989; Stock, et al., 1989; Tucker, et al., 1989; Nagai, et al., 1990). The wild-type sequence of colicin Ia contains no cysteines, and as expected, mercurial derivatization of wild-type colicin Ia results in low R_{der}'s and does not result in identifiable binding sites (Table VI).

Ten different serines distributed throughout the sequence were targetted for mutagenesis. Serine was chosen because it is isosteric to cysteine, and particular sites for mutagenesis were identified based on the finding that partially buried cysteines result in the

most useful derivatives (Dao-Pin, et al., 1987). Serines that are bracketed by a charged residue and a non-polar residue, and thus likely to be partially buried, were identified for mutagenesis. Furthermore, the x-ray structure of a fragment of colicin A (Parker, et al., 1989; Parker, et al., 1992) was used to identify by sequence comparison (BESTFIT, UWGCG) serines in colicin Ia that are likely to be partially buried. Colicin A is a channel-forming colicin that is 24% identical to colicin Ia, and the solved colicin A fragment is equivalent to the carboxy-terminal quarter of colicin Ia. For the amino-terminal three-quarters of the molecule, for which a homologous structure does not exist, secondary structure prediction (Garnier, et al., 1978; Finer-Moore & Stroud, 1984) was used to identify serines that were likely to be involved in secondary structures other than coil or turn, since these are often disordered.

Serines 68, 171, 219, 263, 392, 462, 522, 526, 547, and 615 were targetted for substitution. Serines 68, 171, 219, 263, and 392 were identified by secondary structure prediction, and all except 68 are flanked by one hydrophobic and one charged amino acid. In the amino-terminal 100 residues, only serines 14 and 64 are flanked by a hydrophobic and a charged residue, but both are predicted to lie in coil regions. Although serine 68 is flanked by 2 charged groups, it is predicted to be part of an α-helix and was therefore chosen instead of either serine 14 or 64 for substitution. Serines 462, 522, 526, 547, and 615 were identified by sequence and structure comparison with colicin A, and all except 547 are flanked by one hydrophobic and one

charged amino acid. However, if the sequence comparison is accurate and if the two structures are similar, then serine 547 should also be partially buried.

Cloning of Eco RI-Bam HI fragment into pBR322

In order to create the site-directed mutants, a 2.7 kb Eco RI-Bam HI fragment encoding colicin Ia, its immunity protein, and their regulatory elements was amplified from pJK5 using the polymerase chain reaction (PCR) (Saiki, et al., 1988). The Eco RI site was created at nucleotide 711 (using the numbering scheme of (Mankovich, et al., 1986)) of plasmid pJK5, and the Bam HI site was created at nucleotide 3347. The primer used for the creation of the Eco RI site is referred to hereafter as IaEco, and the primer used for the creation of the Bam HI site as IaBam (Table VII). These primers were synthesized by phosphoramidite chemistry at the Biomolecular Resource Center (BRC, UCSF) and were used unpurified.

PCR conditions which confer high fidelity to *Thermus aquaticus* DNA polymerase (Eckert & Kunkel, 1990) were used to generate the 2.7 kb fragment. Since both "high-fidelity" and standard PCR conditions as described in (Kamb, et al., 1989) were used, they are detailed together below.

For the standard PCR reaction, 1 µl of 10 mg/ml DNA template, 1 µl each of two different primers (1 mg/ml), 10 µl of 10x PCR buffer, 10 µl of 8 mM dNTP's (2mM dATP, 2mM dGTP, 2 mM dCTP, 2mM dTTP), 1 µl of 5 units/µl of *Thermus aquaticus* DNA

polymerase (AmpliTaq) (Perkin-Elmer/Cetus), and H_2O to yield a final volume of 100 µl were incubated in a thermocycler (Perkin-Elmer) for 20-25 cycles: 94° C for 1 minute, 50° C for 1 minute, and 72° for 18 minutes. A drop of mineral oil was placed on top of the reaction mixture prior to cycling. The 10x PCR buffer is: 100 mM Tris·HCl, pH 8.3, 500 mM KCl, 20 mM $MgCl_2$, 0.1% gelatin (Pharmacia). For the "high-fidelity" reaction, the same reaction conditions as above were used, except that the final concentration of dNTP's was 4 mM and the 10x buffer was 200 mM Tris·HCl, pH 7.3 at 70° C, 500 mM KCl, and 40 mM $MgCl_2$.

The amplified 2.7 kb fragment was extracted with phenol/$CHCl_3$ and precipitated with ethanol. Standard molecular biology procedures used are as described in (Maniatis, et al., 1982). In order to repair the ends of the DNA, the PCR sample was resuspended in 170 µl H_2O and treated with 4 µl Klenow polymerase (5 units/µl), 5 µl of 8 mM dNTP's, and 20 µl nick-translation buffer at 37° C for 30 minutes. The sample was then re-extracted with phenol/$CHCl_3$, precipitated with ethanol, resuspended, and digested with Eco RI and Bam HI. The Eco RI-Bam HI fragment was ligated at 16° C for 12 hours into pBR322, and the resulting ligation mixture was transformed into competent *E. coli* BSJ72. Insertion into pBR322 at the Eco RI and Bam HI sites results in destruction of the tetracycline resistance gene but leaves the ampicillin resistance gene intact. Thus, transformants that were tetracycline-sensitive but ampicillin-resistant were picked and tested for colicin Ia activity

using a plate assay (see below). Five out of 7 colonies picked were tetracycline-sensitive and ampicillin-resistant, while the other 2 were tetracycline-resistant and ampicillin-resistant. All 5 tetracycline-sensitive, ampicillin-resistant colonies possessed the positive colicin Ia phenotype. Colonies were also mini-prepped and digested with Eco RI and Bam HI to confirm the presence of the insert. The pBR322 plasmid containing the 2.7 kb insert is termed pPBRCOLIA.

The colicin Ia plate assay involves growing up colonies of interest as streaks on LB plates (Miller, 1972). Once the colonies have grown, they are lysed with $CHCl_3$: a drop of $CHCl_3$ is placed on Whatman filter paper which is placed at the bottom of the inverted LB plate. After 5 minutes, the Whatman paper is removed and the LB plate is overlaid with 100 µl of sensitive or resistant *E. coli* and 3 ml of LB containing 0.7% w/v agar (soft agar). After 6-8 hours, the colicin Ia-producing colonies produce a lacuna in the soft agar containing sensitive cells (*E. coli* 294, also called JK362).

Mutagenesis by PCR

Initially, a method using two separate rounds of PCR to generate site-directed mutants was tried (Kammann, et al., 1989; Nelson & Long, 1989; Giebel & Spritz, 1990; Herlitze & Koenen, 1990; Sarkar & Sommer, 1990). The first round of PCR uses a mutant primer and either IaEco or IaBam, whichever one is proximal to the mutagenesis site, as the second primer. The resulting, amplified PCR

product, which contains the mutation and has been termed "megaprimer" (Sarkar & Sommer, 1990), is used as a primer for the second round of PCR, with either IaEco or IaBam, whichever one was not used in the first round, as the second primer. This second round is designed to generate the 2.7 kb Eco RI-Bam HI fragment containing the mutation, but it yielded little or no amplified product. Even when the products of the first round of PCR were gel purified with Gene-Clean (Bio101) and treated with Klenow polymerase, the yield of product was still extremely low. In fact, no detectable 2.7 kb fragment was generated using a 1.5 kb "megaprimer", although low quantities of the 2.7 kb fragment were produced using a shorter "megaprimer" of approximately 500 bases. The failure of the second round of PCR probably stems from both strands rather than the single, desired strand of the "megaprimer" priming DNA synthesis. Since most of the mutations necessitated "megaprimers" greater than 500 bases, the success of this method was not sufficiently general in order for it to be pursued.

In a second mutagenesis method using PCR, two different "megaprimers", one directing synthesis upstream and the other downstream but both coding for the same mutation, were synthesized. The two "megaprimers" were amplified in two separate PCR's. In each PCR, a mutant, oligonucleotide primer was used to direct synthesis with either IaEco or IaBam as the second primer. That is, a mutant primer which directs synthesis in the direction of the Bam HI site, or downstream, was used with the IaBam primer to

generate one "megaprimer". Likewise, a mutant primer which directs synthesis in the direction of the Eco RI site, or upstream, was used with the IaEco primer to generate the second "megaprimer". In a second round of PCR, both "megaprimers" as well as IaEco and IaBam were included to prime synthesis. The desired goal was for the "megaprimers" to initiate several rounds of synthesis and then for the smaller IaEco and IaBam to prime synthesis as the "megaprimers" were used up. In this second round of PCR, 100 ng of each "megaprimer" and 1 μg each of IaEco and IaBam were used. This procedure yielded the 2.7 kb Eco RI-Bam HI fragment with reasonable yield, but ligation and subsequent cloning into pBR322 of this PCR product was difficult. Upon repeated attempts, transformants that were tetracycline-sensitive and ampicillin-resistant were not found, even though the PCR products were gel-purified and treated with Klenow fragment prior to ligation. Similarly, neither gel purification of Eco RI- and Bam HI-digested pBR322 nor further gel-purification of previously purified and digested PCR products resulted in any tetracycline-sensitive and ampicillin-resistant transformants.

Cloning into a phagemid vector

Due to problems with cloning PCR products, a third method of mutagenesis involving PCR and *in vitro* DNA synthesis from single stranded DNA was attempted. For this method, the 2.7 kb Eco RI-Bam HI fragment was cloned from pBRCOLIA into the poly-linker site

within the *lacZ* gene in pSELECT-1 (Promega), a phagemid vector, for subsequent production of single-stranded circles. Insertion into this site results in the loss of *lacZ* activity, as indicated by the white color of colonies plated on LB containing IPTG and Xgal (Ausubel, et al., 1987). Four white, tetracycline-resistant transformants (in *E. coli* BSJ72) were assayed for colicin Ia function by the plate assay and all 4 had a positive colicin Ia phenotype. The resulting phagemid with the colicin Ia insertion is termed pSELCOLIA.

Mutagenesis using PCR and synthesis from single-stranded DNA

Advantage was taken of the fact that the phagemid pSELECT-1 contains a frameshift mutation in the ampicillin resistance gene which renders it ampicillin-sensitive. Mutant primers that direct synthesis towards the EcoRI site, or upstream, were synthesized and used in a standard PCR reaction with a primer which restores the frame of the ampicillin gene, thereby conferring ampicillin resistance. The resulting "megaprimer", which encodes both ampicillin-resistance and the colicin Ia mutation of interest, was used *in vitro* to prime synthesis on single-stranded, phagemid DNA circles with phage T4 DNA polymerase. Single stranded circles were produced from pSELCOLIA using the helper phage R408. The products of the *in vitro* DNA synthesis and ligation reaction were transformed into competent *E. coli* BMH 71-18 *mutS*, and ampicillin-resistant colonies were assayed for colicin Ia activity by the plate

assay. Ninety-three percent of ampicillin-resistant colonies possessed a positive colicin Ia phenotype. Spurious recombination events may have led to the 7% background of ampicillin-resistant but colicin Ia non-producing colonies.

Differential hybridization (Wood, et al., 1985; Kogan & Gitschier, 1990) was used to check for the presence of the mutation. Plasmid DNA from ampicillin-resistant colonies was mini-prepped, dot blotted onto nylon membranes, and probed with radioactive, mutant primer. The probe was prepared by incubating 1 µl of 100 µg/ml oligonucleotide, 2.5 µl of 10x polynucleotide kinase buffer, 10 µl of-γ ^{32}P-ATP (10 µC/µl), 1 µl of 4 units/µl polynucleotide kinase, and 10 µl H_2O for 30 minutes at 37° C and then for 5 minutes at 65° C. The amount of mini-prep DNA that was blotted was determined by quantitation on agarose gels. Approximately 70% of ampicillin-resistant colonies differentially hybridized to the oligonucleotide containing the appropriate mutation. Plasmid from positive clones were mini-prepped and transformed into *E. coli* BSJ72 for subsequent expression and purification.

Serine to cysteine substitutions were created at ten different sites (see above), and these mutants were all functional as determined by the plate assay.

Purification and crystallization of cysteine substitution mutants

Mutants were purified by standard means (Mel & Stroud, 1992), except that 1 mM β-mercaptoethanol and 1 mM dithiothreitol (DTT) were included in the lysis buffer, and 1 mM DTT was included in Buffer C and HPLC buffer to prevent oxidation of cysteines. Although the purity of the mutants is identical to that of wild-type as judged chromotographically, overloaded SDS-PAGE shows minor contaminants (< 1%) in the mutant purification that are absent in the wild-type purification. These impurities may arise from differing proteins or protein levels in *E. coli* BSJ72, in which the mutants are expressed, as compared to *E. coli* 294, in which the wild-type is expressed.

S462C failed to crystallize in a variety of $(NH_4)_2SO_4$ concentrations, while the other 9 mutants formed crystals which are smaller (0.3 mm x 0.1 mm x 0.01 mm) than wild-type crystals. To grow larger mutant crystals for data collection, repeat-seeding techniques were used. One µl of a drop containing many small crystals (~50 µm in the largest dimension) was serially diluted into 6-12 hanging drops, which were formed by the addition of 5 µl of 1-2 mg/ml mutant protein (in 50 mM NaCl, 20 mM citrate buffer, pH 5.2, 1 mM DTT) to 5 µl of 0.9-1.0 M $(NH_4)_2SO_4$, 0.2 M NaCl, 0.02 M citrate buffer, pH 5.2, 1-20 mM DTT. The hanging drop was equililbrated for 24 hours prior to addition of the seeds. Although the quality of these crystals were still inferior to wild-type crystals, 4 of the 9 mutants that crystallized formed crystals large enough for data collection. These 4 mutant crystals (S171C, S263C, S526C, and

S547C) were soaked in 1 mM CH_3HgCl and data were collected at SSRL on film and at CHESS on Kodak image plates (Table VI). Derivative data for the remaining 5 mutant crystals were also collected, but since these crystals were small, the data were of poor quality and unusable.

Heavy Atom data collection

Fifteen data sets (Table VI, 1-15) of derivatives of wild-type colicin Ia and 7 of cysteine mutants (Table VI, 31-37) were collected at SSRL (station 7-1, λ=1.5418 Å or 1.08 Å) and at CHESS (station A1, λ=1.565 Å) on CEA Reflex 25 film. However, only 2 of the 7 mutant data sets, S171C and S547C, diffracted strongly enough to be processed.

Ten data sets of derivatives of wild-type (Table VI, 18-19, 21-30) and 13 of mutant colicin Ia (Table VI, 38-50) were collected on Kodak image plates at CHESS (stations A1, λ= 1.565 Å and F1, λ=0.91 Å). Nine of the 10 wild-type sets and 4 of the 13 mutant data sets diffracted strongly enough to be processed.

Six cryocrystal, derivative data sets (Table VI, 51-56) were collected on MAR image plates at SSRL (station 7-1, λ=1.08 Å), and 4 of these diffracted strongly enough to be processed.

A total of 56 heavy atoms and conditions were assayed at synchrotrons, and a total of 34 data sets were collected and processed (Table VI). The unit cell dimensions of the derivatives were within experimental error of the those of the wild-type.

Phasing of colicin Ia

In order to determine the positions of bound heavy atoms, difference Pattersons (Patterson, 1934) using $(F_p-F_{ph})^2$ coefficients were calculated, typically from 20-5 Å, in the asymmetric unit of the Patterson (u=0 to 1/4; v=0 to 1/2; w=0 to 1/2). Harker sections (Harker, 1936) were searched for peaks by hand and using the program HASSP[16], which had been modified to accept CCP4 maps[17]. The Harker sections are u=0, v=0, v=1/2, and w=1/2, and the sites found on the Harkers are: u=0,v=±2x, w=±2y; u=±2x, v=0,w=1/2±2z; u=1/2±2x, v=1/2, w=1/2±2z; u=±2x, v=±2y, w=1/2; and u=1/2±2x, v=1/2±2y, z=1/2. If peaks were found, then the difference Patterson was recalculated, but with only those reflections having ΔF's[18] less than 3-5σ of the ΔF distribution. Reflections were identified as having large ΔF's and eliminated from the calculation with DELFCUT (PG). Difference Pattersons were then searched for the presence of the original site, in order to ensure that the site was not the result of only a few large differences. If the site were still present, then the resolution cut-off of the difference Patterson was increased to determine whether the site was reliable for phasing beyond 5 Å.

Prior to calculation of difference Pattersons, native and derivative data were scaled by local scaling (Matthews & Czerwinski,

---

[16]T. Terwilliger, personal communication.

[17]C. Bystroff, personal communication.

[18]$\Delta F=|F_p-F_{ph}|$, where F_p is the native amplitude and F_{ph} is the derivative amplitude.

1975) using either LOCALSC or LOCAL (CCP4). Anisotropic scaling, using ANISOSC (CCP4), fails to correct for systematic differences between data sets as well as local scaling, as determined by comparison of anisotropically or locally scaled $\langle F_{ph} \rangle$ against $\langle F_p \rangle$ as a function of resolution.

Using native data collected on film, no interpretable difference Patterson sites were found for any of the derivatives. Numerous resolution and ΔF cut-offs were tried but failed to yield solvable difference Pattersons. Due to the possibility that the uninterpretability of the difference Pattersons stems from the noisiness of the native and some of the derivative data, diffraction data were re-processed and filtered prior to reduction using MULTICUT (PG). Observations were excluded from the data set on the basis of intensity and an I/σ ratio. The noise level of the data set was established by first scaling all data and determining a mean intensity level at which R_{symm} is unacceptably high, for example 30-40%. Observations with intensities less than this noise value as well as observations with I/σ ratios less than 3 were removed, resulting in an overall, typical exclusion of 67% of observations. After filtering, the data were rescaled, post-refined, and once more rescaled before being truncated. The exclusion of unreliable observations leads to a decrease in the R_{symm} for the native film data from 12.7% to 6.1%, with similar decreases for the derivative data. Using these filtered data, difference Pattersons remained insoluble, except for 0.5 mM TlK_3Cl_6, which appeared to have a

heavy atom site at 0.039, 0.195, 0.172. This site failed to yield interpretable maps, even upon solvent flattening (Wang, 1985), and was later determined to be spurious by difference Fourier methods (see below, Identification of isomorphous derivatives).

Since standard difference Pattersons failed to yield interpretable sites, origin-removed as well as sharpened difference Pattersons (Stout & Jensen, 1989) were calculated, but these too failed to yield interpretable sites for either filtered or non-filtered film data.

Identification of Isomorphous Derivatives

However, when native, image plate data were used instead of native, film data in difference Pattersons, both 0.5 mM TlK_3Cl_6 and 0.1 mM Nb_6Cl_{14} derivatives produced large, unambiguous sites (Figures 6a and 6b). These two derivative data sets are themselves recorded on film. Therefore, the problems in solving difference Pattersons seem not to be due to data collection on film *per se*, but the lack of reliability of the native film data, as evidenced by an R_{symm} of 30% (Table III) if stringent rejection criteria are not applied. The problems in the native, film data may arise from systematic differences between the two synchrotrons, LURE and SSRL, at which the data were collected.

Contemporaneous with the identification of the thallium and niobium derivatives, a mercurial (1 mM CH_3HgCl) derivative of mutant S171C recorded on film was found by difference Pattersons

to yield a useful site. However, this site was identified only when underivatized, mutant colicin Ia (S171C, S263C, S392C, or S547C) rather than underivatized, wild-type colicin Ia was used as the native data. It should be noted that the underivatized mutants had also been soaked in 1 mM CH_3HgCl, but probably because of prior oxidation of the cysteines failed to form derivatives, as confirmed subsequently by difference Fouriers. This restriction to using mutant native data likely indicates that the mutants are non-isomorphous with wild-type colicin Ia, possibly because of a mutation introduced by PCR in the production of the Eco RI-Bam HI fragment (see above, Cloning of Eco RI-Bam HI fragment into pBR322). It is also possible that the different genetic backgrounds in which the wild-type and mutants are expressed may lead to this systematic difference, possibly from differences in post-translational modification.

A component of the systematic difference ($1/\sqrt{2}$ root-mean-square) was removed by correction of the mutant, derivatized amplitudes. The correction required calculating the difference between wild-type, underivatized F_p's and mutant, underivatized F_p's ($F_{pmutant} - F_{pnative} = F_{pdiff}$), and subtracting this difference from F_{ph}'s of derivatized S171C ($F_{phS171C} - F_{pdiff} = F_{phS171Ccorrected}$). The 0.3% of reflections for which the correction resulted in negative amplitudes were set to 0. Difference Pattersons calculated with wild-type F_p's and corrected S171C F_{ph}'s resulted in an interpretable peak (Figure 6c). These corrected amplitudes were then used instead of the observed amplitudes.

The heavy atom sites from the thallium, niobium, and mercury derivatives were checked with cross Fouriers and were refined with a modified version of DICKERSON (Dickerson, et al., 1968) and subsequently with a modified[19] version of HEAVY (Terwilliger, et al., 1987). For refinement in HEAVY, the occupancies and positions of the heavy atoms were initially set to those values determined with DICKERSON. Origin-removed Patterson refinement was used in HEAVY, and once changes in occupancy and position had converged, phased refinement (Blundell & Johnson, 1976) was used. Occupancies and B-factors were often set by hand upon inspection of the distributions of $|F_p - F_{ph}|/f_h$ [20] and $\langle \alpha_p - \alpha_h \rangle$[21] as a function of resolution (Dodson, 1976). Double difference maps (Blundell & Johnson, 1976) were checked for minor sites that had not been included in the phasing. The thallium and mercury derivatives are modelled as single sites, and the niobium derivative is modelled as 4 sites (Table VIII). The major niobium site is modelled as a tetrahedral, bipyramidal Nb_6Cl_{12} coordination complex (Vaughan, et al., 1950), while the three minor sites are modelled as single niobium atoms (Table VIII).

Phases, figures of merit, and phase probabilities (Blow & Crick, 1959) in the form of Hendrickson-Lattman coefficients (Hendrickson & Lattman, 1970; Hendrickson, 1971) were calculated using HEAVY (Table IX). Electron density calculated from these phases was

---

[19] V. Ramalingam, personal communication.

[20] f_h is the heavy atom structure factor.

[21] α_p is the protein phase and α_h is the heavy atom phase.

solvent-flattened (Wang, 1985) using a solvent mask of 65%, and combined phases (Bricogne, 1976) were calculated. Phased refinement of the derivatives using either HEAVY or PHARE (Bricogne, 1982) with these solvent-flattened phases failed to improve the combined phase set as monitored by R_{Cullis} (Cullis, et al., 1961) and figures of merit. However, these phases were used to identify two other, albeit weak derivatives, 1 mM $PtCl_4$ and 0.1 mM terpyridine Pt(II) chloride (Tables VI, VIII, and IX), by difference Fouriers. The $PtCl_4$ derivative, which was recorded on image plates, is modelled as 2 major and 2 minor sites, while the terpyridine Pt(II) derivative (Table VIII), which was recorded on film, is modelled as 2 major and 1 minor sites (Table VIII). Double difference maps were once again used to find minor sites.

The positions, occupancies, and B-factors for these five derivatives were refined, and phases, figures of merit, and Hendrickson-Lattman coefficients were calculated using the program HEAVY (Table IX). The electron density resulting from these phases was solvent flattened, with an initial solvent mask of 60%, which was recalculated and increased to 65% after 6 cycles and then recalculated at 65% every 6 cycles thereafter; several cycles beyond convergence for a total of 28 cycles were run. For calculation of the 60% mask, the map was averaged twice with an 8 Å radius; for the 65% mask, the map was averaged twice with a 4 Å radius. The phase shift from the MIR phases after solvent flattening was 50° and the mean figure of merit improved from 0.51 to 0.75. Again, phased

refinement with these solvent-flattened phases yielded no appreciable gains. In order to improve the solvent mask, it was manually edited using PRISM (Chen, et al., 1990) and MASKEDIT (PG). However, editing proved to be very cumbersome since it was done on a point-by-point basis in sections, and it yielded minimal gain as determined from visual inspection of maps.

Solvent flattened phases were also calculated from single isomorphous (SIR) maps, in order to determine whether any of the derivative sets contained errors and were therefore degrading the combined phase set. Best phases from the thallium, niobium, and mercury derivatives were separately used for phasing and the resulting maps were solvent flattened. However, none of the SIR solvent flattened maps were as good as the MIR solvent flattened map as determined by visual inspection.

Due to the weak intensities of higher resolution reflections, sharpened F_p's, calculated with a B-factor of 70, were used for map calculation. However, the density in these maps was disconnected, and these maps were not used for building.

Electron density from MIR, solvent-flattened maps (65% solvent envelope) was plotted on mini-maps using PLUTO (CCP4) and regions of connectivity were identified. An α-helical, poly-alanine model composed of 623 residues in 67 fragments (Model 1) was built to the MIR, solvent-flattened density using FRODO (Jones & Thirrup, 1986). Efforts were made to build with O (Jones, et al., 1991), but the BONES algorithm resulted in bones atoms running through the

central axis of α-helices rather than taking a helical route. Subsequent solvent masks for solvent flattening were computed from this fragmentary model (Model 1). The model was used in both phase combination and density replacement for improvement of phases. In phase combination, the MIR, solvent-flattened phases were combined (Bricogne, 1976) with model phases, and maps were calculated from the recombined phases. In density replacement, model density was used to replace map density after scaling with MAPCOMBINE (PG), and phases were calculated from the recombined map. At 3.4 Å, neither technique improved the maps considerably, as determined from visual inspection.

The colicin Ia, fragmentary model (Model 1) was refined by rigid body rotation and translation as well as by positional refinement using XPLOR (Brünger, et al., 1987). The R-factor dropped from 58% to 50% and the free R-factor (Brünger, 1992) dropped to 54% with rigid body refinement; the R-factor dropped to 39% and the free R-factor to 51% with positional refinement. Refinement by molecular dynamics using the slow cool algorithm resulted in a further drop in the R-factor to 36% and in the free R-factor to 50%. These refined models were used for phase combination and map combination, but the resulting maps were not much improved as determined by visual inspection.

The peptide conformations that resulted from slow cooling were non-standard, so this model was manually rebuilt to MIR density, which was solvent-flattened using a 75% solvent mask

calculated from Model 1. Questionable portions of Model 1 were eliminated to yield Model 2, which is more connected than Model 1, containing 482 alanine residues and 28 αhelical fragments.

Density Modification Techniques

Electron density was modified by skeletonization (Baker, et al., 1992; Bystroff, et al., 1992), density matching (Zhang & Main, 1990a), and squashing (Main, 1990; Zhang & Main, 1990b) as well as solvent flattening (Wang, 1985). In order to follow the progress of these methods quantitatively, a free R-factor (Brünger, 1992) was calculated. Approximately 2-3% of randomly chosen reflections (free set) were excluded from map calculation, and after density modification of the map, their amplitudes were calculated by back-transformation using SFC (CCP4). The calculated amplitudes were zonally scaled to the observed amplitudes using SCALENEW (CCP4) or LCFSCALE (CCP4), and the free R-factor was computed using FREER (PG). In subsequent rounds of density modification, the calculated values of the reflections in the free set were included in map calculations.

For solvent flattening, the free R-factor indicates that attenuation of negative protein densities lead to errors in the map. If negative protein density (after addition of a F(000) term) is attenuated by a factor between 0.0 and 0.5, the free R-factor rises between 2-3% as compared to runs in which there is no attenuation.

Therefore, negative protein density was left unattenuated and the solvent region was set to its average value.

The free R-factor was also used to set the solvent content of masks computed from the fragmentary, poly-alanine model. While a 70% solvent mask computed from Model 1 resulted in a 2% higher free R-factor than the original 65% mask computed from MIR phases, a 75% solvent mask computed from Model 1 resulted in a slightly lower free R-factor (~45%) than the 65% mask. Therefore, the 75% rather than the 70% solvent mask was used for further cycles of solvent flattening, and Model 2 was built to these flattened maps.

Furthermore, the free R-factor was used to gauge whether recombination of calculated phases with MIR phases as opposed to using solely calculated phases yield better final maps. It appears that this depends on the solvent mask used. For the 65% mask computed from MIR phases, using calculated phases raises the free R-factor by 2%, while for the 70% mask computed from Model 1, using calculated phases results in a lower free R-factor for the first 20 cycles, after which it begins to rise. Therefore, it appears that recombination with MIR phases is useful for the 65% solvent mask, but may not be as useful for the 70% mask, at least at the beginning of the run. Towards the end of the run, it appears that errors, which are not corrected by recombination to the MIR phases, accumulate and result in a rising free R-factor. During the course of model building, both recombined phase and calculated phase maps were examined and were not very qualitatively different.

For skeletonization, the free R-factor actually rises with progressive cycles, and for skeletonization in combination with several cycles of solvent flattening, the free R-factor rises with each skeletonization cycle and falls with each solvent-flattening cycle. However, the free R-factor in combined runs does not fall as much as it does in runs in which solvent flattening alone is used. The errors created in skeletonization probably arise from the representation of helical paths as straight-line paths. That is, just like in the BONES algorithm, the skeleton probably runs through the center of α-helices rather than adopting a spiral course.

Furthermore, histogram matching in combination with solvent flattening using DENMATCH (PG) does not lower the free R-factor more than solvent flattening alone, and in fact raises it after 30 cycles. Histogram-matched, solvent-flattened maps appear to have more disconnected density than simply solvent-flattened maps. Similarly, squashing does not improve the map more than solvent flattening alone as determined by visual inspection. A free R-factor was not determined for squashing since the program does not output calculated phases and amplitudes.

Description of Structure

The high Wilson B-factor for data collected at room temperature reflect the sharp decrease in diffraction intensities at higher resolution, resulting in an effective resolution less than the nominal 3.4 Å. This is apparent in the multiple isomorphous

replacement (MIR), solvent-flattened maps in which most of the density has a connected, tube-like appearance (Figure 7) characteristic of α-helices at low or medium resolution. The large number of such connected, tubular regions reflect the highly α-helical nature of colicin Ia, which by CD measurements is 66% α-helical and 34% random coil (Mel & Stroud, 1992a). Although the tubes have indications of side chains in many portions, sequence could not be fit with confidence into the effectively low resolution map. However, the placement of helices could be carried out with confidence because of the connected nature of most of the density. A model consisting of 482 alanine residues, which is slightly greater in number than that predicted by CD, in standard α-helical conformation has been built in 28 different fragments. As indicated by the agreement with the number of α-helical residues observed by CD, this model accounts for the large majority of density in these maps. Without sequence assignment, fitting connections between helices has not been attempted.

Overall structure of colicin Ia , its packing in the unit cell and effect on solvent flattening

Colicin Ia has three α-helical domains arranged in a "Y"-shape (Figure 8), with a long stalk, termed the Stalk domain, and two shorter arms, termed Arm 1 and Arm 2. The overall dimensions from the base of the Stalk domain to the top of the two arms is 95 Å and from Arm 1 to Arm 2 is 75 Å.

The 8 "Y"-shaped molecules in the unit cell pack (Figures 9a and 9b) such that continuous 95 Å x 85 Å solvent channels run along the **a** axis throughout the crystal, accounting for its 79% solvent content. Arm 1 and Arm 2 from crystallographically symmetry-related molecules form a wall of protein along the **c** = 0 and 1/2 planes. These walls are connected by Stalk domains running along the **c** axis.

This unusual packing leads to an anisotropic improvement of phases in solvent flattening. The presence of large solvent spaces interspersed by walls of protein along the **c** axis leads to strong low-order terms along the **c** axis for the solvent envelope (Figure 10). The low-order terms along the **a** and **b** axes are much weaker, reflecting the presence of essentially continuous walls of density along these directions. Since each reflection is convoluted by the transform of the solvent envelope, solvent flattening leads to greater phase improvement along **c** rather than **a** or **b**. Thus, although solvent flattening is expected to greatly improve phases because of the high solvent content of the crystal, this improvement is localized along one axis of the crystal.

Stalk Domain

The stalk domain contains five long αhelices (Figure 11), two of which continue into and form portions of Arm 1. These two helices, Arm 1 α1 and Arm 2 α2, are 70 and 50 Å long respectively. The other three helices join to Arm 2: Stalk α1 and α2 are both 70 Å

long and join to one side of Arm 2 while Stalk α3 is 50 Å long and joins to the opposite side of Arm 2. The density for these long helices, whose axes point in the direction of the **c** axis, is the most improved by solvent flattening. While density in the MIR map is weak and disconnected (Figure 12a), it is connected and clearly interpretable in the solvent-flattened map (Figure 12b). Crystal contacts are made by the Stalk region of one molecule to the Stalk region of another molecule across a 2-fold symmetry axis running along the **b** axis at **c** = 1/4 and 3/4.

Arm 1

Arm 1 (Figure 13) contains several short helices as well as the two long helices (Arm 1 α1 and Arm 1 α2) that abut the Stalk domain. The mercury derivatized to mutant S171C maps (Table III) to the top of this domain at helix Arm 1 α1 (Figure 14). Since wild-type colicin Ia does not bind mercurial compounds (data not shown), it is likely that the mercurial position identified in mutant S171C corresponds residue 171. Although this residue was identified, sequence could not be built from this point because of the uninterpretability of loop connections between helices. Crystal contacts are made by Arm 1 of one molecule with Arm 1 of a crystallographically symmetry-related molecule across a 2-fold symmetry axis running along the **a** axis at **c** = 0 and 1/2. Without sequence assignment, the molecular boundary between the two symmetry-related molecules cannot be determined unambiguously.

Arm 2

Arm 2 appears to be a compact bundle of approximately 18 α helices and probably corresponds to the channel-forming domain of colicin Ia. The 10 α-helix bundle of the channel-forming fragment of colicin A can be superimposed on 10 helices of this domain (Figure 15a), which appear to form a sub-domain of Arm 2 and has been termed sub-domain 1 (Figure 15b). Helix Stalk α3 appears to join with sub-domain 1, although the connection into this sub-domain may be through a loop that is not observed at this resolution. The remaining 8 helices of Arm 2 which do not superimpose on the colicin A fragment abut helices Stalk α1 and α2, and have been termed sub-domain 2 (Figure 15b). Arm 2 of one molecule contacts Arm 2 of another crystallographically-related molecule. As with Arm 1, the molecular boundary between symmetry-related molecules is not completely clear.

Conclusions from structure

Colicin Ia has been found to be an unusually elongated "Y"-shaped molecule with three highly α-helical domains. This elongated shape agrees with hydrodynamic studies which defined an axial ratio of 15 to 20 for this molecule (Konisky & Richards, 1970). The maximum axial ratio of 2 to 3 as measured from the structure (Figure 16) using GEM[22] indicates that either the molecule is not best

[22]Eric Fauman, personal communication.

described as an ellipse or that the arms might bend in solution to yield this very high axial ratio. Since the molecule is 95 Å from the bottom of the Stalk domain to the top of the arms, it seems unlikely that bending of the arms could result in an axial ratio any greater than 5. Because of the concentration of mass at the top of the "Y" and the paucity of mass at the bottom of the "Y", an ellipsoidal shape appears not to be an appropriate description of the molecule. Both colicins A and E1 have the same asymmetric feature as determined by hydrodynamics. Colicin A (Cavard, et al., 1988) has a hydrodynamic axial ratio of 8 to 10 while colicin E1 (Schwartz & Helinski, 1971) has a hydrodynamic axial ratio similar to that of colicin Ia. Therefore, the asymmetric "Y"-shape found for colicin Ia is likely to be common to these colicins and perhaps to all the channel-forming colicins.

The physiological relevance of this elongated shape may be in bridging across the periplasmic space from the outer membrane to the inner membrane. From studies of colicin A (Bénédetti, et al., 1992), it appears that colicins may be in contact with the outer membrane and the external medium while they form channels in the inner membrane. Thus , the elongated shape may be necessary to contact both outer and inner membranes simultaneously.

The three structural domains observed for colicin Ia probably correspond to the three functional domains identified for other colicins. Because the 10 helix motif of the colicin A fragment (Parker, et al., 1989; Parker, et al., 1992) is also found in the colicin E1

fragment (Wormald, et al., 1990), which shares the same amount of identity to colicin A as does colicin Ia, it is likely that the same motif is present in colicin Ia. Since a sub-domain (number 1) of Arm 2 is superimposable on the colicin A fragment, Arm 2 probably corresponds to the ion channel-forming domain of colicin Ia.

The colicin A channel-forming fragment is equivalent to an 18 kD channel-forming fragment of colicin Ia (Ghosh, et al., 1992). This 18 kD fragment, whose amino-terminus is residue 451 and whose carboxy-terminus is probably the carboxy-terminus of the intact molecule, is slightly shorter than the colicin A fragment but about the same size as the colicin E1 channel-forming fragment (Wormald, et al., 1990). By sequence comparison, the amino-terminus of the 18 kD fragment would correspond to the eighth residue of helix 1 of the colicin A fragment and its likely carboxy-terminus would correspond to the colicin A fragment without its last three residues. Therefore, the 18 kD fragment is likely to be sub-domain 1.

Ion channels formed by the 18 kD colicin Ia fragment differ substantially from those formed by the intact molecule in conductance, open times, and voltage dependence. These differences may arise from portions of the protein amino-terminal to the 18 kD fragment being involved in forming the ion channel of the intact molecule. Since the 18 kD fragment appears to correspond only to sub-domain 1, sub-domain 2 is a likely candidate for the putative portion necessary to form the intact channel. Furthermore, proteolytic digestion of colicin Ia (Mel, 1992) associated with

liposomes shows that 93 residues amino-terminal to the 18 kD channel-forming fragment are protected from digestion by the membrane. These residues may occupy sub-domain 2 and may have a role in formation of the intact ion channel.

Differences in voltage-dependence, gating kinetics, and ion selectivities between the channel-forming fragments and intact molecules of colicins A and E1 have also suggested that portions outside of these fragments may be involved in forming the intact molecule ion channel. Studies with proteolytic and genetic truncations of colicin A (Frenette, et al., 1989) have shown a pH-dependent interaction of the channel-forming domain with the central third of the molecule, the receptor-binding domain. Additionally, ion channel recordings with colicin A-E1 fusion proteins also suggest the interaction of the same two domains (Bénédetti, et al., 1991). Therefore, it appears that an understanding of ion channel formation and function of these colicins will require an understanding of the intact molecule rather than fragments.

By analogy with colicins A and E1, the putative translocation domain of colicin Ia would span the amino-terminal third (residues 1 to ~200) and the putative receptor-binding domain the central third (residues ~201 to ~400) of colicin Ia. Thus, the location of residue 171 at the top of Arm 1 in colicin Ia identifies this position as either the end of the translocation or the beginning of the receptor-binding domain. Since Arm 2 is likely to be the channel-forming domain, Arm 1 and the Stalk domain would then constitute the translocation

and receptor-binding domains, although from our data it is not clear which is which.

The low resolution structure of colicin Ia is a step towards understanding the mechanism of membrane insertion and ion channel-formation and function for these colicins. Since the ion channel-forming fragments of these colicins do not fully mimic the properties to the intact molecule, studies will need to focus on the intact molecules in order to elucidate their mechanism of action. This structure directly demonstrates the unusual shape of intact colicin Ia as well as its tripartite domain structure and the relationship of these to functional domains.

Phasing for cryocrystal data

Diffraction data to 2.8 Å were collected from flash-frozen crystals of colicin Ia (see above, Cryocrystallography). However, the cryocrystal data are non-isomorphous with the room temperature data, as evidenced by an R_{scale} of 36%. The non-isomorphism stems from the 1.6% difference in the c unit cell axis between these two data collection conditions. Since phases calculated for room temperature data are not readily applicable to the cryocrystal data set, an attempt was made to collect thallium and niobium data for flash-frozen crystals.

Three data sets were collected for various times of thallium soaks. All three data sets were collected from crystals which were initially soaked in 0.1 mM TlK_3Cl_6 for 43 hours. Crystals for the first

set were soaked in 0.5 mM TlK_3Cl_6 for an additional 3 hours; crystals for the second set were soaked in 0.5 mM TlK_3Cl_6 for an additional 13 hours; and crystals for the third set were soaked in 0.5 mM TlK_3Cl_6 for an additional 10 days. Although all three sets were isomorphous in cell dimension and had high R_{der}'s (30%, 31%, 38% respectively), none yielded an interpretable difference Patterson against any of the cryo-native sets at any resolution tried (the high resolution cut-off was varied between 8-2.8 Å). The three cryo-thallium derivative sets agree internally: their R_{scale} is 16-18%, indicating that they are reliably measured. However, the uninterpretability of the difference Pattersons points to non-isomorphism between the cryo-thallium set and the cryo-native set, which probably results from some aspect of the freezing.

A single cryo-niobium data set was collected from a crystal that had been soaked for 30 hours in 0.1 mM Nb_6Cl_{14}. An attempt was also made to collect a longer soak time, but after 12 days the niobium-soaked crystals failed to diffract beyond 4-5 Å, even after 3 days of backsoaking. The cryo-niobium data set is isomorphous to the cryo-native data set with respect to unit cell dimensions and has a high R_{der} (31%), but like the cryo-thallium derivative fails to yield an interpretable difference Patterson. Interestingly, the R_{scale} between the cryo-thallium and cryo-niobium data sets is 20%, lower than the R_{der} of either to the cryo-native data set.

Anomalous difference Pattersons were computed for both derivatives, but these failed to yield any convincing sites.

Therefore, in order to obtain phases for the low temperature data, Model 2 was refined by rigid body rotation and translation, and by positional refinement against the cryocrystal data set using XPLOR. The final R-factor for the refinement is 40%. The phases calculated from the refined structure were applied to the low temperature data set, and maps calculated with weighted $2F_O$-F_C coefficients (Main, 1979) were solvent-flattened, skeletonized, and squashed. A free R-factor experiment resulted in a 75% solvent mask computed from Model 1 being used in solvent-flattening. Parameters for skeletonization were optimized; the largest change was in the maxdens parameter, which was set to 3.5-4σ. As before, skeletonization alone raises the free R-factor and in combination with solvent-flattening does not lower it more than solvent-flattening alone. Squashing results in some portions of the map becoming more connected, but other portions remained disconnected and difficult to interpret.

In a second method of obtaining phases for the cryocrystal data, electron density calculated from the MIR, solvent-flattened 3.4 Å data was shrunk to fit in the cryocrystal unit cell. Phases to 3.4 Å were calculated from this shrunk map and were refined and extended to 2.8 Å using squashing (70 steps of extension and 70% solvent mask). These maps appear to have greater connectivity and appear more interpretable than the maps calculated from refinement of Model 1 to the cryocrystal data.

REFERENCES

Arndt, U. W., Champness, J. N., Phizackerley, R. P. & Wonacott, A. J. (1973) *J. Appl. Cryst. 6*, 457-463.

Arndt, U. W., Crowther, R. A. & Mallett, J. F. W. (1968) *J. Phys. E: Sci. Instrum. 1*, 510-516.

Arndt, U. W., Gilmore, D. J. & Wonacott, A. J. (1977) In *The rotation method in crystallography.* Arndt, U. W. & Wonacott, A. J., eds. North-Holland Publishing Company, Amsterdam, pp. 207-218.

Arndt, U. W. & Wonacott, A. J. (1977) *The Rotation Method in Crystallography.* North-Holland Publishing Company, Amsterdam.

Ausubel, F. M., Brent, R., Kingston, R. E., Moore, D. D., Seidman, J. G., Smith, J. A. & Struhl, K. (1987) *Current protocols in molecular biology.* John Wiley & Sons, New York.

Azaroff, L. V. (1955) *Acta Cryst. 8*, 701-704.

Baker, D., Bystroff, C., Fletterick, R. J. & Agard, D. A. (1992) *Acta Cryst.* Submitted.

Blow, D. M. & Crick, F. H. C. (1959) *Acta Cryst. 12*, 794-802.

Blum, M., Metcalf, P., Harrison, S. C. & Wiley, D. C. (1987) *J. Appl. Cryst. 20*, 235-242.

Blundell, T. L. & Johnson, L. N. (1976) *Protein Crystallography.* Academic Press, New York.

Bricogne, G. (1976) *Acta Cryst. A32*, 832-846.

Bricogne, G. (1982) In *Computational Crystallography.* Sayre, D., ed. Oxford University Press, New York, pp. 223-230.

Brünger, A. T. (1992) *Nature 355*, 472-475.

Brünger, A. T., Kuriyan, J. & Karplus, M. (1987) *Science 235*, 458.

Bystroff, C., Baker, D., Fletterick, R. J. & Agard, D. A. (1992) *Acta Cryst.* Submitted.

CCP4 (1979) S.E.R.C. [U.K.] Collaborative Computing Project No. 4, Daresbury Laboratory, Warrington, U.K.

Chen, H., Sedat, J. W. & Agard, D. A. (1990) In *Handbook of biological confocal microscopy.* Pawley, J. B., ed. Plenum Press, New York, pp. 141-150.

Choe, S. (1987) Ph. D. Thesis, University of California, Berkeley.

Crick, F. H. C. & Magdoff, B. (1956) *Acta Cryst. 9*, 901.

Cullis, A. F., Muirhead, H., Perutz, M. F., Rossmann, M. G. & North, A. C. T. (1961) *Proc. R. Soc. London A:265*, 15-38.

Dao-Pin, S., Alber, T., Bell, J. A., Weaver, L. H. & Matthews, B. W. (1987) *Protein Eng. 1*, 115-123.

Dickerson, R. E., Weinzierl, J. E. & Palmer, R. A. (1968) *Acta Cryst. B24*, 997-1003.

Dodson, E. J. (1976) In *Crystallographic Computing Techniques.* Ahmed, F. R., ed. Munksgaard, Copenhagen, pp. 259-268.

Durbin, R. M., Burns, R., Moulai, J., Metcalf, P., Freymann, D., Blum, M., Anderson, J. E., Harrison, S. C. & Wiley, D. C. (1986) *Science 232*, 1127-1132.

Eckert, K. A. & Kunkel, T. A. (1990) *Nucleic Acids Research 18*, 3739-3744.

Elder, M. (1985) *Methods Enzymol. 114*, 199-211.

Finer-Moore, J. & Stroud, R. M. (1984) *Proc. Nat. Acad. Sci. U.S.A. 81*, 155-159.

Fourme, R. & Kahn, R. (1985) *Methods Enzymol. 114*, 281-299.

Fox, G. C. & Holmes, K. C. (1966) *Acta Cryst. 20*, 886-891.

French, S. & Wilson, K. (1978) *Acta Cryst. A34*, 517-525.

Garnier, J., Osguthorpe, D. J. & Robson, B. (1978) *J. Mol. Biol. 120*, 97-120.

Giebel, L. B. & Spritz, R. A. (1990) *Nucleic Acids Research 18*, 4947.

Green, D. W., Ingram, V. M. & Perutz, M. F. (1954) *Proc. R. Soc. London A:225*, 287-307.

Harker, D. (1936) *J. Chem. Phys. 4*, 381.

Harrison, S. C., Winkler, F. K., Schutt, C. E. & Durbin, R. M. (1985) *Methods Enzymol. 114*, 211-237.

Hatfull, G. F., Sanderson, M. R., Freemont, P. S., Raccuia, P. R., Grindley, N. D. F. & Steitz, T. A. (1989) *J. Mol. Biol. 208*, 661-667.

Hendrickson, W. A. (1971) *Acta Cryst. B27*, 1472-1473.

Hendrickson, W. A. & Lattman, E. E. (1970) *Acta Cryst. B26*, 136-143.

Herlitze, S. & Koenen, M. (1990) *Gene 91*, 143-147.

Hope, H. (1988) *Acta Cryst. B44*, 22-26.

Hope, H., Frolow, F., von Boelhen, K., Makowski, I., Kratky, C., Halfon, Y., Danz, H., Webster, P., Bartels, K. S., Wittman, H. G. & Yonath, A. (1989) *Acta Cryst. B45*, 190-199.

Howard, A. J., Gilliland, G. L., Finzel, B. C., Poulos, T. L., Ohlendorf, D. H., & Salemme, F. R. (1987) *J. Appl. Cryst. 20*, 383-387.

Jones, T. A. & Thirrup, S. (1986) *EMBO J. 5*, 819-822.

Jones, T. A., Zou, J.-Y., Cowan, S. W. & Kjeldgaard, M. (1991) *Acta Cryst. A47*, 110-119.

Kahn, R., Fourme, R., Gadet, A., Janin, J., Dumas, C. & Andre, D. (1982) *J. Appl. Cryst. 15*, 330-337.

Kamb, A., Weir, M., Rudy, B., Varmus, H. & Kenyon, C. (1989) *Proc. Nat. Acad. Sci. U.S.A. 86*, 4372-4376.

Kammann, M., Laufs, J., Schell, J. & Gronenborn, B. (1989) *Nucleic Acids Research 17*, 5404.

Kogan, S. C. & Gitschier, J. (1990) In *PCR Protocols.* Innis, M. A., Gelfand, D. H., Sninsky, J. J. & White, T. J., eds. Academic Press, Inc., New York, pp. 288-299.

Main, P. (1979) *Acta Cryst. A35*, 779-785.

Main, P. (1990) *Acta Cryst. A46*, 372-377.

Maniatis, T., Fritsch, E. F. & Sambrook, J. (1982) *Molecular Cloning.* Cold Spring Harbor Laboratory, Cold Spring Harbor, New York.

Mankovich, J. A., Hsu, C. & Konisky, J. (1986) *J. Bacteriol. 168*, 228-236.

Matthews, B. W. & Czerwinski, E. W. (1975) *Acta Cryst. A31*, 480-487.

Matthews, B. W., Klopfenstein, C. E. & Colman, P. M. (1972) *J. Phys. E. 5*, 353-359.

Mel, S. F. & Stroud, R. M. (1992) *Biochemistry* Submitted.

Mel, S. F. (1992) Ph. D. Thesis, University of California, San Francisco.

Miller, J. H. (1972) *Experiments in Molecular Genetics.* Cold Spring Harbor Laboratory Press, Cold Spring Harbor, New York.

Miyahara, J., Takahashi, K., Amemiya, Y., Kamiya, N. & Satow, Y. (1986) *Nuclear Instruments and Methods in Physics Research A246,* 572.

Morimoto, H. & Uyeda, R. (1963) *Acta Cryst. 16,* 1107-1119.

Morlon, J., Lloubès, R., Varenne, S., Chartier, M. & Lazdunski, C. (1983) *J. Mol. Biol. 170,* 271-285.

Nagai, K., Oubridge, C., Jessen, T. H., Li, J. & Evans, P. R. (1990) *Nature 348,* 515-520.

Nelson, R. M. & Long, G. L. (1989) *Analytical Biochemistry 180,* 147-151.

Parker, M. W., Pattus, F., Tucker, A. D. & Tsernoglou, D. (1989) *Nature 337,* 93-96.

Parker, M. W., Postma, J. P. M., Pattus, F., Tucker, A. D. & Tsernoglou, D. (1992) *J. Mol. Biol. 224*, 639-657.

Parker, M. W., Tucker, A. D., Tsernoglou, D. & Pattus, F. (1990) *Trends Biochem. Sci. 15*, 126-129.

Patterson, A. L. (1934) *Phys. Rev. 46*, 372.

Petsko, G. A. (1985) *Methods Enzymol. 114*, 147-156.

Phillips, W. C. (1985) *Methods Enzymol. 114*, 300-316.

Phillips, W. C. & Rayment, I. (1985) *Methods Enzymol. 114*, 316-329.

Rossmann, M. G., Leslie, A. G. W., Abdel-Meguid, S. S. & Tsukihara, T. (1979) *J. Appl. Cryst. 12*, 570-581.

Saiki, R. K., Gelfland, D. H., Stoffel, S., Scharf, S. J., Higuchi, R., Horn, G. T., Mullis, K. B. & Ehrlich, H. A. (1988) *Science 239*, 487-491.

Salles, B., Weisemann, J. M. & Weinstock, G. M. (1987) *J. Bacteriol. 169*, 5028-5034.

Sarkar, G. & Sommer, S. G. (1990) *BioTechniques 8*, 404-407.

Schein, S. J., Kagan, B. L. & Finkelstein, A. (1978) *Nature 276*, 159-163.

Sonoda, M., Takano, M., Miyahara, J. & Kato, H. (1983) *Radiology 148*, 833.

Stock, A. M., Mottonen, J. M., Stock, J. B. & Scutt, C. E. (1989) *Nature 337*, 745-749.

Stout, G. H. & Jensen, L. H. (1989) *X-ray structure determination.* John Wiley & Sons, New York.

Subbiah, S. (1991) *Science 252*, 128-133.

Teng, T.-Y. (1990) *J. Appl. Cryst. 23*, 387-391.

Terwilliger, T. C., Kim, S.-H. & Eisenberg, D. (1987) *Acta Cryst. A43*, 1-5.

Tucker, A. D., Baty, D., Parker, M. W., Pattus, F., Lazdunski, C. & Tsernoglou, D. (1989) *Protein Eng. 2*, 399-405.

Vaughan, P. A., Sturdivant, J. H. & Pauling, L. (1950) *J. Am. Chem. Soc. 72*, 5477-5486.

Waleh, N. S. & Johnson, P. H. (1985) *Proc. Nat. Acad. Sci. USA 82*, 8389-8393.

Wang, B.-C. (1985) *Methods Enzymol. 115*, 90-112.

Weaver, C. A., Redborg, H. & Konisky, J. (1981) *J. Bacteriol. 148*, 817-828.

Whitting, B. R., Owen, J. F. & Rubin, B. H. (1988) *Nuclear Instruments and Methods in Physics Research A266*, 628-635.

Wilson, A. J. C. (1949) *Acta Cryst. 2*, 318-321.

Winkler, F. K., Schutt, C. E. & Harrison, S. C. (1979) *Acta Cryst. A35*, 901-911.

Wood, W. I., Gitschier, J., Lasky, L. A. & Lawn, R. M. (1985) *Proc. Nat. Acad. Sci. U.S.A. 82*, 1585-1588.

Wooster, W. A. (1964) *Acta Cryst. 17*, 878-882.

Zhang, K. Y. J. & Main, P. (1990a) *Acta Cryst. A46*, 41-46.

Zhang, K. Y. J. & Main, P. (1990b) *Acta Cryst. A46*, 377-381.

Table I. Native Synchrotron Data Collected at LURE and SSRL

	Maximum Resolution (Å)									
	10.39[b]	7.42	6.08	5.28	4.73	4.32	4.00	3.74	3.53	3.35
Rmerge[a] cumulative	.050	.051	.062	.078	.085	.091	.100	.110	.117	.127
Rmerge[a] by resolution bin	.050	.052	.113	.202	.133	.149	.208	.352	.491	.887
$\langle I \rangle / \langle \sigma_I \rangle$	8.57	10.98	6.04	3.52	5.31	4.81	3.48	2.18	1.51	0.83
Number of Observations	2701	4818	6324	6303	4717	3887	3970	3247	2025	1923
Unique Observations	883	1410	1457	1429	1339	1345	1326	1241	953	963
% Complete	100	99.6	95.2	84.6	73.3	65.3	59.0	52.3	41.2	39.0

$$^{a}R_{merge} = \frac{\sum_h \sum_i |I_{h,i} - I_h|}{\sum_h \sum_i I_{h,i}}$$

[b]The low resolution cut-off for the data set is 20 Å.

Table II. Native Synchrotron DataCollected at CHESS on Image Plates

	Maximum Resolution (Å)									
	10.39[b]	7.42	6.08	5.28	4.73	4.32	4.00	3.74	3.53	3.35
R_{merge}[a] cumulative	.046	.050	.060	.071	.080	.090	.101	.112	.122	.127
R_{merge}[a] by resolution bin	.046	.052	.086	.132	.123	.160	.224	.308	.409	.456
$\langle I \rangle / \langle \sigma_I \rangle$	13.03	11.73	7.78	5.26	5.68	4.46	3.19	2.28	1.69	1.46
Number of Observations	2090	5114	8051	8931	9778	10731	11239	10765	10083	6771
Unique Observations	634	1416	1898	2198	2406	2718	2875	3057	3141	2445
% Complete	.680	.940	.989	.984	.980	.978	.958	.968	.967	.810

[a] $R_{merge} = \dfrac{\sum_h \sum_i |I_{h,i} - I_h|}{\sum_h \sum_i I_{h,i}}$

[b] The low resolution cut-off for the data set is 20 Å.

Table III. Native Synchrotron Data Collected at LURE and SSRL with less stringent rejection criteria and without a resolution cut-off

	Maximum Resolution (Å)									
	10.39[b]	7.42	6.08	5.28	4.73	4.32	4.00	3.74	3.53	3.35
Rmerge[a] cumulative	.098	.096	.108	.125	.140	.158	.183	.216	.256	.300
Rmerge[a] by resolution bin	.098	.094	.164	.263	.223	.280	.415	.684	1.211	2.180
$\langle I \rangle / \langle \sigma_I \rangle$	4.91	5.65	3.80	2.64	3.09	2.52	1.69	0.97	0.55	0.30
Number of Observations	3208	6051	8627	9685	10935	11860	12919	13260	13704	12662
Unique Observations	883	1461	1895	2187	2432	2750	2943	3128	3232	3388
% Complete	100	99.3	99.9	100	100	99.9	99.5	99.6	99.3	97.6

$$^{a}R_{merge} = \frac{\sum_h \sum_i |I_{h,i} - I_h|}{\sum_h \sum_i I_{h,i}}$$

[b]The low resolution cut-off for the data set is 20 Å.

Table IV. Native Cryocrystal dataCollected at SSRL on MAR Image Plates

	Maximum Resolution (Å)									
	8.73[b]	6.22	5.09	4.42	3.95	3.61	3.34	3.13	2.95	2.80
Rmerge[a] cumulative	.036	.039	.044	.046	.049	.054	.059	.066	.072	.077
Rmerge[a] by resolution bin	.036	.041	.054	.050	.055	.073	.104	.153	.203	.239
$\langle I \rangle / \langle \sigma_I \rangle$	17.2	15.7	12.9	13.3	12.5	9.9	7.1	4.9	3.7	2.9
Observations	4392	8581	10887	12941	14263	15447	16129	15988	15911	11053
Unique Observations	1176	2150	2720	3200	3686	3952	4374	4435	4892	3491
% Complete	.973	.979	.968	.959	.951	.947	.939	.929	.924	.678

[a] $R_{merge} = \frac{\sum_h \sum_i |I_{h,i} - I_h|}{\sum_h \sum_i I_{h,i}}$

[b] The low resolution cut-off for the data is 30 Å.

Table V. Heavy Atom Data Screened withrotating anode x-rays

	Soak Conditions	Soak Time	Unit cell	Rder[a]
1	1% sat. Yb_2O_3	12 days	66.0 x 177.7 x 290.1	0.10
2	10 mM $PtCl_4$	40 days	65.6 x 176.3 x 289.6	0.32
3	1 mM $PtCl_4$	7 days	66.4 x 175.8 x 290.4	0.19
4	10% sat. PCMBS	9 days	NA Weak diffraction	NA
5	1% sat. PCMBS	21 days	65.7 x 176.9 x 289.4	0.11
6	10% sat. mersalyl	12 days	65.4 x 177.1 x 289.5	0.09
7	10% sat. $UO_2(NO_3)_2$	15 days	64.5 x 180.0 x 292.1	0.20

Table V. Heavy Atom Data Screened withrotating anode x-rays

	Soak Conditions	Soak Time	Unit cell	Rder[a]
8	1% sat. $UO_2(NO_3)_2$	29 days	65.3 x 181.1 x 292.0	0.16
9	1% sat. K_2PtI_6	17 days	66.3 x 176.8 x 290.0	0.22
10	10 mM TlK_3Cl_6	Immediately cracks crystal	NA	NA
11	1 mM TlK_3Cl_6	17 days	65.1 x 178.2 x 289.7	0.18
12	0.5 mM TlK_3Cl_6	15 days 0.1 mM, 4 days 0.5 mM	65.7 x 175.0 x 288.4	0.13
13	0.1 mM TlK_3Cl_6	11 days	65.4 x 175.0 x 288.4	0.08
14	10 mM $Gd(CH_3COO)_3$	21 days	65.9 x 177.0 x 291.0	0.13

Table V. Heavy Atom Data Screened withrotating anode x-rays

	Soak Conditions	Soak Time	Unit cell	Rder[a]
15	10% sat. HgI_2	25 days	66.1 x 176.7 x 289.8	0.11
16	1 mM Ta_6Cl_{14}	14 days	65.8 x 177.4 x 290.3	0.08
17	0.1 mM Nb_6Cl_{14}	19 days	65.1 x 181.0 x 285.7	0.33
18	1 mM chloro-(2,2':2''-terpyridine) Pt (II)	23 days	NA Crystals fall apart and crack	NA
19	0.1 mM chloro-(2,2':2''-terpyridine) Pt (II)	29 days	66.3 x 173.5 x 288.1	0.36
20	1 mM $OsCl_3$	13 days	65.7 x 176.6 x 289.7	0.12
21	10 mM Na_3IrCl_6	18 days	65.7 x 176.3 x 292.5	0.34

Table V. Heavy Atom Data Screened withrotating anode x-rays

	Soak Conditions	Soak Time	Unit cell	Rder[a]
22	10 mM $UO_2(CH_2COO)_2$	19 days	64.2 x 179.9 x 289.2	0.19
23	1% sat. $Pb_3(C_6H_5O_7)_2$	31 days	67.4 x 176.2 x 290.2	0.09
24	1% sat. $KAuI_4$	33 days	66.4 x 174.8 x 289.9	0.11
25	1% sat. K_2PtBr_6	35 days	66.1 x 174.1 x 288.1	0.21
26	1 mM $(NH_4)_2IrCl_6$	38 days	NA No diffraction	NA
27	0.1 mM $(NH_4)_2IrCl_6$	4 days	65.9 x 174.7 x 289.1	0.11

[a] $R_{der} = \frac{\sum|F_p - F_{ph}|}{\sum F_p}$, where F_p is the native amplitude and F_{ph} is the derivative amplitude; both were collected using rotating anode x-rays on a Siemens area detector.

Table VI. Heavy Atom Soaks collected at synchrotrons

	Soak Conditions	Soak Time	Source	d_{min}	R_{symm}[a]	R_{der}[b]
1	10 mM Na_3IrCl_6	12 days	CHESS film, SSRL film	5.0 Å	0.12	0.20
2	1 mM TlK_3Cl_6	12 days	CHESS film, SSRL film	No diffraction	NA	NA
3	1% sat. K_2PtI_6	12 days	CHESS film, SSRL film	4.0 Å	0.18	0.22
4	1% sat. Yb_2O_3	12 days	CHESS film, SSRL film	3.4 Å	0.19	0.16
5	1 mM Ta_6Cl_{14}	12 days	CHESS film, SSRL film	3.4 Å	0.20	0.15

Table VI. Heavy Atom Soaks collected at synchrotrons

	Soak Conditions	Soak Time	Source	d_{min}	R_{symm}[a]	R_{der}[b]
6	0.1 mM Nb_6Cl_{14}	20 days	SSRL film	3.4 Å	0.17	0.30
7	0.1 mM terpyridine Pt(II) chloride	13 days	SSRL film	3.4 Å	0.21	0.21
8	0.5 mM TlK_3Cl_6	15 days 0.1 mM, 5 days 0.5 mM	SSRL film	3.4 Å	0.18	0.20
9	1 mM $(NH_4)_2IrCl_6$	14 days	SSRL film	No diffraction	NA	NA
10	0.1 mM $(NH_4)_2IrCl_6$	8 days	SSRL film	3.4 Å	0.18	0.13
11	1% sat. K_2PtBr_6	14 days	SSRL film	3.4 Å	0.22	0.27

Table VI. Heavy Atom Soaks collected at synchrotrons

	Soak Conditions	Soak Time	Source	d_{min}	R_{symm}[a]	R_{der}[b]
12	10 mM $UO_2(NO_3)_2$	20 days	SSRL film	3.4 Å	0.28	0.31
13	10 mM $PtCl_4$	14 days	SSRL film	3.4 Å	0.22	0.31
14	$Hg(CH_3)_2$	4 days	SSRL film	3.4 Å	0.22	0.19
15	1% sat. $KAuI_4$	14 days	SSRL film	3.4 Å	0.13	0.21
16	1% sat. $Pb_3(C_6H_5O_7)_2$	14 days	SSRL film	3.4 Å	0.22	0.19[c]

Table VI. Heavy Atom Soaks collected at synchrotrons

	Soak Conditions	Soak Time	Source	d_{min}	R_{symm}[a]	R_{der}[b]
17	1 mM Na_3IrCl_6	19 days	CHESS film	3.4 Å	0.17	0.15
18	0.5 mM TlK_3Cl_6	19 days, only 1 crystal in set diffracts	CHESS Image Plate	3.4 Å	0.16	0.16
19	0.5 mM Nb_6Cl_{14}	9 days	CHESS Image Plate	No diffraction beyond 5 Å	NA	NA
20	1% sat. $TlNO_3$	20 days	CHESS film	3.4 Å	ND	ND
21	1 mM CH_3CH_2HgCl	5 days[d]	CHESS Image Plate	3.4 Å	0.14	0.15

Table VI. Heavy Atom Soaks collected at synchrotrons

	Soak Conditions	Soak Time	Source	d_{min}	R_{symm}[a]	R_{der}[b]
22	1 mM $PtCl_4$	5 days[d]	CHESS Image Plate	3.4 Å	0.15	0.30
23	1 mM CH_3HgCl	5 days[d]	CHESS Image Plate	3.4 Å	0.14	0.16
24	1 mM PCMBS	5 days[d]	CHESS Image Plate	3.4 Å	0.15	0.11
25	1 mM HgCl	5 days[d]	CHESS Image Plate	3.4 Å	0.12	0.12
26	0.1 mM Nb_6Cl_{14}	5 days[d]	CHESS Image Plate	No Diffraction	NA	NA

Table VI. Heavy Atom Soaks collected at synchrotrons

	Soak Conditions	Soak Time	Source	d_{min}	R_{symm}[a]	R_{der}[b]
27	0.1 mM TlK_3Cl_6	5 days	CHESS Image Plate	Weak diffraction	NA	NA
28	0.5 mM TlK_3Cl_6	Soaked and mounted as in 8, data collected 1 year after soak	CHESS Image Plate	3.4 Å	0.12	0.16
29	1% sat. Lutetium Acetate	20 days	CHESS Image Plate	3.4 Å	0.14	0.14
30	1% sat. methyl amine tungstate	19 days	CHESS Image Plate	3.4 Å	0.11	0.12
31	S171C in 1 mM CH_3HgCl	5 days	SSRL film	3.5 Å	0.22	0.29
32	S547C in 1 mM CH_3HgCl	5 days	SSRL film	3.5 Å	0.19	0.25

Table VI. Heavy Atom Soaks collected at synchrotrons

	Soak Conditions	Soak Time	Source	d_{min}	R_{symm}[a]	R_{der}[b]
33	S615C in 1 mM CH_3HgCl	5 days	SSRL film	Weak	NA	NA
34	S526C in 1 mM CH_3HgCl	5 days	SSRL film	Weak	NA	NA
35	S219C in 1 mM CH_3HgCl	5 days	SSRL film	Weak	NA	NA
36	S263C in 1 mM CH_3HgCl	4 days	SSRL film	Weak	NA	NA
37	S392C in 1 mM CH_3HgCl	5 days	SSRL film	Weak	NA	NA

Table VI. Heavy Atom Soaks collected at synchrotrons

	Soak Conditions	Soak Time	Source	d_{min}	R_{symm}[a]	R_{der}[b]
38	S171C in 1 mM CH_3HgCl	8 days[e]	CHESS Image Plate	3.4 Å	0.16	0.26
39	S547C in 1 mM CH_3HgCl	8 days[e]	CHESS Image Plate	3.4 Å	0.19	0.31
40	S526C in 1 mM CH_3HgCl	8 days[e]	CHESS Image Plate	3.4 Å	0.17	0.26
41	S392C in 1 mM CH_3HgCl	8 days[e]	CHESS Image Plate	Weak	NA	NA
42	S522C in 1 mM CH_3HgCl	8 days[e]	CHESS Image Plate	Weak	NA	NA

Table VI. Heavy Atom Soaks collected at synchrotrons

	Soak Conditions	Soak Time	Source	d_{min}	R_{symm}[a]	R_{der}[b]
43	S68C in 1 mM CH_3HgCl	8 days[e]	CHESS Image Plate	Weak	NA	NA
44	S263C in 1 mM CH_3HgCl	8 days[e]	CHESS Image Plate	3.4 Å	0.15	0.25
45	S219C in 1 mM CH_3HgCl	8 days[e]	CHESS Image Plate	Weak	NA	NA
46	S615C in 1 mM CH_3HgCl	8 days[e]	CHESS Image Plate	Weak	NA	NA
47	S547C in 2 mM CH_3HgCl	2 days	CHESS Image Plate	No diffraction	NA	NA

Table VI. Heavy Atom Soaks collected at synchrotrons

	Soak Conditions	Soak Time	Source	d_{min}	R_{symm}[a]	R_{der}[b]
48	S171C in 2 mM CH_3HgCl	2 days	CHESS Image Plate	Weak diffraction	NA	NA
49	S263C in 2 mM CH_3HgCl	2 days	CHESS Image Plate	Weak diffraction	NA	NA
50	S526C in 2 mM CH_3HgCl	2 days	CHESS Image Plate	Weak diffraction	NA	NA
51	0.1 mM Nb_6Cl_{14}	30 hours	SSRL MAR Image Plate	2.8 Å	0.11	0.31
52	0.1 mM Nb_6Cl_{14}	12 days, backsoak 21 hours	SSRL MAR Image Plate	< 5 Å	ND	ND

Table VI. Heavy Atom Soaks collected at synchrotrons

	Soak Conditions	Soak Time	Source	d_{min}	R_{symm}[a]	R_{der}[b]
53	0.1 mM Nb_6Cl_{14}	12 days, backsoak 3 days	SSRL MAR Image Plate	< 5 Å	ND	ND
54	0.5 mM TlK_3Cl_6	43 hours 01. mM, 3 hours 0.5 mM	SSRL MAR Image Plate	2.8 Å	0.07	0.30
55	0.5 mM TlK_3Cl_6	43 hours 01. mM, 13 hours 0.5 mM	SSRL MAR Image Plate	2.8 Å	0.10	0.29
56	0.5 mM TlK_3Cl_6	43 hours 01. mM, 10 days 0.5 mM	SSRL MAR Image Plate	2.8 Å	0.07	0.38

[a] $R_{symm} = \frac{\sum_h \sum_i |I_{h,i} - I_h|}{\sum_h \sum_i I_{h,i}}$

[b] $R_{der} = \frac{\sum |F_p - F_{ph}|}{\sum F_p}$, where F_p is the native amplitude and F_{ph} is the derivative amplitude.

[c] Calculated from one-half of the data set against filtered native data.

[d] Citrate buffer was excluded from the soaking solution, which was left unbuffered.

[e] 1.1 M $(NH_4)_2SO_4$ was was replaced with 1.1 M Na_2SO_4 in the soaking solution.

Table VII. Primers used for mutagenesis of colicin Ia

PRIMERS	SEQUENCES 5' TO 3'
IaEco	AAAGAATTCGTCCGGTTTTTGTATTGCAC
IaBam	ATTGGATCCTTTTGCTGTCCATCAGGGCA
amp[a]	GTTGCCATTGCTGCAGGCATCGTGGTG
S68C	TTCGATATCACATCGGGTTGG
S171C	TATACGAAGACAATCAGCATCAG
S219C	TTCCAGCTCGCACAACCGGGT
S263C	CCGTCTTAAGGCATTCCGTCAC
S392C	ATTTACCGCACATTCAGCAGAG
S462C	TTTCTGAGACGCATTTCAGGAACTCT
S522C	CAGCTTCACACACTCAAGGGC
S526C	GACGATATATCGCACAGCTTCACA
S547C	GTCAGCAAGACATGTAAATTTTCC
S615C	TTTCCACAAGGCATTCATCAATCAGC

[a]Primer used to restore frame of *amp* gene.

Table VIII. Heavy Atom Positions

Derivative	Atom	Occupancy	x	y	z	B
TlK_3Cl_6	1. Tl	1.32	.1629	.1870	.4736	50.0
Nb_6Cl_{14}	1. Nb	1.16	.3303	.1017	.3385	17.0
	Nb	1.16	.3008	.0906	.3416	17.0
	Nb	1.16	.2794	.1024	.3466	17.0
	Nb	1.16	.3089	.1134	.3435	17.0
	Nb	1.16	.3222	.0999	.3483	17.0
	Nb	1.16	.2875	.1042	.3369	17.0
	Cl	1.16	.3390	.1149	.3390	17.0
	Cl	1.16	.3297	.0883	.3368	17.0
	Cl	1.16	.2707	.0892	.3462	17.0
	Cl	1.16	.2801	.1157	.3484	17.0
	Cl	1.16	.3545	.0991	.3445	17.0
	Cl	1.16	.3203	.0863	.3481	17.0
	Cl	1.16	.2955	.0999	.3539	17.0
	Cl	1.16	.3297	.1128	.3503	17.0
	Cl	1.16	.3142	.1041	.3312	17.0
	Cl	1.16	.2800	.0912	.3348	17.0
	Cl	1.16	.2552	.1049	.3406	17.0
	Cl	1.16	.2894	.1177	.3370	17.0
	2. Nb	0.75	.0991	.0905	.4586	17.0
	3. Nb	0.65	.3957	.1257	.3116	17.0
	4. Nb	0.60	.0437	.1345	.4937	17.0
CH_3HgCl S171C	1. Hg	1.16	.1524	.4208	.4620	30.0
$PtCl_4$	1. Pt	0.75	.2196	.0957	.0039	35.0
	2. Pt	0.70	.2256	.0823	.0003	35.0
	3. Pt	0.35	.1537	.0904	.4578	35.0
	4. Pt	0.30	.1606	.1881	.4740	35.0

Table VIII. Heavy Atom Positions

Derivative	Atom	Occupancy	x	y	z	B
terpyridine Pt(II) Cl	1. Pt	0.75	.3973	.1247	.3109	30.0
	2. Pt	0.55	.3990	.1099	.3113	30.0
	3. Pt	0.25	.3055	.1147	.3424	30.0

Table IX. Phasing Statistics

	Maximum Resolution (Å)								
	Total	11.27	7.26	5.72	4.87	4.31	3.91	3.60	3.35
Mean figure of merit	.52	.62	.61	.57	.51	.47	.48	.47	.39
0.5 mM TlK_3Cl_6	Unit Cell: 65.78 x 177.43 x 290.80[d]								
R_{der}[a]	0.22	0.15	0.15	0.22	0.23	0.21	0.26	0.28	0.28
R_{Cullis}[b]	.70	.53	.60	.68	.79	.80	.79	.87	.89
f_H / e[c]	1.07	1.21	1.27	1.20	1.06	0.93	.87	.93	.91
0.1 mM Nb_6Cl_{14}	Unit Cell: 65.93 x 176.96 x 289.24								
R_{der}[a]	0.30	0.41	0.31	0.29	0.27	0.28	0.30	0.31	0.29
R_{Cullis}[b]	.72	.61	.72	.74	.75	.77	.83	.76	.75
f_H / e[c]	1.02	1.26	1.15	1.05	0.53	0.59	0.87	1.13	1.46
1 mM CH_3HgCl S171C	Unit Cell: 66.05 x 176.36 x 289.48								
R_{der}[a]	.21	.13	.12	.19	.22	.23	.28	.30	
R_{Cullis}[b]	.73	.59	.73	.87	.74	.83	.73	.83	
f_H / e[c]	.80	.86	.99	0.91	0.73	.68	.75	.78	
1 mM $PtCl_4$	Unit Cell: 65.94 x 175.90 x 289.53								
R_{der}[a]	.27	.24	.21	.27	.29	.26	.32	.33	.32
R_{Cullis}[b]	.70	.71	.68	.75	.67	.66	.71	.72	.88
f_H / e[c]	.74	.64	.80	.86	.71	.67	.69	.77	.89
0.1 mM terpyridine Pt(II) chloride	Unit Cell: 65.96 x 176.17 x 290.43								
R_{der}[a]	.22	.16	.16	.20	.22	.23	.25	.27	.26
R_{Cullis}[b]	.74	.70	.68	.70	.78	.76	.78	.85	.81
f_H / e[c]	.72	.66	.76	.86	.72	.64	.65	.70	.76

[a]$R_{der}=\frac{\sum|F_p-F_{ph}|}{\sum F_p}$, where F_p is the native amplitude and F_{ph} is the derivative amplitude.

[b]$R_{Cullis}=\frac{\sum||F_p\pm F_{ph}| - F_{h\ calc}|}{\sum|F_p\pm F_{ph}|}$, where F_p is the native amplitude, F_{ph} is the derivative amplitude for centric reflections, and $F_{h\ calc}$ is the calculated heavy atom structure factor.

[c]f_H / e is the phasing power; f_H is the mean amplitude of the heavy atom structure factor and e is the r.m.s lack-of-closure error.

[c]Unit cell dimensions for the native are 66.00 x 176.20 x 290.20 Å.

Figure Legends

Figure 1. Crystal of colicin Ia grown by the vapor diffusion from 1.08 M $(NH_4)_2SO_4$, 200 mM NaCl, 20 mM citrate buffer, pH 5.2. The magnification is ~80-fold.

Figure 2. Non-linearity correction for CEA 25 Reflex film. The exposure saturates at a value of 1600. The corrected density is 16-fold lower in scale than the observed density; the corrected density is a real*8 number while the observed density is an integer*2 value (on a scale of 0-4096). The parameters of the cubic polynomial fit are A=9.32429678, B=6.627302036 x 10^{-1}, C=-1.5459198 x 10^{-3}, D=1.277181458 x 10^{-6}, where the function is: $D + Ax + Bx^2 + Cx^3$.

Figure 3. Refinement protocol for MAR image plate data used in DENZO.

Figure 4. Polarization of synchrotron beams. Data from a single film were processed and reduced with varying polarization values, and the resulting R_{symm} was calculated. (a) Data collected at SSRL. (b) Data collected at LURE, for which the polarization has been measured as 90.3% horizontal.

Figure 5. Wilson Plot of colicin Ia diffraction. o Data collected at room-temperature. The Wilson B-factor was calculated from 5.0 to 3.4 Å and is 76 $Å^2$. ◘ Data collected at ~100 K. The Wilson B-factor was calculated from 3.4 to 2.95 Å and is 55 $Å^2$.

Figure 6. Difference Pattersons showing the u=0 Harker section; the extents are v=1/2 and w=1/2. (a) 0.5 mM TlK_3Cl_6. (b) 0.1 mM Nb_6Cl_{14}. (c) 1 mM CH_3HgCl of S171C.

Figure 7. Cross-eyed stereo view of typical density in the 3.4 Å map. The electron density map was calculated from 20-3.4 Å using MIR, solvent-flattened phases and contoured at 1σ.

Figure 8. Cross-eyed stereo view of a ribbon representation of the overall structure of colicin Ia. The model consists of 482 α-helical alanines in 28 separate fragments.

Figure 9. Cross-eyed stereo view of the packing of colicin Ia in the unit cell. (a) Ten molecules are shown to illustrate the packing; the unit cell contains 8 molecules of colicin Ia. The direction of unit cell axes (a=66.0 Å, b=176.2 Å, c=290.2 Å) are indicated on the figure. A wall of protein formed by Arm 1 and Arm2 at the **c**=0 and 1/2 planes are connected by Stalk domains which point in the direction of the **c** axis. (b) Projection along the **a** axis of one unit cell of room temperature colicin Ia. Phases were calculated with MIR, solvent-flattened phases.

Figure 10. Transform of the solvent envelope as a function of resolution. O Amplitude of the solvent envelope along the **c** axis (calculated for 00l reflections). □ Amplitude of the solvent envelope along the **b** axis (calculated for 0k0 reflections). Δ Amplitude of the solvent envelope along the **a** axis (calculated for h00 reflections). The high amplitudes along the **c** axis reflect the strong low-order terms representing the alternation of walls of protein separated by large solvent spaces. There is much less low-order modulation along the **a** and **b** axes.

Figure 11. Cross-eyed stereo view of a ribbon representation of the Stalk domain.

Figure 12. Cross eyed stereo view of electron density for Stalk a1. (a) MIR electron density calculated from 20-3.4 Å with a contour level of 1σ. (b) MIR, solvent-flattened electron density calculated from 20-3.4 Å with a contour level of 1σ.

Figure 13. Cross-eyed stereo view of a ribbon representation of Arm 1.

Figure 14. Cross-eyed stereo view of a difference Fourier map calculated from 20-3.4 Å of the mercurial derivative of S171C with a contour level of 5σ. The map is calculated from (F_{ph} - F_p) coefficients and MIR, solvent-flattened phases; corrected amplitudes were used for the derivative.

Figure 15. Cross-eyed stereo view of Arm 2. (a) The superposition of the colicin A channel-forming fragment with sub-domain 1 (see b). Colicin A is represented as the clear trace and the N-terminus, C-terminus, and residues 80 and 100 are indicated on the figure. Helices for colicin Ia are show as black traces. (b) Ribbon representation of Arm 2. Sub-domain 1, which superimposes with the colicin A fragment, is shown in light gray, and sub-domain 2 is shown in dark gray.

Figure 16. Cross-eyed stereo view of an elliptical representation of the length and direction of primary axes of colicin Ia.

FIGURE 1

FIGURE 2

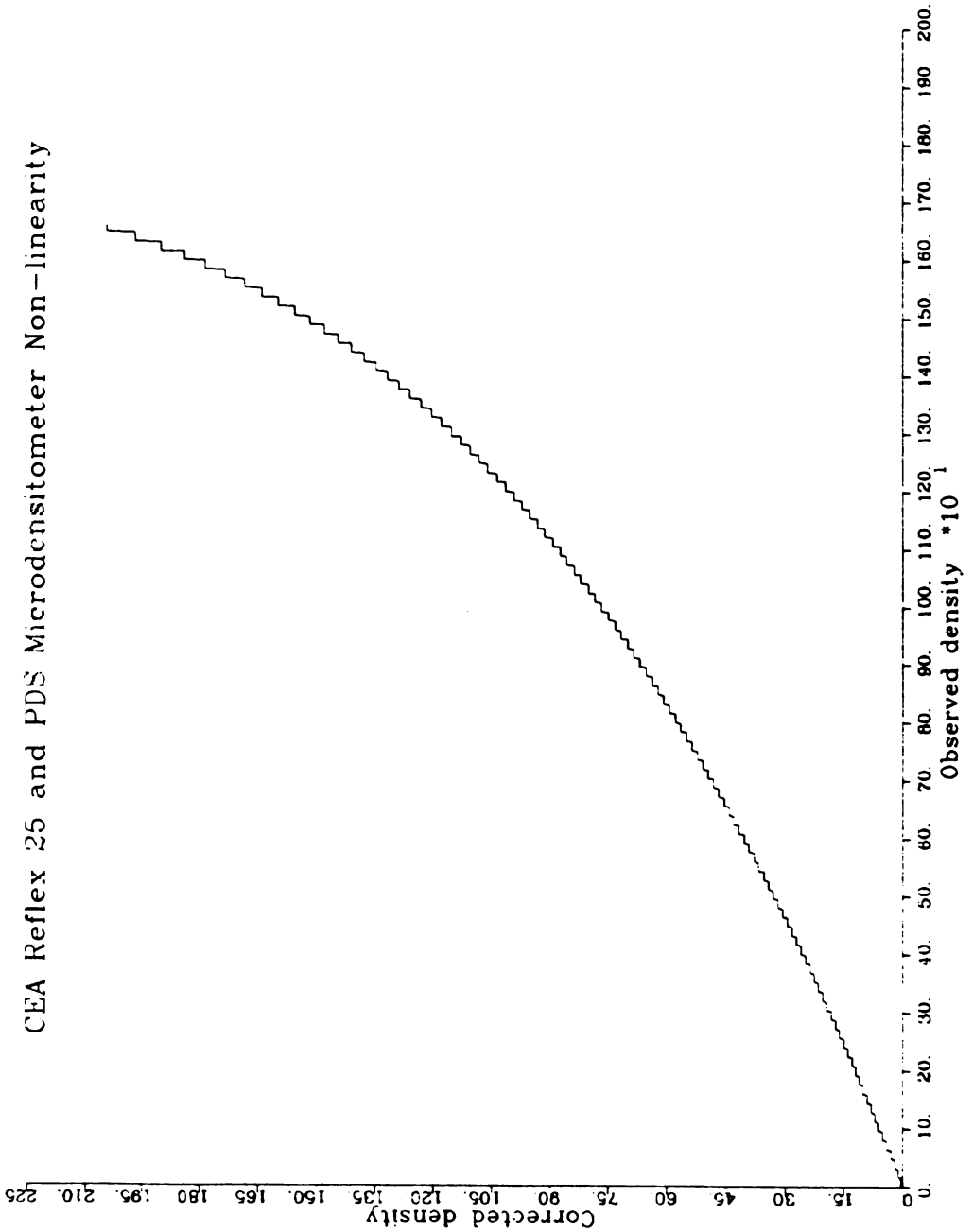
CEA Reflex 25 and PDS Microdensitometer Non-linearity
Corrected density
0 15 30 45 60 75 90 105 120 135 150 165 180 195 210 225
Observed density *10^-1
0. 10. 20. 30. 40. 50. 60. 70. 80. 90. 100. 110. 120. 130. 140. 150. 160. 170. 180. 190. 200.

FIGURE 3

```
UNIT CELL 65.15 174.72 284.70 90.0 90.0 90.0
LATTICE C
MOSAICITY .2
WAVELENGTH 1.08
SPINDLE AXIS 1 1 0
VERTICAL AXIS 0 0 1
MONOCHROMATOR SSRL
(pixel size on MAR image plate)
RASTER .15
(FILM THICKNESS .203 )
CRYSTAL ROTZ 34.533 ROTY -6.449 ROTX -7.465
DISTANCE 220.585
Y SCALE 0.99868
(mar research "corrected" frames as opposed to "spiral")
FORMAT MAR_CORR
(film length and width are in millimeters)
FILM LENGTH 180. WIDTH 180.
FILM ROTATION 0.0
RECORD LENGTH 1200
NUMBER OF RECORDS 1200
OVERLAP SPOT
ERROR POSITIONAL .02
;

BOX PRINT 4.5 1.05 SPOT RADIUS .325
BACKGROUND RADIUS .5
USE NO BEAM

RESOLUTION LIMITS 30. 15.
FIT CRYSTAL ROTZ
GO GO GO GO GO GO GO


FIT Y SCALE X BEAM Y BEAM USE NO BEAM
GO GO GO GO GO GO GO

RESOLUTION LIMITS 30. 10.
FIT RADIAL OFFSET ANGULAR OFFSET
GO GO GO GO GO GO

RESOLUTION LIMITS 30. 8.
FIT CRYSTAL ROTX ROTY
REFINE PARTIALITY
GO GO GO GO GO GO GO

RESOLUTION LIMITS 30. 7.
GO GO GO GO GO

RESOLUTION LIMITS 30. 6.0
FIX DISTANCE
FIT A* B* C*
GO GO GO GO GO GO GO GO GO

RESOLUTION LIMITS 30. 5.
GO GO GO GO

RESOLUTION LIMITS 30. 4.
FIX A* B* C*
FIT DISTANCE
GO GO GO GO GO GO GO

FIT A* B* C*
GO GO GO GO GO GO GO

FIX CRYSTAL ROTX ROTY ROTZ
FIT CASSETTE ROTX ROTY ROTZ
RESOLUTION LIMITS 30. 4.0
GO GO GO GO GO GO GO GO

FIX CASSETTE ROTX ROTY ROTZ
FIT CRYSTAL ROTX ROTY ROTZ
GO GO GO GO GO GO GO

RESOLUTION LIMITS 30. 3.4
GO GO GO GO GO GO GO

FIX DISTANCE
FIT A* B* C*
GO GO GO GO GO GO GO

FIX A* B* C*
FIT DISTANCE
GO GO GO GO GO GO GO

FIT A* B* C*
GO GO GO GO GO GO GO

RESOLUTION LIMITS 30. 3.2
GO GO GO GO GO GO GO

RESOLUTION LIMITS 30. 2.8
GO GO GO GO GO GO GO GO GO GO

RESOLUTION LIMITS 30.0 2.8
PROFILE FITTING RADIUS 25.
CALCULATE
GO

END OF PACK
```

FIGURE 4a

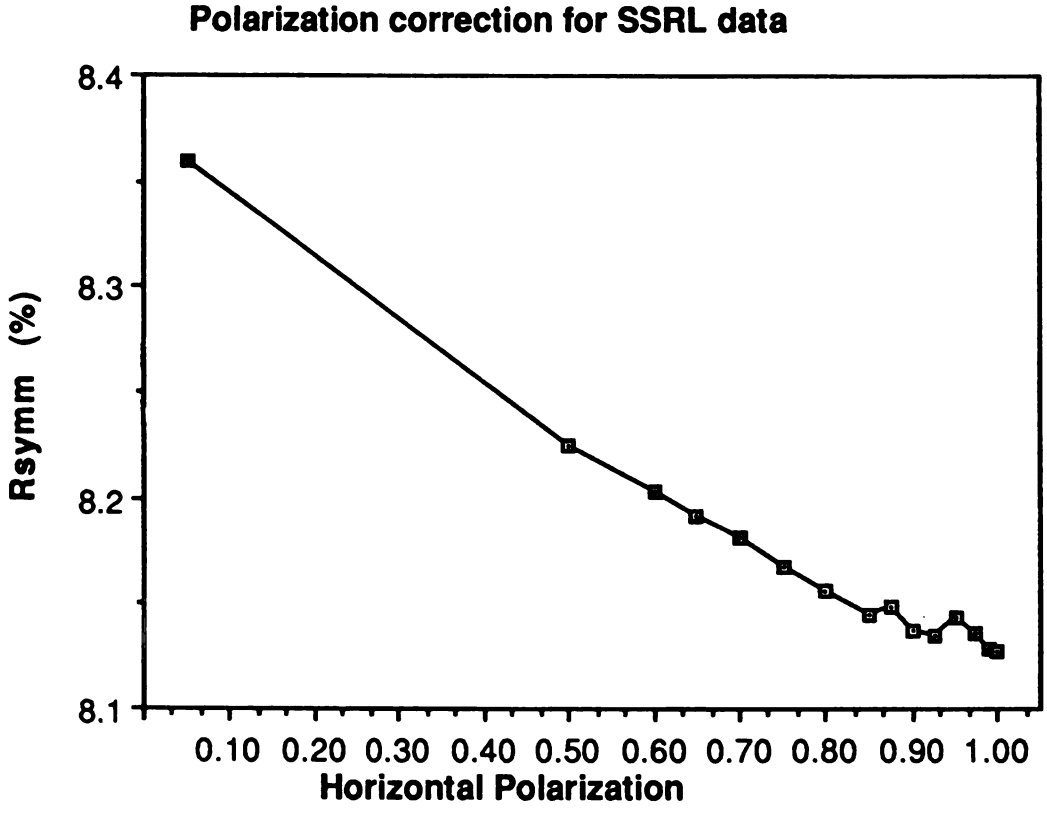
Polarization correction for SSRL data
8.4
8.3
8.2
8.1
Rsymm (%)
0.10 0.20 0.30 0.40 0.50 0.60 0.70 0.80 0.90 1.00
Horizontal Polarization

FIGURE 4b

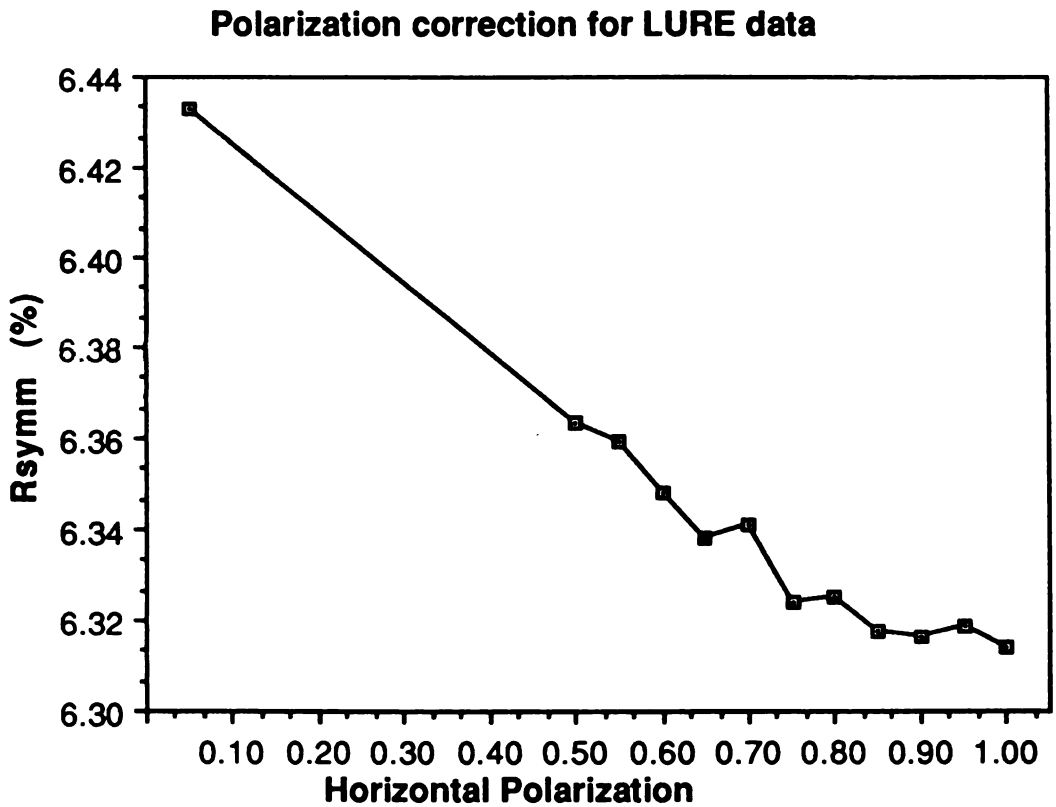
Polarization correction for LURE data
Rsymm (%)
6.44
6.42
6.40
6.38
6.36
6.34
6.32
6.30
0.10 0.20 0.30 0.40 0.50 0.60 0.70 0.80 0.90 1.00
Horizontal Polarization

FIGURE 5

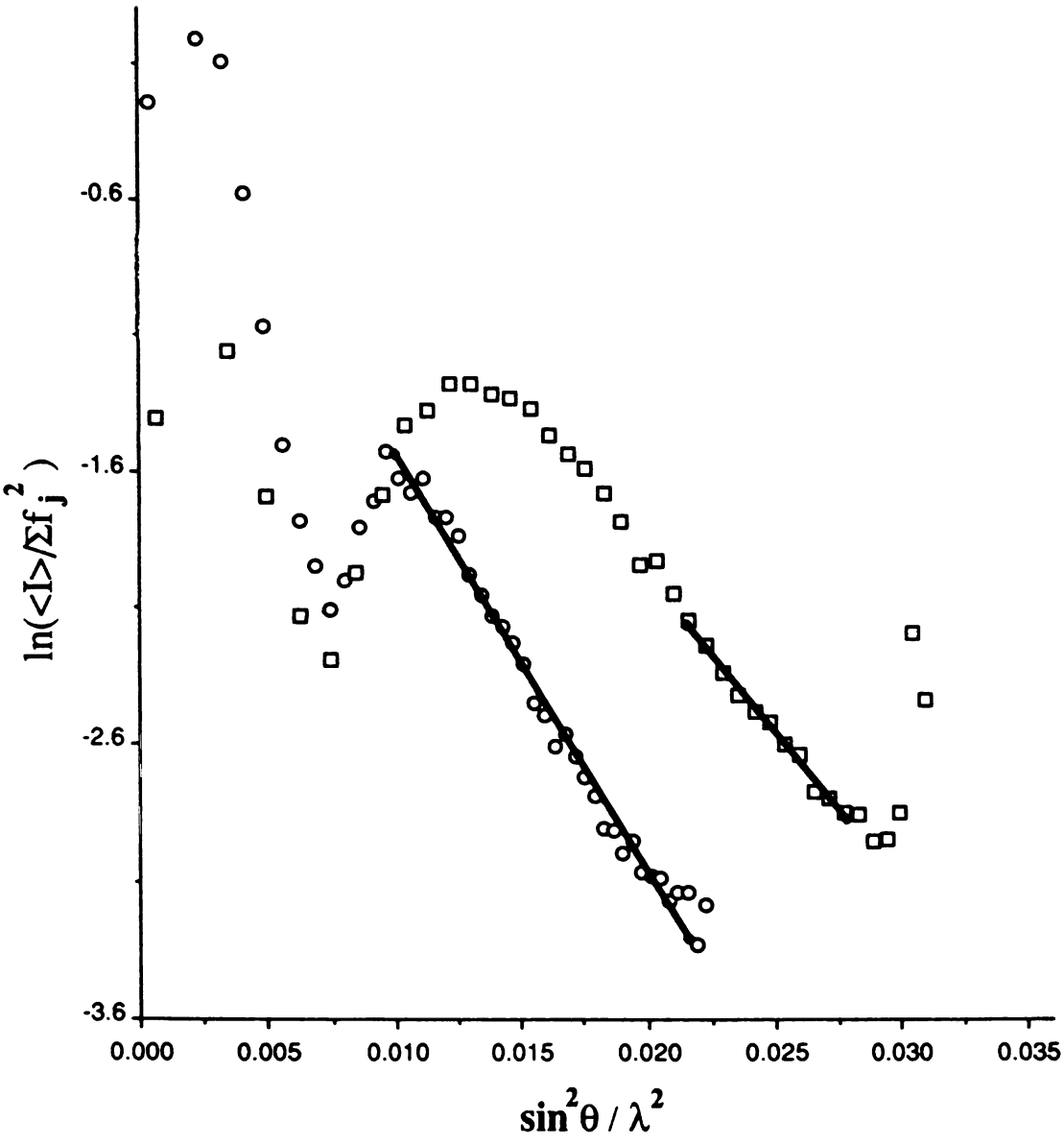
-0.6
-1.6
-2.6
-3.6
0.000
0.005
0.010
0.015
0.020
0.025
0.030
0.035
ln(<I>/Σf_j^2)
sin^2θ / λ^2

FIGURE 6a

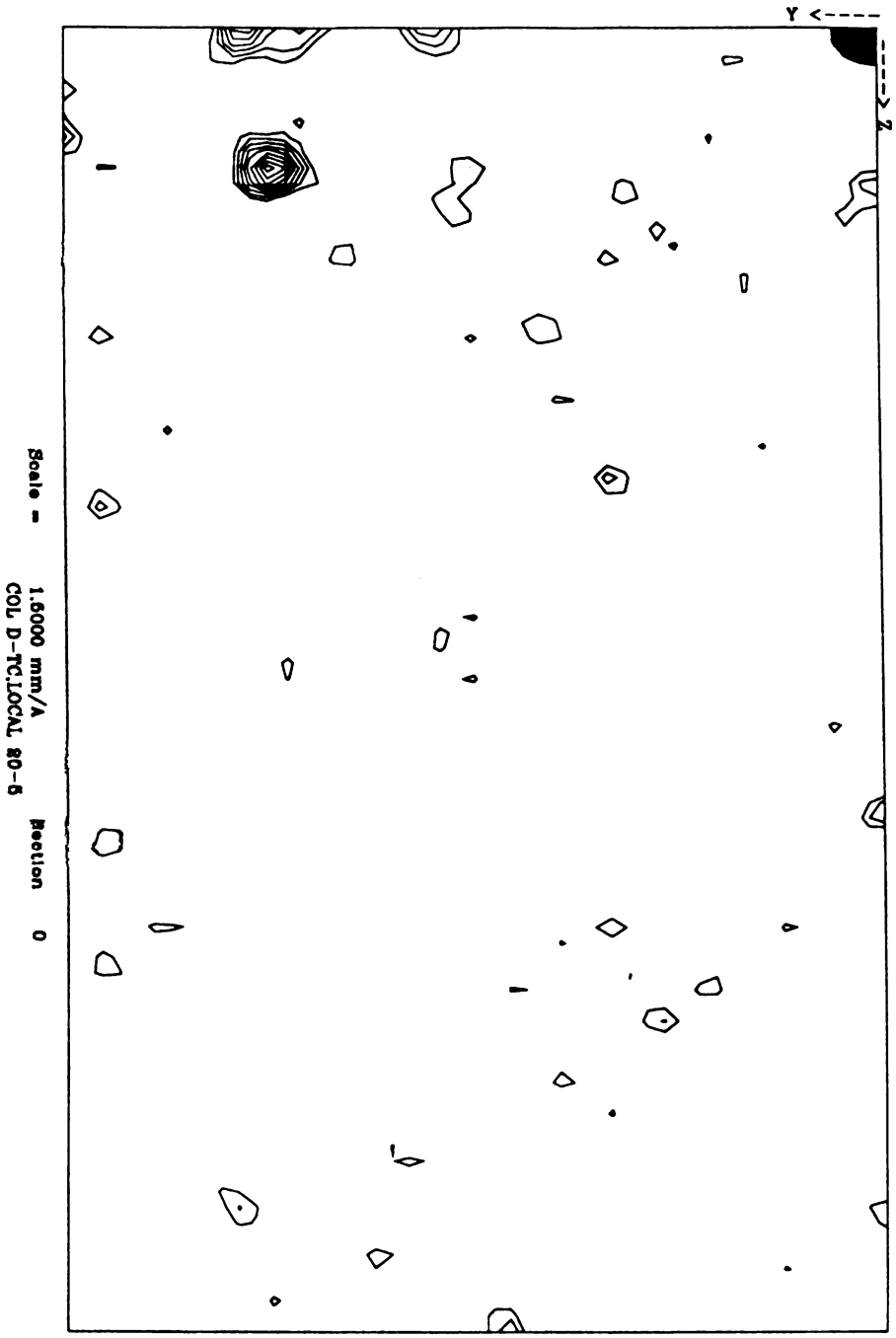

FIGURE 6b

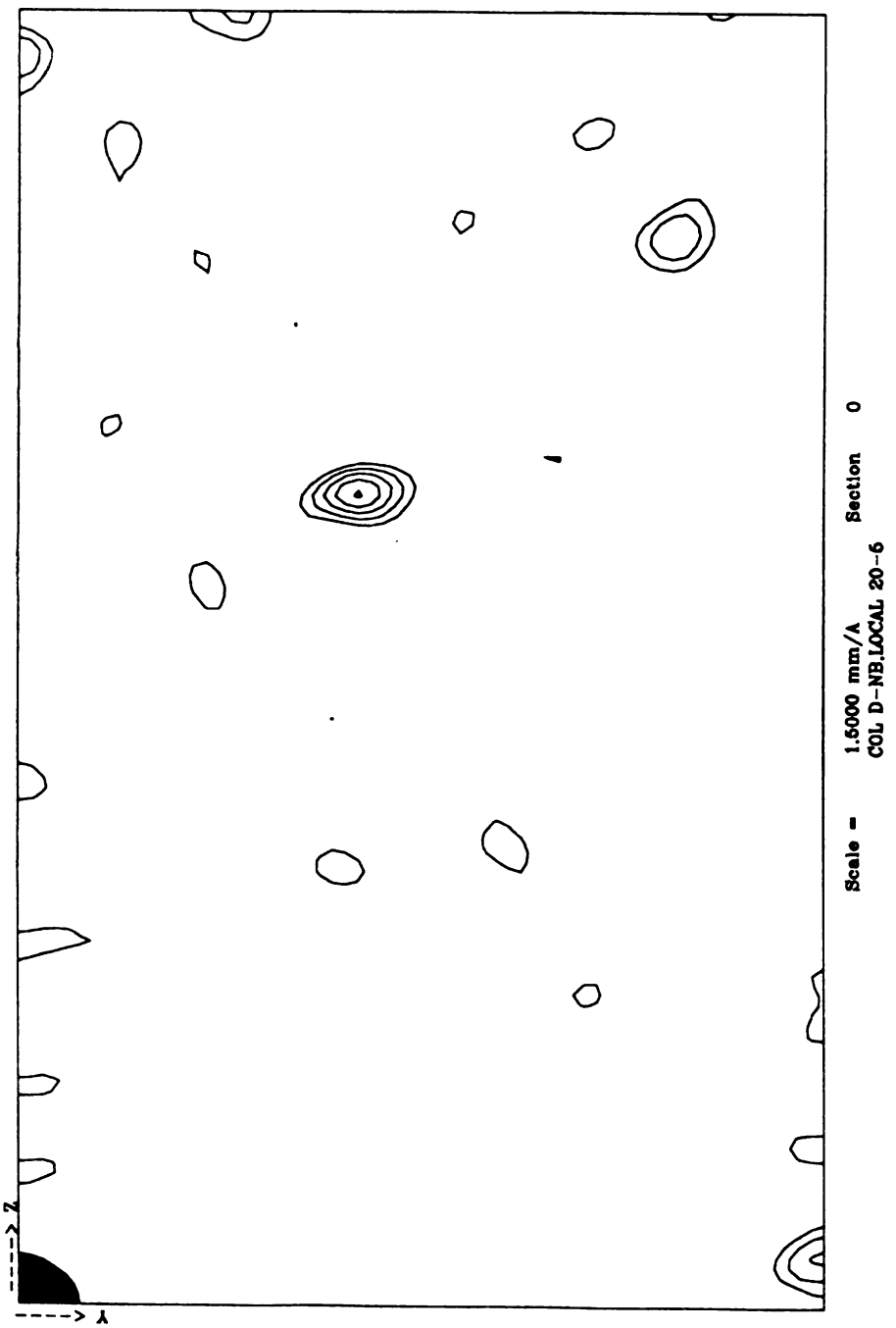

FIGURE 6c

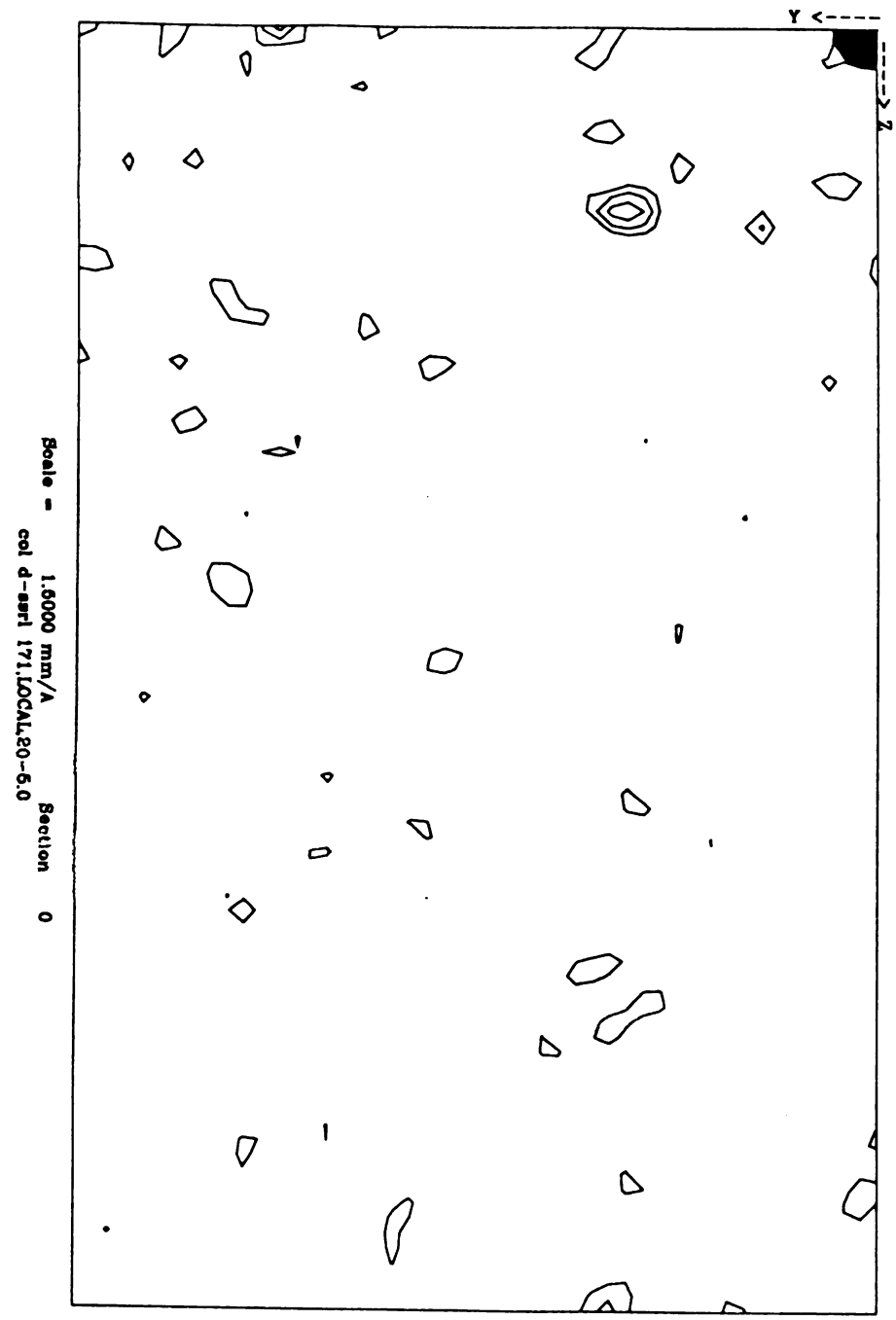

FIGURE 7

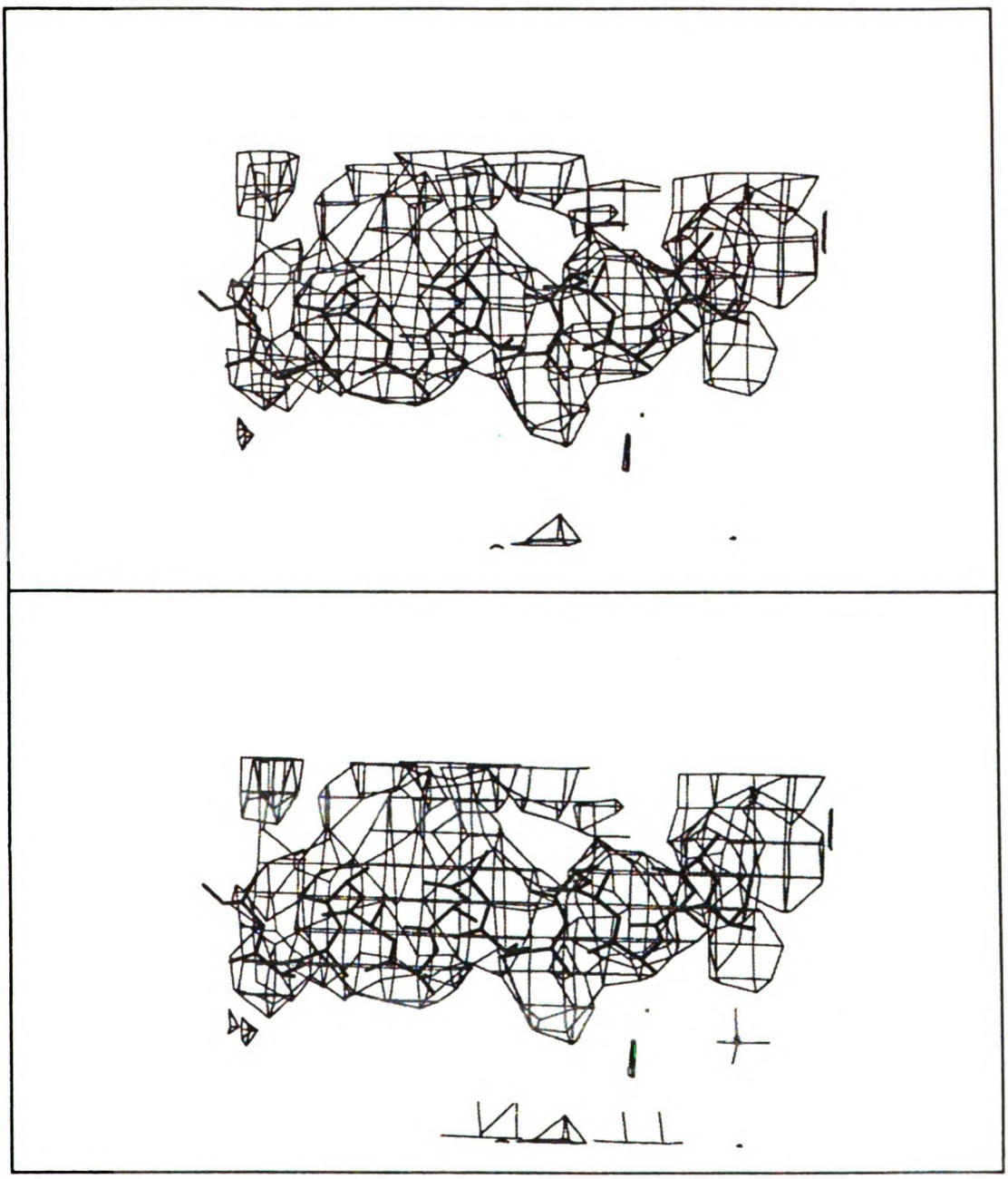

FIGURE 8

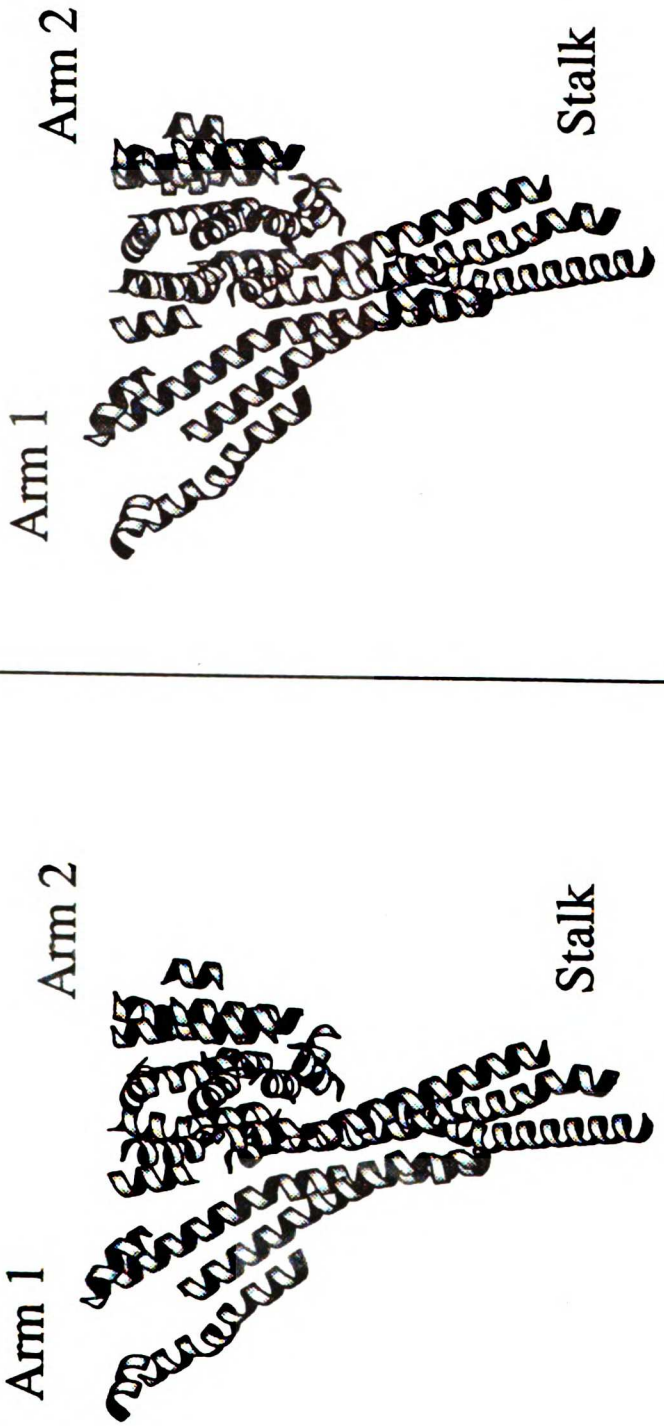

FIGURE 9a

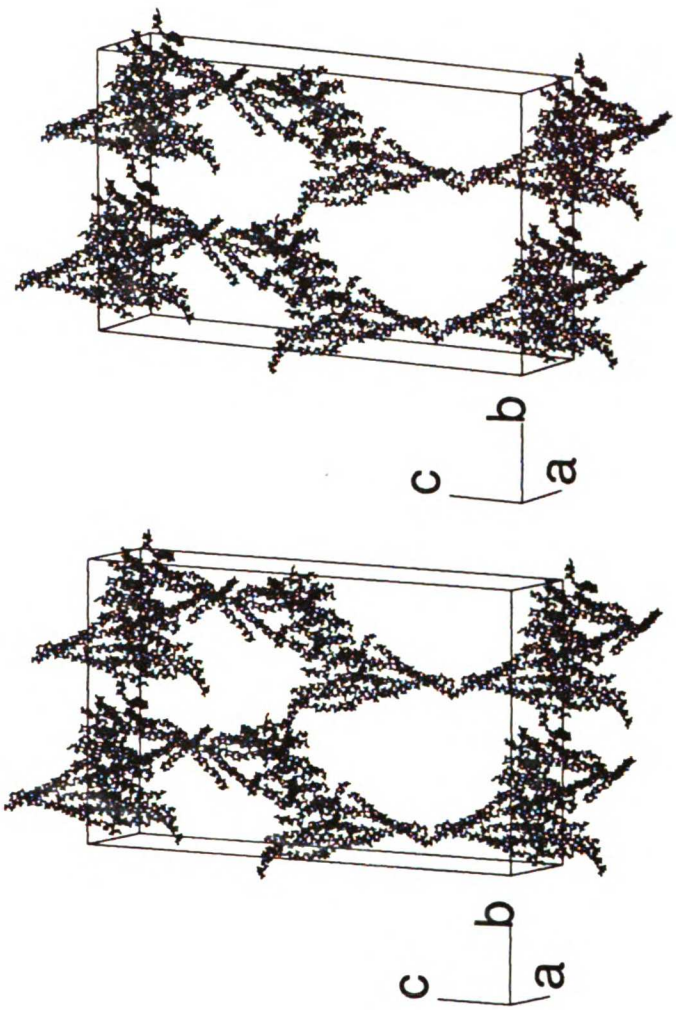

FIGURE 9b

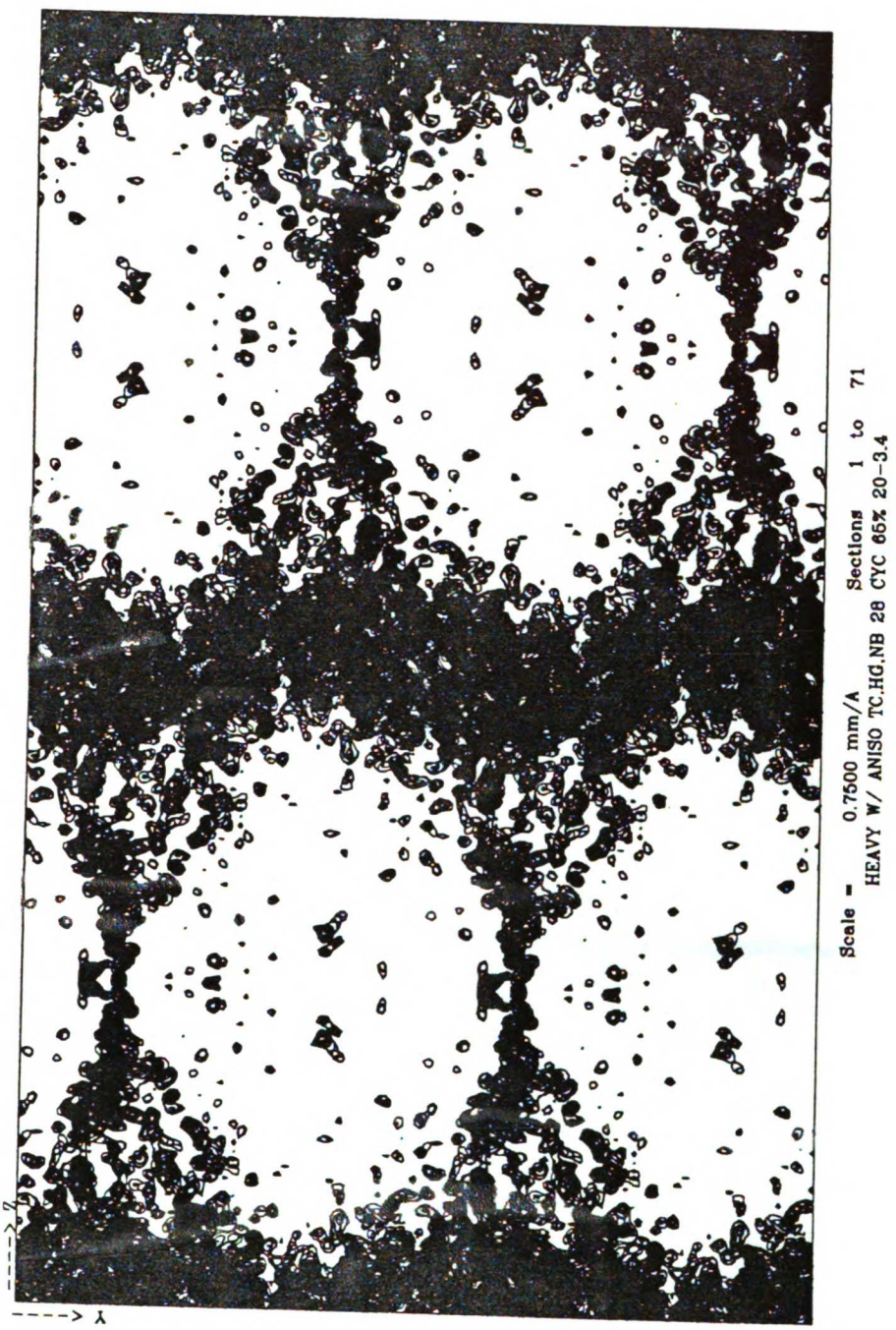
Scale = 0.7500 mm/A Sections 1 to 71
HEAVY W/ ANISO TC,HG,NB 28 CYC 65% 20-3.4
----> Z
----> X

FIGURE 10

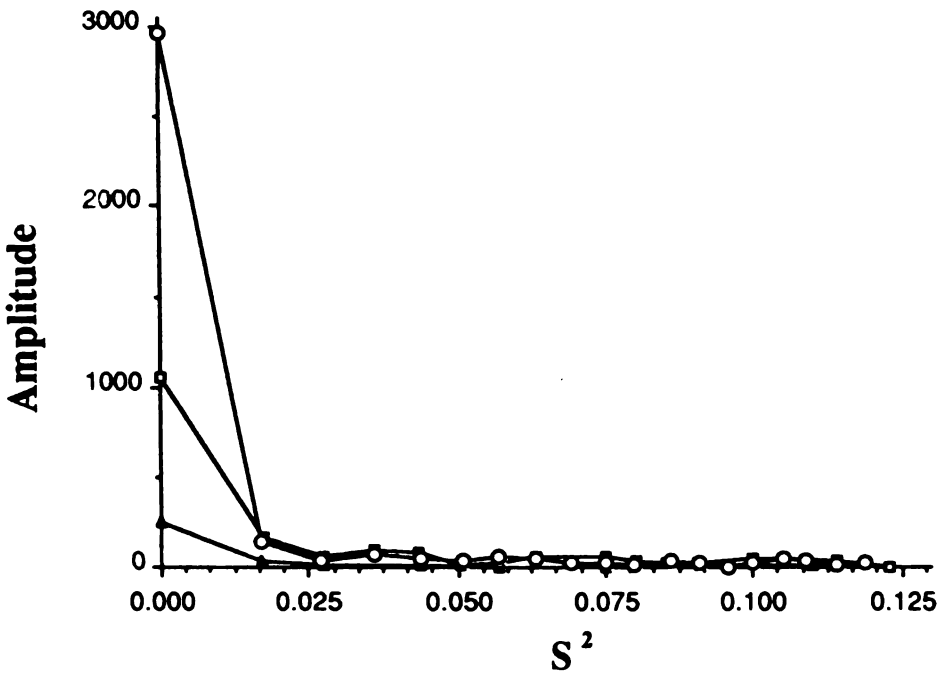

FIGURE 11

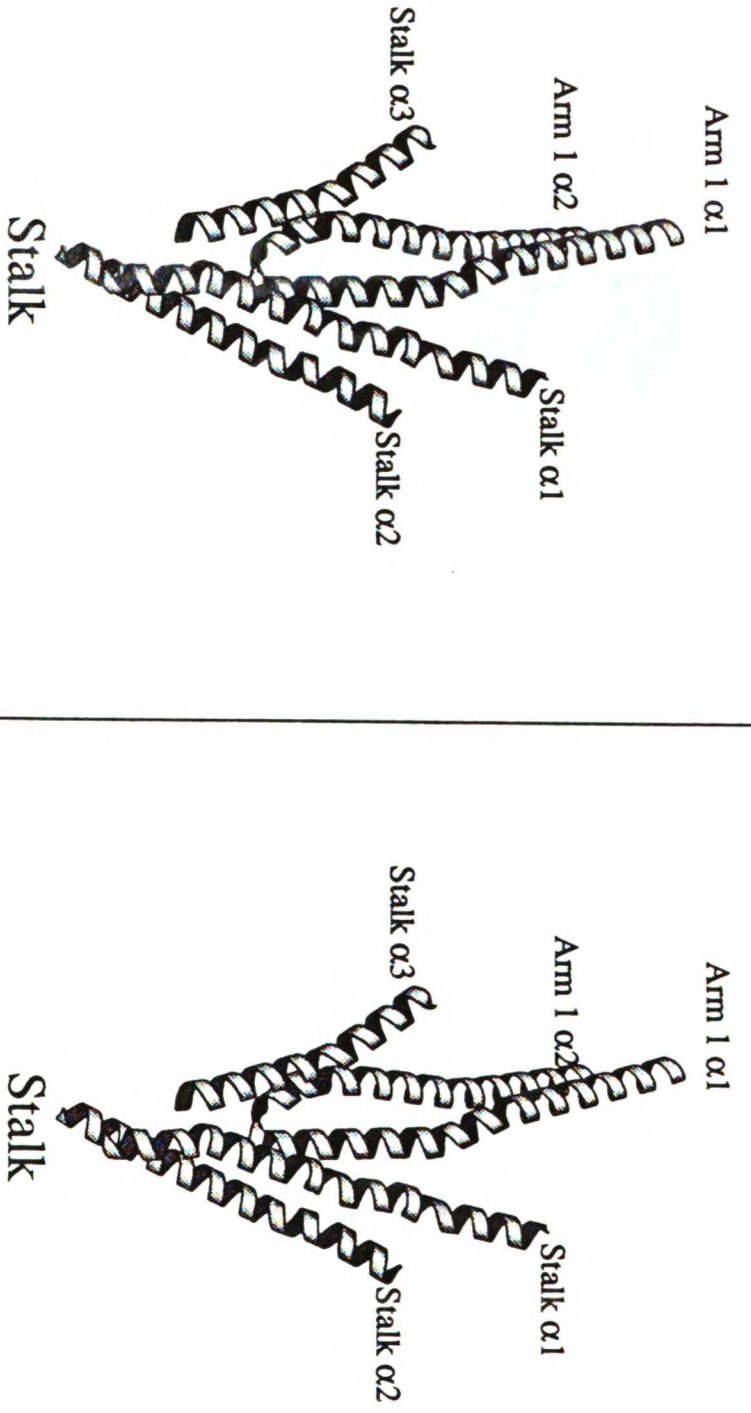
Arm 1 α1
Arm 1 α2
Stalk α3
Stalk
Stalk α1
Stalk α2
Arm 1 α1
Arm 1 α2
Stalk α3
Stalk
Stalk α1
Stalk α2

FIGURE 12a

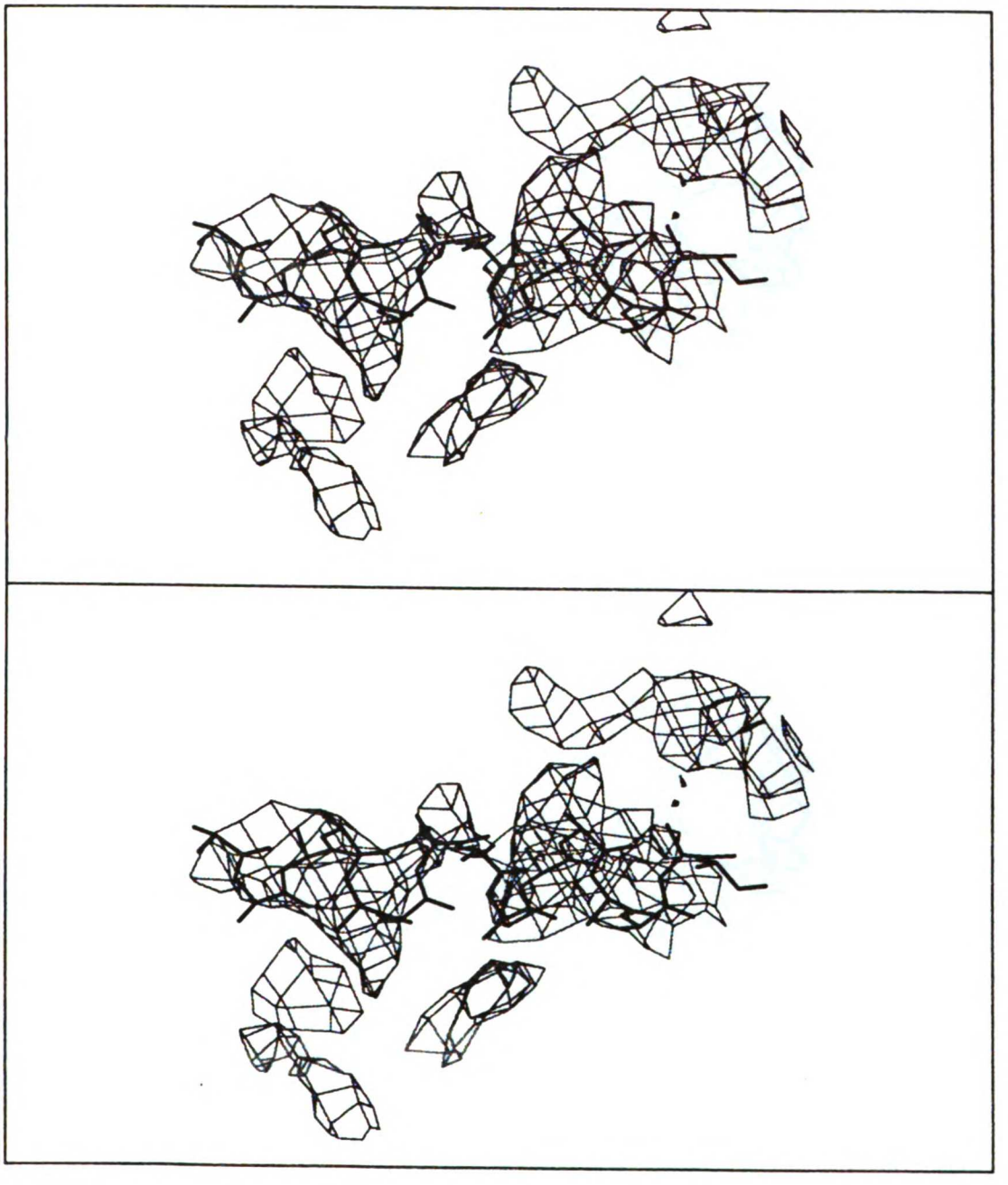

FIGURE 12b

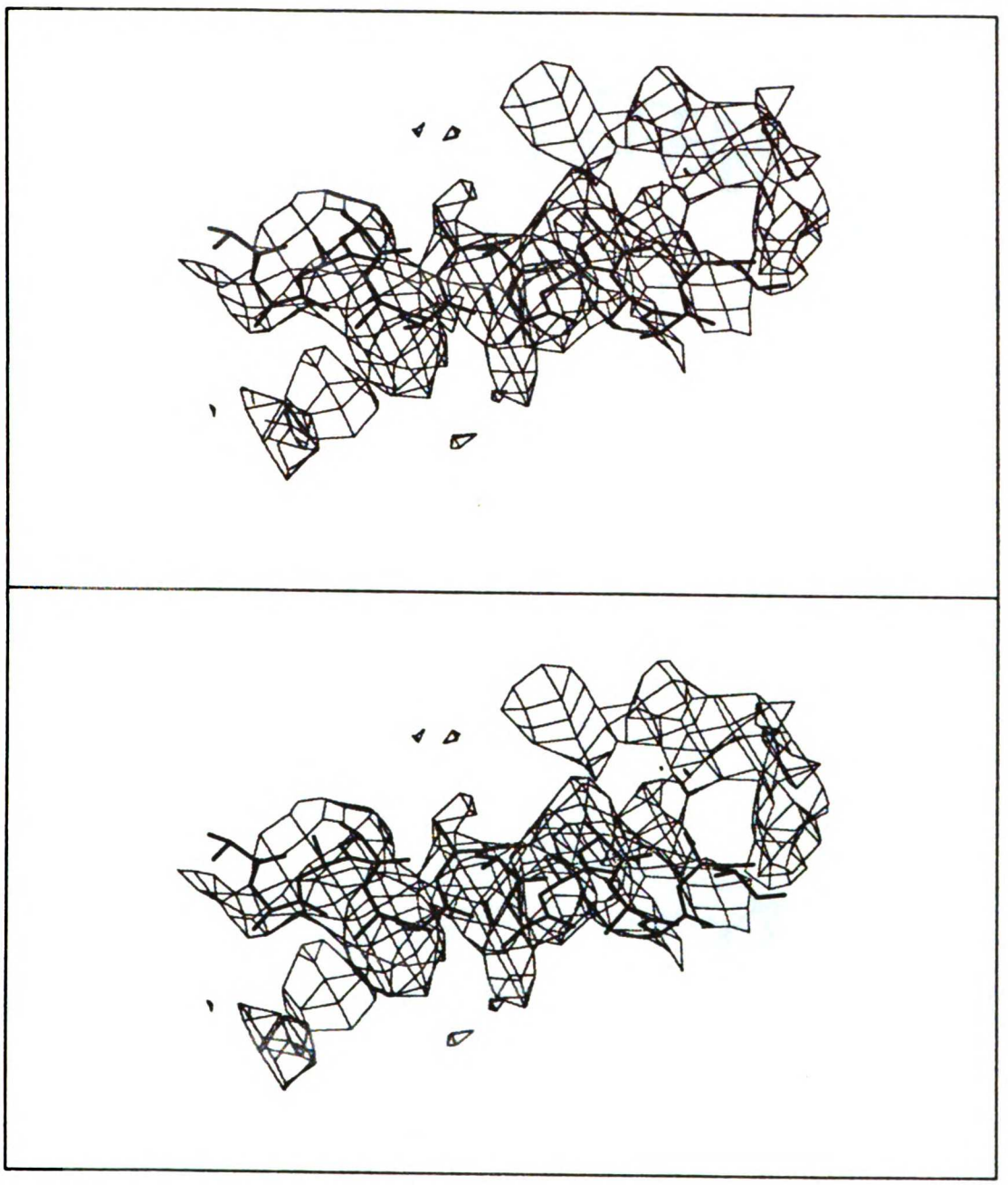

FIGURE 13

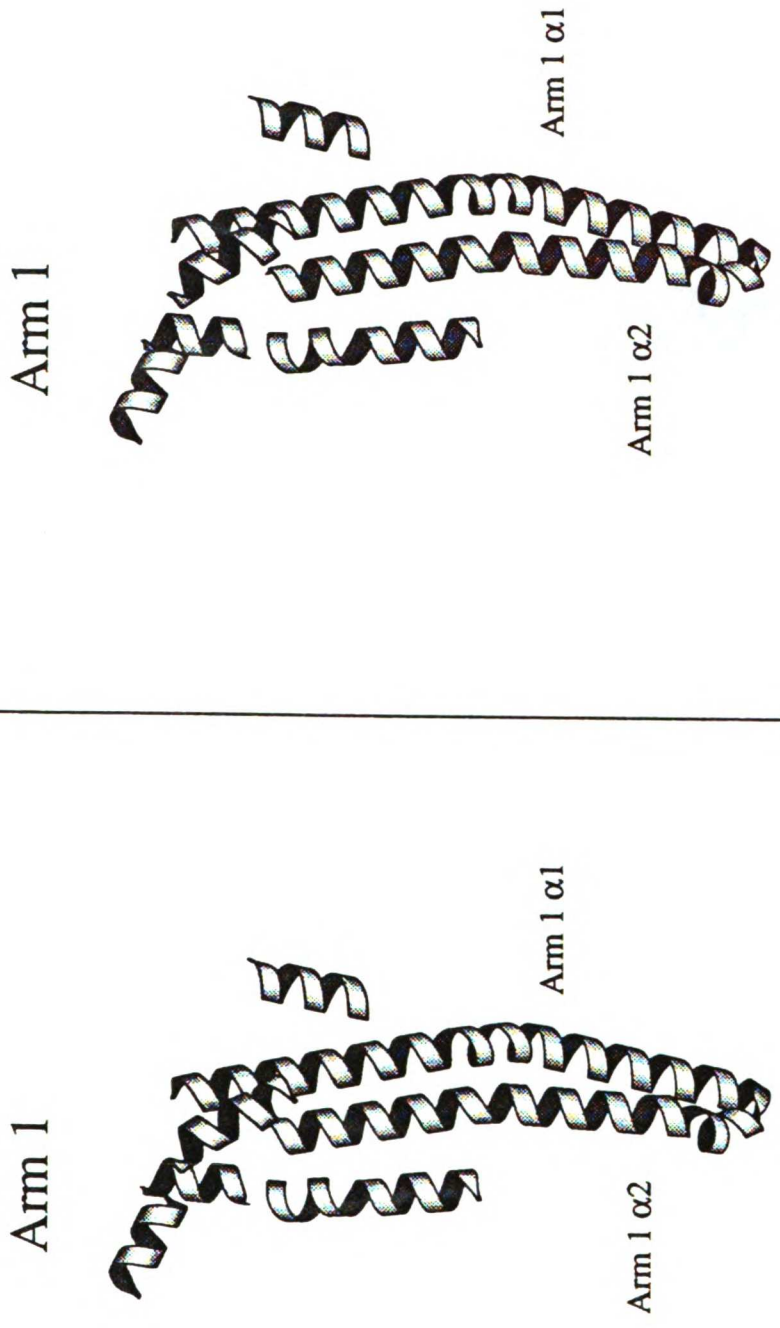

FIGURE 14

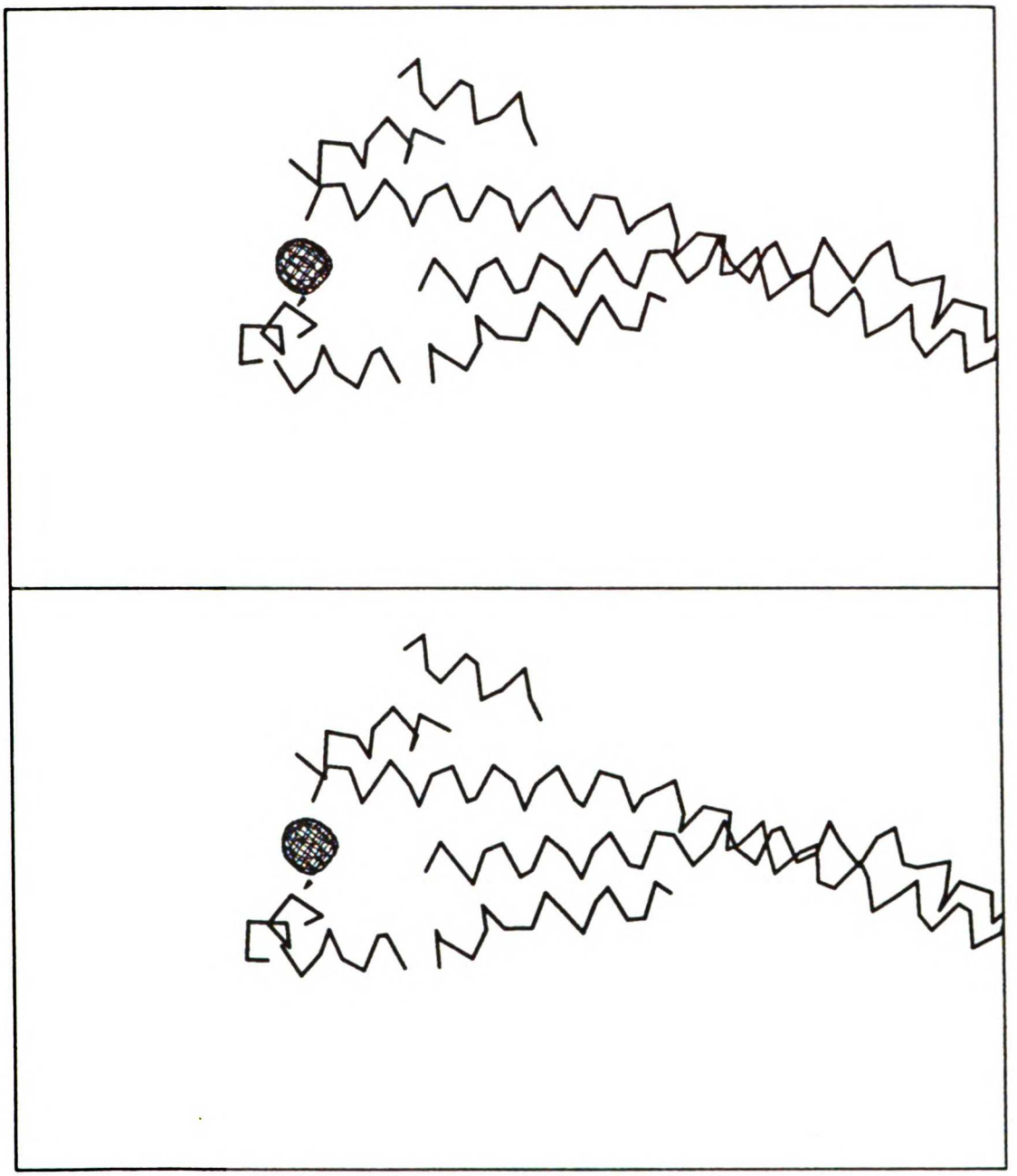

FIGURE 15a

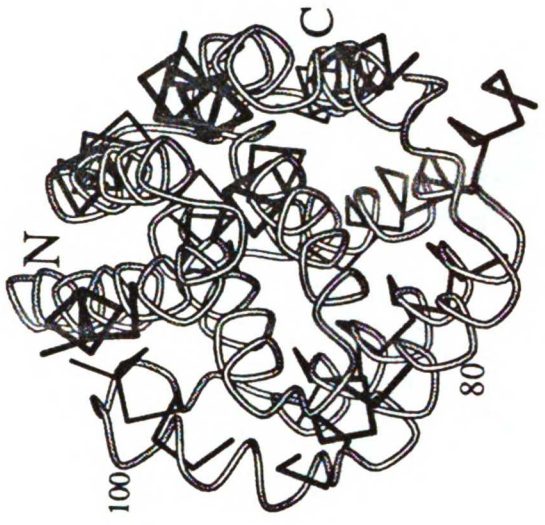

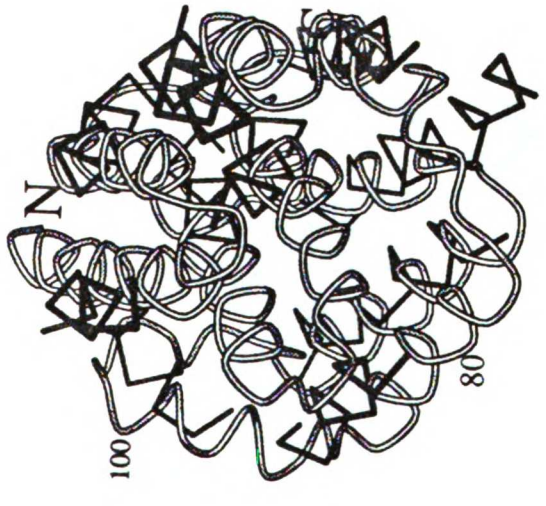

FIGURE 15b

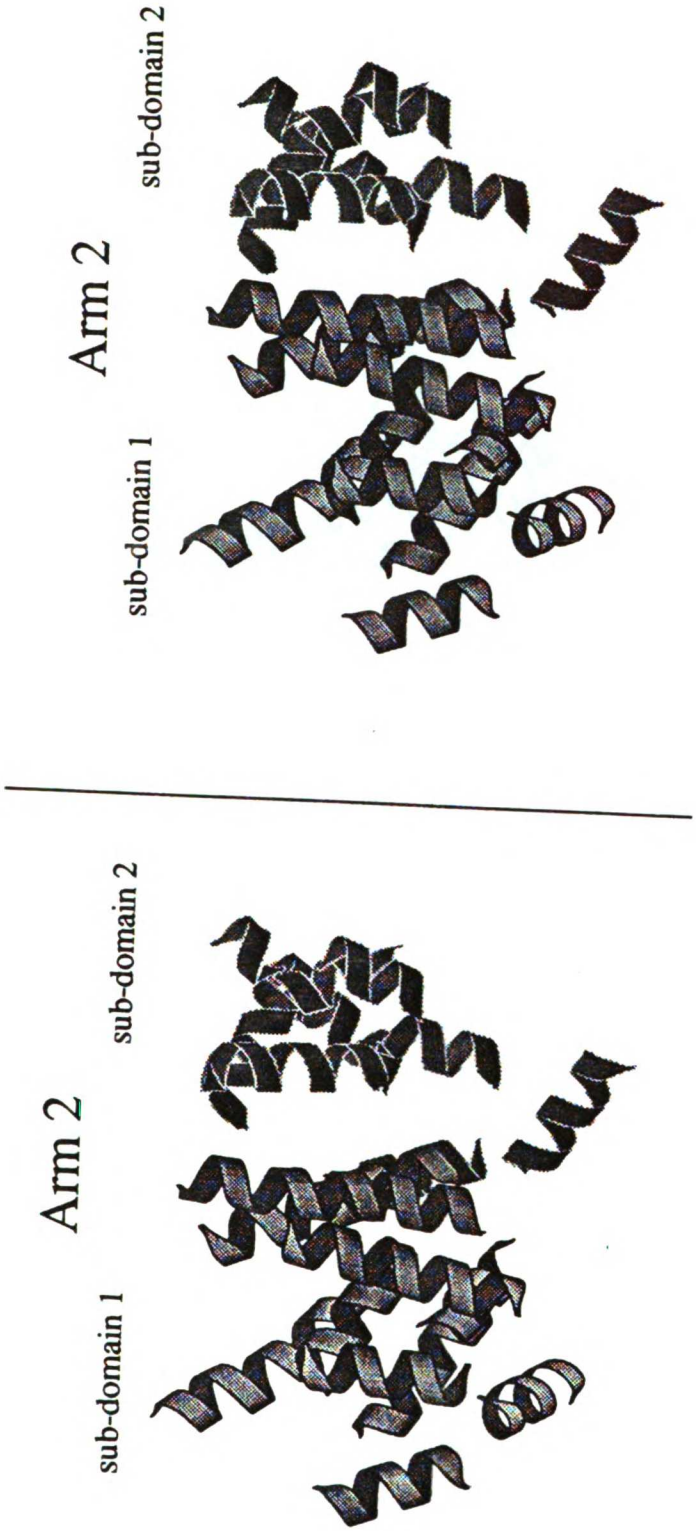

FIGURE 16